AD NUMBER

AD877170

LIMITATION CHANGES

TO:

Approved for public release; distribution is unlimited.

FROM:

**Distribution authorized to U.S. Gov't. agencies and their contractors;
Administrative/Operational Use; SEP 1970. Other requests shall be referred to Army Aviation Materiel Labs., Fort Eustis, VA.**

AUTHORITY

USAAMRDL ltr, 14 May 1971

AD

USAAVLABS TECHNICAL REPORT 70-53

TURBINE BLADE/DISK FABRICATION INVESTIGATION

By

George W. Kelch

Richard W. Nelson

September 1970

U. S. ARMY AVIATION MATERIEL LABORATORIES
FORT EUSTIS, VIRGINIA

CONTRACT DAAJ02-68-C-0071

PRATT & WHITNEY AIRCRAFT
FLORIDA RESEARCH AND DEVELOPMENT CENTER
WEST PALM BEACH, FLORIDA

180

DISCLAIMERS

The findings in this report are not to be construed as an official Department of the Army position unless so designated by other authorized documents.

When Government drawings, specifications, or other data are used for any purpose other than in connection with a definitely related Government procurement operation, the United States Government thereby incurs no responsibility nor any obligation whatsoever; and the fact that the Government may have formulated, furnished, or in any way supplied the said drawings, specifications, or other data is not to be regarded by implication or otherwise as in any manner licensing the holder or any other person or corporation, or conveying any rights or permission, to manufacture, use, or sell any patented invention that may in any way be related thereto.

DISPOSITION INSTRUCTIONS

Destroy this report when no longer needed. Do not return it to the originator.

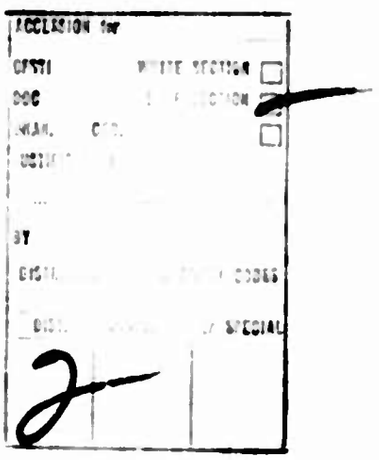

DEPARTMENT OF THE ARMY
U. S. ARMY AVIATION MATERIEL LABORATORIES
FORT EUSTIS, VIRGINIA 23604

The research described herein was conducted by the Florida Research and Development Center of Pratt & Whitney Aircraft under the technical management of Mr. Edward T. Johnson, Propulsion Division, US Army Aviation Materiel Laboratories.

The object of this research was to investigate, through analytical studies and experimental testing, several blade-to-disk attachment concepts to determine the optimum concept for use on future small, high-temperature axial turbine rotors.

Appropriate technical personnel of the US Army Aviation Materiel Laboratories have reviewed this report and concur with the conclusions contained herein.

Task 1G162203D14413
Contract DAAJ02-68-C-0071
USAAVLABS Technical Report 70-53
September 1970

TURBINE BLADE/DISK FABRICATION INVESTIGATION

FINAL REPORT

by

George W. Kelch
Richard W. Nelson

Prepared by

Pratt & Whitney Aircraft
Florida Research and Development Center
West Palm Beach, Florida

for

U.S. ARMY AVIATION MATERIEL LABORATORIES
FORT EUSTIS, VIRGINIA

ABSTRACT

This report describes an investigation of blade/disk attachment methods for small gas turbine engines. The investigation included analytical and experimental evaluations of selected attachment methods potentially suitable for a 2-lb/sec axial flow turbine with 2500°F turbine inlet temperature.

A literature survey of attachments for small axial flow turbines yielded six candidate methods for further analytical study. The three most promising approaches were evaluated experimentally to determine the superior attachment technique. This attachment scheme was optimized by additional uniaxial experimental testing and final proof-testing by subjecting biaxial specimens to cyclic loads at the attachment design temperature.

TABLE OF CONTENTS

TABLE OF CONTENTS (Continued)

TABLE OF CONTENTS (Continued)

LIST OF ILLUSTRATIONS

LIST OF ILLUSTRATIONS (Continued)

LIST OF ILLUSTRATIONS (Continued)

LIST OF ILLUSTRATIONS (Continued)

LIST OF ILLUSTRATIONS (Continued)

LIST OF ILLUSTRATIONS (Continued)

LIST OF TABLES

LIST OF TABLES (Continued)

LIST OF SYMBOLS

B.M.	Burst Margin
$\mathcal{L}$	Centerline
ID	Inner Diameter, in.
L	Distance, in.
N	Rotational Speed, rpm
OD	Outer Diameter, in.
P_t	Total Blade Pull, lb
R	Radius, in.
$T_{cooling\ air}$	Cooling Air Temperature, °F
T_{gas}	Gas Stream Temperature, °F
T_{metal}	Airfoil Metal Temperature, °F
V_{tip}	Blade Tip Velocity, ft/sec
Δ	Differential
ΔH	Turbine Stage Work, Btu/lb
η	Adiabatic Efficiency
σi	Stress at Point i, lb/in^2
Φ	Cooling Effectiveness Parameter

1.0 INTRODUCTION

Future U. S. Army aviation and vehicle applications will require small gas turbine engines with high power-to-weight ratios, improved efficiency over a wide power range, and ease of field maintenance. Simplicity and low cost are additional requirements, which dictate a minimum number of engine parts and make single-stage, high-work turbines desirable.

To achieve the high stage work levels required, operation at the maximum levels of turbine inlet temperature, aerodynamic loading, and wheel speed allowed by performance and life goals is necessary. Studies of small turbines indicate that the maximum allowable wheel speed is governed by the attachment stress limitations. Optimized attachment methods that reduce rotor weight and improve cooling air sealing are therefore vital parts of the advanced technology necessary for the successful development of small, high-temperature engines.

An analytical and experimental program was conducted to evaluate attachment concepts that are potentially suitable for small gas turbine engines defined by the design parameters given in Table I.

TABLE I. TURBINE DESIGN PARAMETERS

Parameter	Value
Turbine Inlet Temperature - °F	2300-2500
Airflow Rate - lb/sec	2-5
Compressor Pressure Ratio	10:1
Turbine Adiabatic Efficiency - %	83-85
Turbine Tip Speed - ft/sec	1500-1900
Number of Turbine Stages	1
Cooling Technique	Air
Design Life (at Maximum Gas Temperature) - hr	1000

This program was accomplished in the following five tasks:

Task I. A literature survey of blade/disk attachment methods and selection of a maximum of six candidate methods

Task II. Design analysis of the prospective methods to select the three most promising approaches, and design of test specimens for the chosen attachment configurations

Task III. Uniaxial test specimen fabrication

Task IV. Uniaxial screening tests to determine tensile, fatigue and stress rupture strength characteristics of the three selected methods

Task V. Selection and redesign of the most suitable attachment method, optimization of the final attachment design by uniaxial test specimen evaluations, and proof testing by subjecting biaxial specimens to cyclic loads at the predicted attachment design temperature

2.0 TASK I - FABRICATION STUDY

OBJECTIVES

The objectives of the fabrication study were (1) to survey published literature, manufacturing vendors, and patent disclosures for potential blade/disk attachment techniques; and (2) to select six promising attachment methods for detailed analysis.

2.1 LITERATURE SURVEY

A survey of the published literature was conducted to obtain information on turbine blade/disk attachment methods. Table II lists the reference sources used in the survey. Since the available literature contained relatively few references dealing specifically with turbine blade attachments for small gas turbines, a patent search and a manufacturing vendor survey were also undertaken to uncover novel attachment designs. Bicasting was the most promising fabrication technique uncovered by the vendor survey; the patent search revealed very little technical information. The literature reviewed is presented in Section 9 (Selected Bibliography), and a summary of pertinent information is contained in Appendix I.

TABLE II. REFERENCE SOURCES

ASTIA, DDC Index	1958 to Date
Author References	-
DDC Search	1950 to Date
Engineering Index	1950 to Date
FRDC Card Catalog	-
NACA, NASA, STAR Index	1952 to Date
Patent Search	to Nov. 1967
Technical Translations	1952 to Dec. 1967
UAC Card Catalog	

2.2 PRELIMINARY SCREENING

The eleven attachment methods listed in Table III were drawn from the literature survey. An initial rating based on engineering judgment was used to screen these techniques for applicability to small high temperature gas turbines. Each of the rating criteria was assigned a weight factor, as shown in Table III, to reflect its importance. Practicality of

sealing blade cooling air and weight effectiveness were given high weight factors because of their significant effects on turbine performance and component life. Manufacturing technology was assigned a high weight factor because advances in technology frequently exceed initial complexity, cost, and development time estimates.

The standard and inverted circumferential fir-tree designs were rated approximately equal in Table III because they are basically similar. The inverted design would provide better sealing of cooling air because of a continuous rim (see Figure 1). Because of additional clamping to restrict spreading of the female fir-tree, however, the inverted fir-tree design was given a lower rating in weight effectiveness and resistance to mechanical and thermal fatigue. The circumferential fir-tree with a split disk would require a high level of manufacturing technology to ensure proper assembly of the disk halves. The weight effectiveness rating for this design was low because of the massive joint required to reduce stress considerations.

The brazed, welded, cast, and forged designs were considered to be similar in their cooling air sealing capabilities, vibration damping, heat insulation, and resistance to mechanical and thermal fatigue. The brazed and welded designs would permit the use of optimized materials for the blade and disk. The integral cast joint would require the use of relatively low-strength cast materials for the disk, thus lowering its weight effectiveness rating.

The dovetail design was eliminated from further study after preliminary calculations indicated that its weight effectiveness was insufficient to meet the performance requirements of this program.

The various pinned attachment methods were fundamentally similar and scored well in all categories, except cooling air sealing and weight effectiveness. The pin-in-sectional shear design rated slightly higher because of its continuous rim, which simplifies the sealing problem. The vibration damping characteristics of this scheme were judged to be slightly better than the two other pin designs under consideration, but not sufficient to merit an excellent rating in Table III. Because of the similarity of the pinned attachments, only one was selected to permit a wider scope of analysis for the overall program.

The bicasting process consists of two separate pours. In the turbine rotor application, the blades are individually formed by investment casting with coring as required for cooling passages. The blades are then positioned in the final mold, and the disk is cast onto the blades in the second pour. Compared to an integral rotor casting, the bicast process simplifies the coring required for cooling passages and permits separate optimization of pouring parameters for the blades (thin sections) and the disk (thick sections) to improve the final microstructure. Mechanical locks can be designed into the joint between blades and disk, but maximum joint strength requires a metallurgical bond. This would normally require surface melting of the blade material (first casting) during the second pour, but it possibly

TABLE III. PRELIMINARY ATTACHMENT DESIGN RATING

Attachment Design Considered	Practicality of Scaling Air	Weight Effectiveness	Capability For Vibration Damping
WEIGHT FACTOR	3	3	2
1. Standard Fir-Tree (Solid Forged Disk - Cast Blades)	2	3	3
2. Inverted Circumferential Fir-Tree (Forged Disk - Cast Blades)	3	2	3
3. Circumferential Fir-Tree With Split Disk (Forged Disk - Cast Blades)	3	1	2
4. Brazed (Solid Forged Disk - Cast Blades)	4	4	1
5. Electron Beam Welded (Solid Forged Disk - Cast Blades)	4	4	1
6. Integral Casting (Cast Disk - Cast Blades)	4	3	1
7. Integral Forged (Forged Disk - Forged Blades)	4	4	1
8. Dovetail (Forged Disk - Cast Blades)	1	0	3
9. Pin-In-Longitudinal Shear (Forged Disk - Cast Blades)	1	1	3
10. Pin-In-Sectional Shear (Forged Disk - Cast Blades)	2	1	3
11. Pin-In-Compression (Forged Disk - Cast Blades)	1	1	3

Weight Factor	Influence
3	High
2	Medium
1	Low

Rating Number	Rating
4	Excellent
3	Good
2	Fair
1	Poor
0	Inadequate to Fulfill Program Requirements

ticality Sealing Air	Weight Effectiveness	Capability For Vibration Damping	Optimized Use Of Both Blade and Disk Material	Insulation of Heat Conduction From Blade To Disk	Resistance To Mechanical And Thermal Fatigue	Required Manufacturing Technology	Initial Cost and Replacement Cost	Overall Rating	Selected For Analysis In Task III
3	3	2	2	2	2	3	1	-	-
2	3	3	4	3	4	3	2	54	Yes
3	2	3	4	3	3	3	2	52	Yes
3	1	2	4	2	2	1	2	37	No
4	4	1	4	1	1	3	3	50	Yes
4	4	1	4	1	1	3	3	50	Yes
4	3	1	2	1	1	2	2	39	Yes
4	4	1	2	1	1	1	1	38	No
1	0	3	4	3	4	3	4	44	No
1	1	3	4	3	3	4	4	48	No
2	1	3	4	3	3	4	4	51	Yes
1	1	3	4	3	3	4	4	48	No

could be achieved by diffusion heat treatment in some applications. A bicast rotor should be comparable to an integral cast rotor with respect to air sealing, vibration damping, heat conduction, and fatigue. However, the bicast rotor would rate higher than the integral casting in optimization of blade and disk materials and, as a result, higher in weight effectiveness because of the improvement in disk properties. Insufficient joint strength data and manufacturing experience for the bicast process prevented consideration of this attachment method within the scope of the contract. Because of the potential advantages of this approach, a preliminary bicast joint strength evaluation was conducted under a separately funded program. Results of this program are reported in Appendix II.

2.3 PRELIMINARY SELECTION

- The standard fir-tree is a promising approach if the difficulty associated with sealing blade cooling air can be overcome; high fabrication costs are anticipated due to the close tolerances required. The split disk design in conjunction with a fir-tree root offers improved coolant sealing; however, the attendant stress concentrations require a massive attachment joint. The other mechanical attachment methods (pinned, dovetail, etc.) suffer from low weight effectiveness and difficulty in sealing blade cooling air.

- The fabricated attachments (welded and brazed) have good strength-to-weight ratios. Good sealing capability is offset by the high conductivity heat path to the disk. In addition, nondestructive inspection techniques must be developed to ensure sound joints.

- Integral blade/disk attachments lack the advantage of optimized use of blade and disk materials, thereby limiting their weight effectiveness. Good blade sealing capability is offset by high heat conduction to the disk.

The overall ratings of the preliminary screening (indicated in Table III) resulted in the selection of the six attachment methods shown in Figure 2 for detailed design analysis.

3.0 TASK II - AEROMECHANICAL DESIGN

OBJECTIVES

The objectives of this task were (1) to define turbine geometry and blade/disk attachment loads, (2) to select the three most promising attachment concepts from the six methods selected under Task I, and (3) to design uniaxial test specimens for experimental evaluation of the three selected attachments.

3.1 TURBINE DESIGN

A preliminary turbine design was conducted to define a small, high temperature, single-stage turbine within the guidelines previously presented in Table I. A turbine inlet temperature of 2500°F, a blade tip speed of 1900 ft/sec, and an air flowrate of 2 lb/sec were selected as the most difficult combinations of parameters for the attachment design since this condition combined the maximum attachment temperature and stress with the smallest size. To fix the turbine mainstream and cooling air inlet conditions, a compressor efficiency of 80%, combustor pressure loss of 5%, and cooling air temperature increase (between compressor discharge bleed to turbine airfoils) of 50°F were assumed to be representative for an advanced engine in this class. The cooling air supply temperature was thus 640°F for a sea level static compressor inlet condition.

The stringent goals of the turbine design required materials with superior high temperature strength characteristics. Therefore, advanced turbine alloys and coatings were selected for the design study:

Vane Airfoils	- NX188 (PWA 643) with AlCrMg coating (PWA 64)
Blade Airfoils	- Directionally solidified SM 200 (PWA 664) with PWA 64 coating
Disk	- Astroloy (PWA 1013)

The one exception to these materials was for the integral attachment design where cast Udimet 700 (PWA 656) properties were assumed for rotor blades and disk. With the advanced materials, the vanes were limited by erosion to a hot spot vane metal temperature of 1880°F, and the blades were limited by creep to an average metal temperature of 1635°F. Peak gas temperatures of 2820°F at vane inlet and 2276°F (relative) at blade inlet were obtained using a burner exit temperature profile representative of small combustors. Assuming that the airfoils were convection cooled, the gas stream, cooling air, and critical metal temperatures permitted calculation of cooling effectiveness parameters. Using the empirical effectiveness-cooling airflow relations of Figure 3, the required cooling air was 1.2% and 1.9% of engine airflow for vanes and blades, respectively. Consistent with previous engine experience, it was assumed that the disk and platforms could be cooled by normal cooling air leakage, or 0.7% of engine airflow.

A parametric study was conducted to select the turbine annulus area and radius that would provide good efficiency with a reasonable blade pull load on the disk. Results of 15 turbine mean line designs using three

values of annulus area and five values of root radius are shown in Figure 4. Rotor speed is included for each point. Any appreciable increase in efficiency above the 83% for the design point radius of 2.25 in. would require a prohibitively small root radius, further restricting the attachment size and making the design increasingly difficult. Similarly, the design point annulus area of 6.5 sq in. represented a good compromise between efficiency and blade pull.

A turbine airfoil axial chord of 0.5 in. was selected as the minimum size that permitted formation of internal cooling air passages with current casting technology and was the best compromise between the manufacturing limitations and efficiency.

Figure 5 shows the final turbine elevation. The airfoils were designed for free vortex flow resulting in the root and tip velocity triangles shown in Figure 6. Airfoil spacing was chosen to provide moderate aerodynamic loading with maximum tangential loading coefficients of 0.924 for the vane and 0.990 for the blade. Root and tip contours were designed with smooth static pressure distributions. Blade final contours are shown in Figures 7 and 8.

The preliminary turbine analysis resulted in a rotor with a root radius of 2.25 in., and 28 blades having a total blade pull of 57,600 lb at 81,600 rpm. Design features of the final study turbine are summarized in Table IV.

3.2 ATTACHMENT ANALYSIS AND DESIGN

3.2.1 Design Criteria

Design analyses were conducted on the six attachment techniques in two steps. First, a preliminary one-dimensional thermal and stress analysis was conducted for each concept to establish the attachment's relative size, geometry, and feasibility. The design criteria used in the initial evaluation are listed below:

Parameter	Design Limit
• Tensile Stress	100% of 1500 hr* stress rupture or 75% of 0.2% yield strength
• Bearing Stress (Based on mating surface area)	100% of 0.2% yield strength
• Bending Stress	45% of 1000 hr stress rupture or 45% of 0.2% yield strength
• Shear Stress	40% of 1000 hr stress rupture or 40% of 0.2% yield strength

Parameter	Design Limit
• Braze Tensile	None allowed
• Braze Shear Stress (Based on 50% wetted area)	90% of braze shear strength
• Weld Stresses (Based on 90% weld efficiency)	100% of weaker parent material strength

*The 1500-hr rather than 1000-hr life was used to provide a safety margin against a catastrophic failure occurring at the design goal.

Second, detailed design analyses were conducted to refine and optimize each attachment if the preliminary design indicated that the concepts were feasible. Two-dimensional thermal analysis was conducted to determine the attachment temperature and thermal gradient, and was used in the input of the stress analysis. These analyses included an elastic stress analysis as the attachment design was being refined, followed by a more detailed elastic/plastic stress analysis to include the effect of load redistribution with plastic deformation. Vibration analyses were conducted on the optimized designs to determine the susceptibility of the attachment to high cycle fatigue. Three possible types of vibration were studied: (1) blade alone, (2) disk alone, and (3) blade-disk coupled. The vibration for each attachment was assumed to be in its least stable direction, axial or tangential.

In addition to the criteria used in the preliminary analysis, the following disk stress limits were applied in the detailed design analyses:

Parameter	Disk Design Limit
• Burst Margin (B.M.)	30% over design speed (B.M. = 1.3)
• Average Stress	80% of ultimate strength/$(B.M.)^2$
• Yield	0.1% residual disk rim growth at 5% above design speed
• Vibratory Stress	50% of Goodman diagram alternating stress
• Radial Stress	110% of 0.2% yield within web 80% of average stress between bolt holes
• Effective Yield Stress	0.2% yield strength
• Effective Creep Stress	110% of 0.1%-1000 hr creep strength for castings 110% of 0.3%-1000 hr creep strength for forgings

Parameter	Disk Design Limit
• Low Cycle Fatigue	1000 cycles

Each attachment method was refined to minimize the ratio of attachment weight to airfoil weight within the limits set by the design criteria.

The blade airfoil and platform were common for all six attachment methods. Stress analysis indicated that the blade platform exceeded the bending stress limit of 45% of the 1000-hr stress rupture strength. The small diameter and high blade speed of this turbine design greatly contributed to the development of high bending stresses; the large gap between blades required a long platform to provide circumferential sealing. The overstressed condition was resolved by providing stiffeners (see Figure 9) to diminish the stress and deflection in the platform when subjected to centrifugal loads.

3.2.2 Standard Fir-Tree

The small size of the turbine dictated the use of a fir-tree root design with as little disk penetration as possible. Excessive reduction of the live rim radius would create an overstress condition in the disk and prohibit the use of a multitooth root configuration. A three-tooth design was required to provide sufficient shear area to support the centrifugal load.

The initial fir-tree configuration consisted of three pairs of beveled teeth with a wedge angle of 40 deg. This design had a 5% excessive pull stress at the first neck of the disk root and high shear stresses (0.5% over allowable) within the teeth. Preliminary analysis indicated that this design would have an attachment-to-airfoil weight ratio of 6.8, which exceeded the preliminary design target of 5, based on previous experience. This result was indicative of the relative inefficiency of mechanical attachments in small turbines. As turbine size is reduced, the manufacturing tolerances and tooth radii cannot be proportionally scaled, resulting in a relative reduction in the tooth loading surface and shear areas. Increasing the disk and fir-tree axial width to regain the required areas increases the attachment weight.

The fir-tree geometry was modified to reduce weight and to distribute more uniformly the stress at each neck in the attachment, resulting in a reduction of the wedge angle to 24 deg. This configuration was subjected to detailed thermal analysis, and the resulting temperature distribution (see Figures 10 and 11) was used in the stress analyses. The elastic/plastic stress analysis (load redistribution among the teeth because of thermal gradients and plastic deformation) indicated that the blade neck and disk neck stresses exceeded the 1500-hr stress rupture strength. The blade neck was overstressed because of the difference in spring rates of the blade root and the more massive adjacent disk material, which resulted in overloading the first tooth pair. The disk neck was overstressed because of the large mass of disk material extending beyond the live rim.

TABLE IV. SELECTED TURBINE DESIGN PARAMETERS	
Engine Airflow Rate	2 lb/sec
Compressor Pressure Ratio	10:1
Compressor Adiabatic Efficiency	80%
Burner Pressure Loss	5%
Design Life, At Maximum Gas Temperature	1000 hr
Number of Turbine Stages	1
Number of Turbine Blades	28
Turbine Inlet Temperature (average)	2500°F
Turbine Inlet Pressure	140 psi
Turbine Pressure Ratio (P_T/P_T)	2.4
Turbine Adiabatic Efficiency (T-T)	83%
Turbine Blade Tip Speed	1900 ft/sec
Turbine Speed	81,600 rpm
Turbine Blade Tip Radius	2.67 in.
Turbine Blade Root Radius	2.25 in.
Turbine Blade Axial Chord	0.5 in.
Total Airfoil Pull	57,600 lb
Turbine Stage Work	136 Btu/lb
Mean Velocity Ratio	0.671
Blade Cooling Air Flow Required	1.9%
Turbine Cooling Air Temperature	640°F
Allowable Blade Metal Temperature	1635°F
Design Blade Tip Clearance	0.009 in.

This problem was relieved by adding radial slots in the disk OD between blades (Figure 12).

The final stress distributions for the fir-tree attachment are presented in Table V. Bending was not found to be a problem in any portion of the standard fir-tree attachment. The bearing and shear stresses were highest within the first tooth of the blade root. The maximum tensile stress occurred in the second neck of the disk, indicating the effect of the loss in area due to the radial disk slots. The final fir-tree design had an attachment-to-airfoil weight ratio of 6.4. Assuming redistribution of load (Figure 13) because of thermal gradients, the first tooth would be subjected to a 55% load increase. Approximately 0.001-in. assembly clearance would be required for the first tooth to reduce the bearing and shear stresses to the allowable level for a 1000-hr life. However, further refinement of the attachment was not justified at this point.

Vibration analyses of the fir-tree design were made to determine if the joint was susceptible to high-cycle fatigue. The joint was assumed to vibrate in the axial direction only since aerodynamic loads and root geometry provided tangential stability. Three possible types of vibration were studied: (1) blade alone, (2) disk alone, and (3) blade-disk coupled. The disk associated with the fir-tree design was so stiff that it did not exhibit any resonant frequencies within the speed range of the engine. Blade-alone and blade-disk calculations for the first mode diverged at high speed because of flexibility in the attachment but were essentially equal at the design operating speed (Figure 14). There were no lower order resonances within the operating speed. Modes such as 18E and 36E, which might be excited by the 18 stator vanes, would be passed through at approximately 80% and 40% of design speed, respectively, and were not considered a problem at the operating point.

3.2.3 Inverted Fir-Tree

Preliminary stress analysis on the inverted circumferential fir-tree (previously shown in Figure 1) indicated that the design was inadequate because of the loss in shear area resulting from the elimination of teeth required to assemble the blades on the disk. The total pull on the attachment was calculated to be 11,027 lb, which was distributed over the three teeth. The shear stress developed in the teeth was 65,700 psi, nearly twice the allowable level. Additional tooth area would not eliminate the problem because of the increase in the total applied load. Part of each blade was acting as dead weight on the remaining root section, making the design excessively large and overweight.

The attachment technique was modified to a split disk concept that permitted the forward and aft sections of the disk to be assembled over the blade circumferential fir-tree, thus eliminating the requirement for a toothless area on the disk. However, this modification did not alleviate the problem because the standard beveled fir-tree teeth induced a high separating force on the disk halves and the design was still overweight

TABLE V. FIR-TREE ATTACHMENT STRESS DISTRIBUTION

CONDITION	RADIAL LOCATION (1)	TOOTH STRESS									NECK TENSILE STRESS		
		BENDING			BEARING			SHEAR					
		ACTUAL	ALLOWABLE (2)	RATIO	ACTUAL	ALLOWABLE (3)	RATIO	ACTUAL	ALLOWABLE (4)	RATIO	ACTUAL	ALLOWABLE (5)	RATIO
1. Uniform Load Distribution	R_1	40,100	56,600	0.71	118,900	126,000	0.94	42,600	50,400	0.85	53,900	61,000	0.89
	R_2	19,300	39,600	0.49	118,900	100,000	1.19	36,500	35,200	1.04	68,500	95,400	0.72
	R_3	16,800	56,600	0.31	103,600	126,000	0.82	32,700	50,400	0.65	52,600	97,500	0.54
	R_4	16,800	45,000	0.37	103,600	100,000	1.03	31,800	40,000	0.79	99,000	95,400	1.04
	R_5	13,900	56,600	0.23	80,000	126,000	0.63	25,100	50,400	0.50	59,000	97,500	0.61
	R_6	24,000	45,000	0.53	80,000	100,000	0.80	25,900	40,000	0.65	100,500	95,400	1.05
2. Condition 1 Plus Thermal Gradient	R_1	54,900	56,600	.97	172,000	126,000	1.37	59,100	50,400	1.18	53,900	61,000	0.89
	R_2	27,500	39,600	.69	172,000	100,000	1.72	50,600	35,200	1.45	93,400	95,400	0.98
	R_3	10,900	56,600	0.19	68,600	126,000	0.54	20,600	50,400	0.41	28,500	97,500	0.29
	R_4	10,900	45,000	0.24	68,600	100,000	0.69	20,200	40,000	0.51	105,000	95,400	1.10
	R_5	9,700	56,600	0.17	61,000	126,000	0.48	18,300	50,400	0.36	39,900	97,500	0.41
	R_6	15,200	45,000	0.34	61,600	100,000	0.62	18,900	40,000	0.47	101,000	95,400	1.06
3. Condition 2 Plus Creep at 1000 hr	R_1	59,700	56,600	1.05	187,200	126,000	1.49	64,400	50,400	1.28	53,900	61,000	0.89
	R_2	29,900	39,600	0.76	187,200	100,000	1.87	55,100	35,200	1.56	100,000	95,400	1.05
	R_3	10,600	56,600	0.19	63,200	126,000	0.50	19,900	50,400	0.39	21,700	97,500	0.22
	R_4	10,600	45,000	0.24	63,200	100,000	0.63	19,600	40,000	0.49	109,000	95,400	1.14
	R_5	7,700	56,600	0.14	45,600	126,000	0.36	14,400	50,400	0.29	26,800	97,500	0.27
	R_6	12,000	45,000	0.27	45,600	100,000	0.46	14,900	40,000	0.37	101,000	95,400	1.06

(1) As illustrated in Figure 16 (Tooth stress at R_3 refers to middle disk tooth; tooth stress at R_4 refers to middle blade tooth, etc. Neck stress at R_3 refers to middle blade neck; neck stress at R_4 refers to middle disk neck, etc.)
(2) 45% of 0.2% yield strength or 45% of 1000 hr stress rupture
(3) 100% of 0.2% yield strength
(4) 40% of 0.2% yield strength or 40% of 1000 hr stress rupture
(5) 75% of 0.2% yield strength or 100% of 1500 hr stress rupture

Note: All stresses are given in psi.

because of the large bolts required to secure the disk halves together. The total pull on the attachment was 22,526 lb, yielding an attachment-to-airfoil weight ratio of 10. A modification of the fir-tree teeth (Figure 15) caused a reduction in the force exerted from the teeth that tended to spread the disk apart. However, this modification did not significantly reduce the weight of the design; bending moments generated near the rim of the disk, as a result of the mass required to secure the blade and stress concentrations around the bolt holes, necessitated a massive disk. No additional analyses were devoted to either the inverted circumferential fir-tree or the split disk designs because of their inherent weight problems.

3.2.4 Welded

The preliminary analysis of the welded attachment indicated that this concept had the potential of being the lightest design with an attachment to airfoil weight ratio of 2.7. The analysis assumed a 100% metallurgical bond capable of developing 90% of the weaker parent material strength.

Detailed thermal analysis defined the welded attachment temperature distribution, as shown in Figures 10(b) and 16. Finite element stress analyses verified that with the assumed weld strengths, the efficiency of the attachment was very good and the disk thickness could be reduced to 0.3 in. with this attachment. The resulting stress distribution for the welded attachment is shown in Figure 17.

The stress distribution indicated that the disk contained a maximum effective stress of 84.6 ksi, which was well below the allowable limit of 126 ksi. The allowable stress in the attachment extension exceeded the maximum effective stress by 10%. The disk burst margin was calculated to be 47% at the average disk temperature of 750°F.

The vibration analysis of this design indicated that the thin disk used with this attachment was more flexible and did exhibit some combined bending effect, as indicated by the frequency shift around 110,000 rpm (see Figure 18), but this is well above the design operating speed. The blade-alone resonant frequency was the same for all attachments and was illustrated in Figure 14. This design was analyzed, assuming the blade platforms acted as shrouds providing damping. If no damping were provided, the design would have 4E excitation at the engine operating speed. Because of limitations in the computer program used in the analysis, the entire blade root extension was input as a single material rather than simulating the change in materials at the weldment. The effect of this variation was considered to be small.

3.2.5 Brazed

The preliminary design of the brazed attachment resulted in a configuration that contained four pairs of fingers to attain sufficient braze area and minimize the attachment ID-to-OD dimension. The total pull of this design

was 8790 lb at the attachment ID. Based on 50% coverage with AMS 2675 braze material, the braze shear stress was 3.5% under the allowable stress of 10,000 psi.

The detailed thermal analysis of the brazed attachment resulted in the temperature distribution indicated in Figures 10(c) and 19. The stress finger segments of the attachment than in the disk to accurately determine the stress levels in the critical areas (see Figure 20). The shear stress at the bond between the brazed fingers of the blade could not be calculated in the elastic/plastic computer program. Normal computation procedures indicated that sufficient braze strength could be obtained with only 50% coverage of the mating surfaces. Any coverage in excess of that would provide a factor of safety for the design. However, each pair of mating fingers must be sufficiently brazed to transmit its share of the radial tensile load to the disk. The design proved to be very efficient with a 3.3 attachment/airfoil weight ratio and required only a 0.4-in.-wide disk for support.

This configuration yielded a maximum effective disk stress 27% below the allowable limit of 126 ksi, whereas the maximum stress in the extension was 10% below the allowable. The calculated burst margin was 34% for the brazed disk, exceeding the minimum requirement of 30%. In addition, the circumferential finger arrangement provided passages that could be used to supply coolant to the blades. For this reason, it was not expected that this design would require additional hardware to maintain the attachment and disk temperature levels.

Because of the geometry of the design, the brazed attachment was considered to be susceptible to vibration in the axial direction only. The vibration analysis of the brazed design indicated no critical resonant frequencies at the operating speed of the engine (see Figure 21). The disk's stiffness was sufficient to prevent any critical frequencies within the entire running range of the engine. The blade-alone mode and blade-disk coupled mode were essentially colinear for the engine running range, indicating no participation by the disk.

3.2.6 Pinned

Preliminary analysis of the pinned root attachment indicated that the technique was unacceptable for the selected turbine guidelines. The design analysis indicated that it was impossible to obtain sufficient pin area to support the applied centrifugal loads and to satisfy the design criteria. The configuration that most nearly satisfied the stress criteria was prohibitively large and bulky (Figure 22). The pin diameter was 0.270 in. with an average shear stress of 33,200 psi and a maximum allowable shear stress of 33,600 psi. The tearout stress in the disk was calculated to be 37,500 psi, which exceeded the allowable limit of 24,000 psi. This attachment scheme had reached the point of diminishing returns. Any further increase in pin size increased attachment weight, resulting in higher stresses. The pinned root attachment was therefore dropped from further consideration.

3.2.7 Integral Cast

Preliminary design analysis for the integral cast attachment indicated that with the high load-carrying efficiency in the attachment zone, this technique had the potential of being relatively lightweight. The total pull at the attachment ID was 8225 lb, which resulted in an attachment to airfoil weight ratio of 3.2.

For this attachment technique, however, the attachment-to-airfoil weight ratio was a deceptive criterion for judging the overall efficiency of the attachment for two primary reasons. First, the homogeneous nature of the attachment zone provided a continuous path with high thermal conductivity that heated the disk live rim to a higher temperature than the other attachment methods and adversely affected material strength. Second, the integral casting technique required by definition that the blade and disk be of one cast material; this required a further degradation in mechanical properties in the disk relative to a forged disk of a dissimilar material.

The two-dimensional thermal analysis of the integral cast attachment resulted in the temperature distribution indicated in Figures 10(d) and 23. Stress analyses indicated a relatively uncomplicated stress pattern similar to that previously presented for the welded attachment. Because of the inferior mechanical properties, this design required a disk width of 0.5 in. at the ID of the attachment and 1.8 in. at the disk bore. This was nearly twice as great as that of the welded attachment disk, yielding a bulky rotor system.

3.3 ATTACHMENT INTERMEDIATE SELECTION

The objective was to select the three most promising attachment methods for experimental evaluation by tensile, stress rupture, and vibrational tests.

3.3.1 Rating Factors

The six attachment methods initially selected for analytical evaluation were rated considering the results of the design analysis in judging each attachment, using the criteria presented below. In addition, each criterion was assigned a weight factor that indicated its relative influence in satisfying the objectives of the program guidelines.

- Joint efficiency (weight effectiveness). This factor was judged to be one of the most important criteria. In meeting the extremely high tip speed specified, the capacity of the attachment to provide a light assembly was considered to be a definite benefit.

- Cooling requirements. All designs could be sealed with can-type coverplates. Lower stressed disks were rated higher because they provided some margin for coverplate bolting without increasing disk weight. Consideration was also given to manufacturing restrictions on airfoil cooling geometry, which would result in higher coolant flow requirements.

- Potential durability. This criterion was judged on the basis of the effect of joint fabrication on material properties that influence high and low cycle fatigue characteristics.

- Effect on rotor system (disk and attachment centrifugal weight, bearing location, coupling method, and shaft design). Axially long disks increased the overhang distance, and heavier rotor system weight decreased the rotor critical speed. This was judged to be directly related to the attachment-plus-Δdisk to airfoil centrifugal weight ratio (the Δdisk was defined as the increase in disk weight relative to the minimum disk weight required for the lightest attachment).

- Consideration of nondestructive testing methods of inspection. The accessibility of loaded surfaces for inspection and the ease of interpreting data (i.e., X-ray) were the prime factors considered.

3.3.2 Rating Explanation

The results of the rating are given in Table VI. The joint efficiency was judged as a function of the attachment-to-airfoil centrifugal weight ratio (see Table VII). Cooling requirement was rated considering the ability of the disk to accommodate the additional weight of the seal coverplate bolting and the quantity of cooling airflow required. The disks for the brazed and welded attachments were not stressed to the design limit, and additional weight could be added to attach the coverplates without increasing disk weight. In addition, since the mating fingers in the disk of the brazed design would be machined circumferentially, the disk remained continuous, potentially providing good sealing that may not require additional coverplates. The integral casting method limited the airfoil cooling passage geometry to simple configurations that required significantly higher coolant flow rates than more efficient designs. The potential durability rating reflected that the fir-tree attachment method did not adversely affect material properties and had favorable vibration and low cycle fatigue characteristics. Conversely, the welded attachment was expected to experience the greatest degradation of properties in the heat affected zone and was rated low. The low rating of the integral cast attachment resulted from the inherent compromise in airfoil and disk properties for this method. Effect on rotor system was judged to be a direct function of the combined attachment-disk parameter given in Table VII. The consideration of nondestructive testing rating reflected that the fir-tree could be completely inspected, whereas X-ray (or ultrasonic) inspection was required for the welded, integral, and brazed designs and did not

TABLE VI. INTERMEDIATE ATTACHMENT DESIGN RATING

	ATTACHMENT DESIGN ANALYZED	Joint Efficiency (Weight Effectiveness)	Cooling Requirements	Potential Durability	Effect on Rotor System	Consideration of Non-Destructive Testing	Overall Rating	Selected for Experimental Evaluation
	Factor Weight	3	3	1	2	2		
1	Welded Attachment (Solid Forged Disk-Cast Blades)	4	4	2	4	2	38	Yes
2	Brazed Attachment (Solid Forged Disk-Cast Blades)	3	4	3	3	1	32	Yes
3	Standard Fir-Tree (Solid Forged Disk-Cast Blades)	1	3	4	1	4	26	Yes
4	Integral Casting (Cast Disk-Cast Blades)	4	1	2	2	2	25	No
5	Inverted Circumferential Fir-Tree (Forged Disk-Cast Blades)	0	-	-	-	-	*	No
6	Pinned Attachment, Sectional Shear (Forged Disk-Cast Blades)	0	-	-	-	-	*	No

Factor Weight	Influence
3	High
2	Medium
1	Low

Rating No.	Rating
4	Excellent
3	Good
2	Fair
1	Poor
0	Inadequate to fulfill program requirements

*Disqualified by Inadequate Rating

TABLE VII. WEIGHT RATIOS

Attachment Method	Attachment/Airfoil Dead Weight	Attachment/Airfoil Centrifugal Weight	(Attachment-Plus-Δ*Disk)/Airfoil Dead Weight	(Attachment-Plus-Δ*Disk)/Airfoil Centrifugal Weight
Standard Fir-Tree	7.87	6.4	13.8	8.77
Welded	3.28	2.67	3.28	2.67
Brazed	4.54	3.3	5.94	4.1
Integral Cast	3.93	3.2	15.2	7.66
Inverted Fir-Tree	-	**	-	-
Pinned	-	**	-	-

*ΔDisk represents additional disk weight required relative to the lightest disk (i.e., ΔDisk = Required disk weight - welded disk weight).
**Inadequate to fulfill program requirement.

yield conclusive results. The multiple fingers of the brazed joint were judged to be the most difficult to inspect.

The overall rating indicated that the welded, brazed, and standard fir-tree were the most promising attachment methods for this program application. These configurations were selected for experimental evaluation.

3.4 TEST SPECIMEN DESIGN

The objective of this effort was to design uniaxial test specimens to permit experimental screening tests of the three attachment methods. These specimens were designed for tensile tests to verify attachment burst margin, vibration tests to determine fatigue resistance, and stress rupture tests to demonstrate high temperature strength characteristics.

Where possible, the specimens were designed to prototype geometry. However, the specimen depth was diminished in some cases to facilitate testing. The tensile and stress rupture specimens for each individual attachment scheme were identical and were designed to have stress levels proportional to that experienced by the attachment under actual engine conditions. The testing of the prototype geometry permitted more accurate evaluation of the significance of notches and fillet radii on the individual attachment design stress concentration factors.

The high cycle fatigue specimens were designed to generate representative stress levels within the attachment region when subjected to a constant radial load and an oscillating transverse load.

3.4.1 Photoelastic Analysis

Photoelastic analysis was used in the test specimen design in addition to the numerical techniques previously discussed in the attachment analysis (Section 2.2). Photoelastic analysis provided a rapid method of modeling the attachment to evaluate both stress levels and stress concentrations with each attachment. Each model was designed to study the stress distribution in the region between the disk live rim and the blade platform. Photoelastic specimens for each of the three selected attachment designs were fabricated from SPM-1 photoelastic grade plastic and examined with a transmission type polariscope. The models were fabricated 10 x scale to permit accurate evaluation of the stress patterns. The photoelastic models were replaced or modified as required during the analysis to optimize each design.

3.4.2 Standard Fir-Tree

The fir-tree attachment models were designed to illustrate the stress pattern in the plane of the disk. Photoelastic analysis of the fir-tree with a root wedge angle of 40 degrees verified that the design was overstressed at the first neck which could be alleviated by increasing the neck area (see Figure 24); however, this did not resolve an overstressed condition resulting from an insufficient tooth shear area.

The second model with the 24-deg root wedge angle contained a modified tooth design that created an additional shear area and an enlarged cross section in the first neck to support the applied load. Photoelastic analysis indicated that the resulting stress distributions were acceptable and that no further modifications were warranted. The design of the fir-tree uniaxial test specimen is indicated in Figure 25.

3.4.3 Welded

The welded attachment models were designed to evaluate the stress pattern in the plane of the disk. Radial and tangential loads were independently applied to the plastic welded attachment model with the resultant stress distribution determined by superposition. As a result of these tests, the weld joint between the blade and disk was relocated 0.145 inch radially outward from the disk OD to an area of lower stress (see Figure 26). Attachment fillet radii were also optimized as a result of this testing.

The welded attachment tensile and stress rupture specimens were designed with three test sections representing the OD, ID, and weld joint, as shown in Figure 27. In this manner the radial load gradient through the region of the joint caused by the variation in radius was simulated by proper consideration of the test section cross-sectional areas. The vibratory specimens were designed to the prototype configuration. The welded design was originally conceived to vibrate in the plane of the disk. Further analysis indicated that installing the blades onto the disk in packets (a series of four blades fabricated as a single unit) offered coolant sealing and fatigue advantages. Fabrication in this manner would have virtually eliminated in-plane vibration, thereby leaving only the axial direction for concern. For this reason, the fatigue test of the welded design was conducted with the transverse load acting in the axial direction.

3.4.4 Brazed

The brazed attachment design was rather unique in that it presented essentially a uniform attachment joint around the disk circumference that minimized the stress variation in the plane of the disk. Thus, the photoelastic model of the brazed attachment was designed to evaluate a section perpendicular to the plane of the disk. The model was designed so that either radial or axial loads could be applied. The radial load simulated the centrifugal load of the airfoil and platform on the attachment, while the axial load represented the differential thermal expansion between the live rim radius and the blade platform. Analysis with the initial brazed attachment model indicated excessive bending stresses at the base of the attachment fingers with the combined thermal expansion and radial strain. The brazed attachment photoelastic test specimen was redesigned to reduce bending stresses across the joint by relocating the fillet radii and to reduce stress concentrations at the extremities of the fingers. Comparison of the photoelastic patterns and model stress magnitudes on the original design resulting from the simulated centrifugal load (Figure 28a) with those resulting from the combined circumferential

thermal growth and centrifugal load (Figure 28b) indicated that the combined load produced bending stresses (σ_f) in the braze fingers which reduce the stress concentrations (σ_e). Comparison of the original design (Figure 28b) with the redesigned model (Figure 29) indicated the reduction of both the bending stress (σ_f) and stress concentration (σ_e) by the attachment redesign.

The test specimens were designed with prototype geometry in the attachment (see Figure 30). The tensile and stress rupture specimens were identical, and the vibratory specimens were designed for bending in the axial direction. The box structure fabricated by the assembled brazed attachment presented superb resistance to fatigue, and no problem areas were anticipated with this design. The specimen was designed to test bending fatigue in the axial direction because the calculations indicated that mode required less energy for excitation.

4.0 TASK III - FABRICATION OF TEST SPECIMENS

OBJECTIVE

The objective of this task was to fabricate the uniaxial specimens designed under Task II for testing under Task IV, using representative blade and disk materials. Table VIII summarizes the number of uniaxial specimens manufactured.

TABLE VIII. UNIAXIAL TEST SPECIMEN QUANTITIES

Specimen Type	Brazed	EB-Welded	Fir-Tree
Tensile	2	2	2
Fatigue	5	5	5
Stress Rupture	5	5	6

4.1 MATERIALS

The Task II turbine design recommended directionally solidified SM 200 (PWA 664) and Astroloy (PWA 1013C) for test specimen materials because of their high strengths at elevated temperatures. However, because of high cost and excessive lead time of these advanced materials, IN 100 (PWA 658) was substituted as the blade alloy, and WASPALOY$_{TM}$ (PWA 1004) was substituted as the disk alloy. The substitute alloys are representative of materials currently being used in high-temperature engines such as the J58 and ST9. As discussed later under Task IV test results, the attachment strength data with the substitute alloys were used as a basis for calculating the longer life potential of attachments made from the advanced materials (directionally solidified SM 200 and Astroloy). All castings were poured from the same master heat to assure uniformity and repeatable test results, and metallurgical inspections were performed to ensure that raw material conformed to PWA specifications.

4.2 PHOTOELASTIC SPECIMENS

Photoelastic models (10X) of each of the three attachment designs selected in Task II were machined from SPM-1 photoelastic grade plastic. A high-speed router was used to trim the plastic to its final dimensions to avoid machining stresses. Where photoelastic analysis indicated that modification was required, plastic was removed by routing or was added by using transparent glue. The glue was allowed to cure for 24 hours before testing of the model was resumed.

4.3 FIR-TREE METALLIC SPECIMENS

The fabrication of the fir-tree metallic test specimens was initiated by machining a template that conformed to the final design contour of the male portion of the root. The template was then used as a guide in the contour grinding of the male sections and in the fabrication of the electrical discharge machining (EDM) electrodes used to form the female sections. The EDM electrodes were undersized to allow for the arc gap required, and to leave stock for later removal of the recast layer associated with this process. The dielectric oil circulated between electrode and work piece for cooling and flushing is partially decomposed because of the high local temperature. The resulting hydrocarbons recombine with elements formed by the removal of parent material to produce a thin recast layer of carbides over the work piece surface. This recast layer was removed by etching with inhibited hydrochloric acid. The male section of the fir-tree was ground to the maximum print specifications. Once a close fit for each set of specimens was obtained, the parts were serialized as matched pairs for the remainder of the machining operation. The female sections were hand-lapped with an elongated tool (contour ground to the geometry of the male fir-tree) until the respective male sections slid easily in the female slots. The extra-length tool was required to prevent rounding over the edges of the female slots during lapping (see Figure 31). The lapping compound was a silicon-base abrasive (No. 150 grit). Final machining of each fir-tree specimen was accomplished on a gear lapping machine. During this operation, a tensile load of 5 lb was maintained along the longitudinal (radial) axis of the specimens. Each specimen pair was lapped until no light could be passed between any mating surfaces when vertically suspended from either end. Upon achieving this condition, the specimen was removed from the machine and approved for testing.

The extreme care taken in the production of the specimens was necessary to ensure that each set of mating teeth was in uniform contact. Both the literature survey and the design analysis indicated that for small turbine attachments, close tolerances were required to avoid undesirable redistribution of the load. Overloading of one set of teeth would cause premature failure of the attachment when subjected to a radial tensile load.

Five clamps were fabricated for testing the fir-tree specimens. The clamp (Figures 32 and 33) was positioned around the joint to provide the circumferential support normally present in a complete disk assembly and to prevent the female part from spreading under radial load.

4.4 WELDED METALLIC SPECIMENS

4.4.1 Machining and Joining

The welded attachment specimens were prepared for fabrication by rough machining rectangular barstock into 4.0 by 1.5 by 0.5-in. pieces. Blade and disk materials were butt-welded by an electron beam directed

through the smallest dimension with sufficient power to provide full penetration (Figure 34). Preliminary welding with the beam located over the center of the joint resulted in cracking on the surface of the joint in the heat-affected zone. Translation of the beam 0.010 in. off-center into the Waspaloy eliminated the surface cracks. The beam power settings used are given in Table IX.

TABLE IX. ELECTRON BEAM-WELD MACHINE SETTINGS

Weld Joints	Material	Thickness (in.)	Beam Location	Power (kv)	Power (ma)	Travel Speed (in./min)	Work Piece Height (in.)
Specimens	Waspaloy IN100	0.5	0.01 in. off center line within Waspaloy	150	45	42	10.0
Samples	Waspaloy IN100	0.4	Over center line	130	10	10	5.5

4.4.2 Heat Treatment

The welded bars were then heat treated as follows to restrengthen the Waspaloy:

Solution - 1850 ±25°F for 1 hour (air cool)

Stabilization - 1550 ±15°F for 4 hours

Precipitation - 1400 ±15°F for 16 hours

4.4.3 Inspection

Post heat-treat X-ray inspection revealed small cracks normal to the weld joint in the heat-affected zone of the IN100. The cracks were apparently caused by loss of ductility in the IN100 as a result of a change in microstructure. The X-ray inspection also indicated a transverse crack in one of the fatigue specimens, signifying a lack of fusion between the two materials. Since only one specimen was obtained from each weld joint, final machining of the specimens was performed in a manner that minimized the number of cracks existing within the specimen test section. However, post-machining X-ray inspection revealed that only one fatigue specimen (shown previously in Figure 27) and two of the tensile/stress rupture specimens were crack-free.

4.4.4 Sample Weld Joints

Additional samples of IN100 and Waspaloy were electron-beam welded to investigate whether the cracks were caused by the welding operation or the subsequent heat treatment. The sample thickness was only 0.400 in. compared to the 0.500 in. for the test specimens, requiring less beam power

and reducing the possibility of crack initiation. Reduced power settings and beam travel speeds were used to attempt to develop a sound weld joint. Radiographic inspection of six samples welded with 95-100% beam penetration showed crack-free joints before and after heat treatment, indicating that the lower beam power may have had a beneficial effect. The power settings for these samples are presented in Table IX. These samples were then machined into stress rupture specimens having cylindrical gage sections and threaded shanks to evaluate joint strength.

4.5 BRAZED METALLIC SPECIMENS

4.5.1 Machining

Blade and disk pieces for the brazed specimens were machined from bar-stock. The attachment fingers were formed by contour grinding.

The initial machining operation on the attachment fingers of the brazed metallic test specimens produced an interference fit of the mating surfaces. Additional material was removed to obtain a 0.003- to 0.005-in. loose fit between each set of specimen mating fingers to allow clearance for nickel plating and braze material flow between mating surfaces.

4.5.2 Brazing

At the brazing temperature, both Waspaloy and IN100 form titanium and aluminum oxide coatings, which cause the braze to "ball-up" and resist flow. For this reason, a 0.0004- to 0.0006-in. nickel plate was electrolytically deposited on the fingers of each specimen (see Figures 35 and 36) followed by an oven bake at 900°F for 30 minutes to ensure a good bond between the nickel plate and parent material. The specimens were placed in a brazing fixture designed to hold them securely during the braze cycle, as shown in Figure 37. Shims were placed in strategic locations to ensure that a 0.002- to 0.004-in. clearance was maintained between each set of specimen mating surfaces. The fixture was Rokide-coated in the area beneath the attachment fingers to prevent the braze from bonding to the fixture. The AMS 4778 braze filler metal was applied with a hypodermic syringe, and all specimens were brazed in a hydrogen atmosphere at 2000°F ±25°F for 20 minutes. Postbraze visual inspection indicated a lack of braze coverage over the area adjacent to the braze fixture base. This was attributed to contamination by the Rokide coating and insufficient heating. The specimens were subjected to a second braze cycle after being inverted in the fixture. After rebrazing, braze buildup was noted on the fatigue test specimens in the space between adjacent fingers. The surplus braze material was machined away before the postbraze heat treatment to avoid diffusing excess boron and silicon (elements present in the braze to lower its melting temperature) into the parent material.

4.5.3 Inspection

X-ray inspection following rebrazing indicated a minimum of 80% braze coverage. X-rays of two sets of fingers of each specimen were simultaneously taken by inserting the film into the center slot and one side slot between the fingers. The process was then repeated for the remaining two sets by turning the specimens to their opposite sides and inserting two more films. In this manner, each set of mated attachment fingers could be inspected individually.

4.5.4 Heat Treatment

Following inspection, the specimens were reloaded into the fixtures and subjected to the following heat treatment to diffuse the braze:

Temperature, °F	Time, hr
1800 ± 25	8
1900 ± 25	8
1950 ± 25	56

The purpose of the lower temperature soaking was to raise the remelt temperature of the braze by diffusing out part of the boron and silicon. A rapid rise to the 1950°F level could have induced remelting of the braze, resulting in possible misalignment of the specimens. Immediately following the 56-hr phase at 1950°F and prior to cooling, the specimens were exposed to an additional heat treatment to restrengthen the Waspaloy material as follows:

1. Fast air cool from 1950° to 1000°F at a rate of 40°F/min
2. Raise to 1550° ± 15°F for 4 hr
3. Cool to 1000°F
4. Raise to 1400° ± 15°F for 16 hr
5. Cool to ambient

The entire diffusion and restrengthening heat treatment cycle was conducted in argon. The specimens were then cleaned, X-rayed, and approved for testing.

5.0 TASK IV - UNIAXIAL SPECIMEN TESTING

OBJECTIVES

The objectives of this task were to evaluate the three selected attachment methods under simulated engine loads, and to select the most suitable method for further testing under Task V. These were accomplished by subjecting the uniaxial models of the fir-tree, welded, and brazed attachment designs to tensile, vibratory fatigue, and stress rupture tests.

5.1 TEST EQUIPMENT

5.1.1 Tensile

The tensile tests were conducted on the Tinius Olsen Universal Tensile Testing Machine shown in Figure 38. This machine has a load capacity of 60,000 lb and is equipped with recording equipment and strain rate controls. The specimens were tested to failure at ambient temperature with a crosshead speed of 0.05 in./min.

5.1.2 Vibration

Vibratory tests were performed at ambient temperature on the resonating beam rig illustrated in Figure 39. The disk portion of the test specimens was clamped securely in the test frame, while the resonant beam was bolted to the blade portion. Known vibratory stresses were applied to the specimen by resonating the beam at controlled amplitudes. Radial load was applied by means of the calibrated coil spring.

5.1.3 Stress Rupture

Stress rupture tests were conducted at 1400°F using the Arcweld Manufacturing Company stress rupture machines shown in Figure 40. These machines have a load capacity of 12,000 lb and temperature capability up to 2200°F. The specimen temperature was stabilized prior to initiation of loading.

5.2 FIR-TREE ATTACHMENT TESTS

5.2.1 Test Procedure and Results

Two metallic fir-tree specimens were tested for ultimate strength at room temperature to verify the calculated burst margin for this configuration. Failure of both specimens occurred at the first neck of the fir-tree in the IN 100 material (see Figure 41). Test data are presented in Table X.

TABLE X. FIR-TREE TENSILE TEST DATA*

Specimen Number	Load to Failure (lb)	Ultimate Strength at** Location of Failure (psi)	Location of Failure
1	13,500	138,500	First neck of blade fir-tree (IN 100)
2	12,750	130,900	First neck of blade fir-tree (IN 100)

*All tests conducted at room temperature

**Does not include stress concentration factor. Minimum room temperature ultimate strength:

IN 100 - 115,000 psi
WASPALOY™ - 180,000 psi

Six specimens were stress-rupture tested at a uniform temperature environment of 1400°F. The applied load was varied from a minimum of 5000 lb to a maximum of 8000 lb to define the stress-time failure line. During tests of the first four specimens, the restraining clamp deformed, allowing the female section to spread slightly (see Figure 42). The contact area of the first two pairs of teeth was thus reduced, resulting in an overstressed joint. Increased bending stresses were transmitted to the first neck of the joints because the load on each tooth pair was applied at a different location. The joint failures were therefore premature, resulting in stress rupture data representative of a minimum strength that can be achieved with the attachment. Progressive clamp refinements during the first four tests eliminated the problem for the remaining two stress rupture specimens. Two new clamps were fabricated from WASPALOY™ using high-strength nuts and bolts for the final two tests, and no clamp deformation could be detected. These specimens also failed in the first neck of the fir-tree in the IN 100 material (see Figure 43). Stress rupture test data are presented in Table XI.

The five specimens scheduled for fatigue testing were strain gaged for load calibration and to ensure proper alignment in the loading fixture. The objective of these tests was to define load combinations (static radial load with alternating bending load) that would yield 10^7 cycles for each attachment configuration. Each specimen was subjected to a static radial load and a vibratory bending load, and cycled until the specimen failed or 10^7 cycles (runout) was reached. If a runout was obtained, the vibratory bending load was increased while maintaining the original static radial load, and the test was continued. This procedure was followed until failure occurred. The applied static load

was varied from 1500 to 2500 lb. The minimum applied vibratory bending stress was 5000 psi and the maximum was 30,000 psi. Each specimen failed in the first neck of the fir-tree in the IN 100 material (see Figure 44). The fatigue data are given in Table XII.

TABLE XI. FIR-TREE STRESS RUPTURE DATA*

Specimen Number	Load (lb)	Stress Level at** Failure Location (psi)	Life (hr)	Location of Failure
3	5,000	51,000	212.1	Small neck of fir-tree (IN 100)
4	7,500	76,500	49.9	Large neck of fir-tree (IN 100)
5	6,000	61,300	340.5	Small neck of fir-tree (IN 100)
6	8,000	82,000	2.9	Small and large neck of fir-tree (IN 100)
7	8,000	82,000	32.4	Large neck of fir-tree (IN 100)
8	7,000	71,500	134.6	Large neck of fir-tree (IN 100)

*All tests conducted at 1400°F.
**Does not include stress concentration factor.

5.2.2 Failure Analysis

Failure analysis of the fir-tree test specimens yielded the following conclusions and observations:

- The test specimen fracture surfaces were typical of the type of test each represented, e.g., tensile, fatigue, or stress rupture.
- All representative failures occurred at the large neck of the fir-tree, just below the blade platform. Failure of the small neck of the attachment during some stress rupture tests was attributed to the spreading of the restraining clamp.

TABLE XII. FIR-TREE VIBRATORY TEST DATA*

Specimen Number	Static Load (lb)	Static** Stress (psi)	Vibratory Stress (psi)	Vibratory Bending Moment (in.-lb)	Cycles to Failure (x 10^6)	Location of Failure
9	2,000	20,000	15,000	148	3.1	Large neck (IN 100)
10	2,000	20,000	30,000	296	0.87	Large neck (IN 100)
11	2,000	20,000	5,000	49.3	>10.0	--
			10,000	98.6	>10.0	--
			15,000	148	3.8	Large neck (IN 100)
12	2,500	25,000	5,000	49.3	>10.0	--
			10,000	98.6	>10.0	--
			15,000	148	2.04	Large neck (IN 100)
13	1,500	15,000	15,000	148	9.6	Large neck (IN 100)

*All tests conducted at room temperature.
**Does not include stress concentration factor.

5.3 WELDED ATTACHMENT TESTS

5.3.1 Test Procedure and Results

The welded attachment metallic test specimens were reexamined by X-ray inspection following final machining to determine the number of crack-free specimens, because some of the cracks were removed by the machining operation. One high-cycle fatigue specimen and two tensile/stress rupture specimens were found to contain no cracks. The latter specimens were distributed so that one crack-free specimen was used for each type of test. Room temperature tests were conducted on the two tensile and five fatigue specimens; stress rupture tests were conducted at 1400°F on five specimens. The fractured specimens are shown in Figures 45, 46, and 47. The data from the tensile, stress rupture, and vibratory stress tests are presented in Tables XIII, XIV, and XV, respectively.

Both tensile specimens failed within the IN 100 heat-affected weld zone. The tensile data indicated that maximum strength was attained from the crack-free specimen and that the weld developed 90% of the IN 100 strength (weaker material at room temperature). Only the crack-free stress rupture specimen failed outside of the weld zone. In this case, the failure occurred in the Waspaloy (weaker material at 1400°F). All the vibratory specimens failed in the IN 100 weld zone.

TABLE XIII. WELDED ATTACHMENT TENSILE TEST DATA*

Specimen Number	Pretest Condition	Load to Failure (lb)	Ultimate** Strength (psi)	Location of Failure
6	Good	9,220	112,500	Weld
9	Weld crack indications by X-ray	7,310	89,200	Weld

*All specimens were Electron Beam welded; heat treated 1850°F 1 hour in Argon, A/C, 1550°F 4 hours, and 1400°F 16 hours (PWA-11-34); and machined to test specimen configuration. Metallic specimens of the welded attachment were designed with modified cross-sectional areas to produce relative stress levels under tensile type loads as would be produced by centrifugal loads. All tests conducted at room temperature.

**Does not include stress concentration factor.
Minimum room temperature ultimate strength:
IN 100 - 115,000 psi
Waspaloy - 180,000 psi

TABLE XIV. WELDED ATTACHMENT STRESS RUPTURE DATA*

Specimen Number	Pretest Condition	Load (lb)	Stress Level** at Failure Location (psi)	Life (hr)	Location of Failure
1	Weld crack indications	7,450	91,000	0.1	Weld
2	Weld crack indications	4,640	56,500	31.0	Weld
3	Good	4,100	54,600	224.6	Waspaloy
4	Weld crack indications	3,730	45,500	76.5	Weld
5	Weld crack indications	4,940	60,200	1.8	Weld

*All specimens were Electron Beam welded; heat treated 1850°F 1 hour in Argon, A/C, 1550°F 4 hours, and 1400°F 16 hours (PWA-11-34); and machined to test specimen configuration. Metallic specimens of welded attachment were designed with modified cross-sectional areas to produce relative stress levels under tensile type loads as would be produced by centrifugal loads. All tests conducted at 1400°F.

**Does not include stress concentration factor.

TABLE XV. WELDED ATTACHMENT HIGH CYCLE FATIGUE DATA*

Specimen Number	Pretest Condition	Static Load (lb)	Static** Stress (psi)	Vibratory Stress (psi)	Vibratory Bending Moment (in.-lb)	Cycles to Failure (x 10^6)	Location of Failure
7	Weld crack indications	4,200	62,200	9,800	30	2.3	Weld
8	Weld crack indications	4,200	62,200	4,900	15	1.75	Weld
10	Weld crack indications	Failed during static loading				0.0	Weld
11	Good	4,200	62,200	4,900	15	>10.0	Weld
			62,200	9,800	30	3.67	Weld
12	Weld crack indications	Failed during static loading				0.0	Weld

*All specimens were Electron Beam welded; Waspaloy heat treated 1850°F 1 hour in Argon, A/C, 1550°F 4 hours, and 1400°F 16 hours (PWA-11-34); and machined to test specimen configuration. All tests conducted at room temperature.

**Does not include stress concentration factor.

5.3.2 Failure Analysis

Failure analysis of the welded test specimens yielded the following conclusions and observations:

- Radiographic inspection showed transverse weld cracks in 75% of the specimens and indications of incomplete fusion on two specimens at the IN 100 fusion line.
- Microstructural examination showed weld metal cracking and intergranular cracks in the IN 100 heat affected zone (see Figures 48 and 49). This cracking was considered to have occurred during welding.
- All weld failures occurred preferentially in the IN 100 fusion line. Examination of the fracture surfaces showed extensive flat areas, which are characteristic of brittle failures (see Figures 50 and 51). The stress rupture weld failures did not exhibit secondary cracking at the fracture face; this also indicates nonductile failure.
- The WASPALOY$_{TM}$ fracture of the crack free stress rupture specimen (previously shown in Figure 46) was irregular and displayed secondary cracking, denoting a stress rupture type of failure.

5.3.3 Sample Weld Specimens

The six additional welded cylindrical specimens were subjected to 1400°F stress rupture testing to evaluate the effects of the welds performed at a reduced power setting, as previously indicated in Table IX. Tests were conducted with stress levels from 30,000 to 70,000 psi to establish a failure line for the sample weld joints. The test data are presented in Table XVI. The three specimens subjected to a stress of 60,000 psi or greater failed during application of the load. Two specimens stressed to 40,000 psi or less ran for more than 1000 hours without failure, and these tests were discontinued. Only one specimen failed within a reasonable time span, making the formulation of a failure line extremely difficult. All failures occurred on the IN 100-side of the weld joint within the heat affected zone. This was typical of the failures exhibited by the attachment test specimens, and it was concluded that the decreased weld power settings did not improve the weld joint strength.

TABLE XVI. ELECTRON BEAM-WELD SAMPLES - STRESS RUPTURE DATA

Sample Number	Load (lb)	Stress (psi)	Life (hr)	Failure Location
1	1,500	60,000	--*	IN 100 heat affected zone
2	1,750	70,000	--*	IN 100 heat affected zone
3	750	30,000	1310.1	**
4	1,000	40,000	1177.8	**
5	1,500	60,000	--*	IN 100 heat affected zone
6	1,250	50,000	77	IN 100 heat affected zone

*Ruptured on loading.
**Discontinued test prior to failure.

5.4 BRAZED ATTACHMENT TESTS

5.4.1 Test Procedure and Results

The test procedures for the brazed specimens were identical to those followed for the welded and fir-tree tests. In the tensile and vibratory tests (room temperature), failure occurred primarily at the OD of the attachment joint in the IN 100 as illustrated in Figures 52 and 53, respectively. The stress rupture tests produced failure at the ID of the attachment in the Waspaloy (see Figure 54). This shift in failure location is caused by the marked decrease in the strength of Waspaloy at 1400°F. In the prototype design, the disk material would experience maximum temperature levels in the 1100°F range in highly stressed areas at the attachment root.

The test data from the tensile, stress rupture, and vibratory tests are presented in Tables XVII, XVIII, and XIX, respectively.

TABLE XVII. BRAZED TENSILE TEST DATA*

Specimen Number	Braze Area (%)	Load (lb)	Ultimate Strength ** (psi)	Location of Failure
6	90	9,300	112,000	Blade radius (IN 100)
7	90	8,300	100,000	Blade radius (IN 100)

*All tests conducted at room temperature.
**Does not include stress concentration factor.
Minimum room temperature ultimate strength:
IN 100 - 115,000 psi
Waspaloy - 180,000 psi

TABLE XVIII. BRAZED STRESS RUPTURE DATA*

Specimen Number	% Braze Area	Load (lb)	Stress** Level (psi)	Life (hr)	Location of Failure
1	90	7,000	84,400	0.9	Disk radius (Wasp)
2	90	6,000	72,400	17.1	Disk radius (Wasp)
3	90	5,500	66,400	8.2	Disk radius (Wasp)
4	90	5,000	60,200	40.0	Disk radius (Wasp)
5	90	4,500	54,300	155.3	Disk radius (Wasp)

*All tests conducted at 1400°F.
**Does not include stress concentration factor.

TABLE XIX. BRAZED VIBRATORY TEST DATA*

Specimen Number	Static Load (lb)	Static** Stress (psi)	Vibratory Stress (psi)	Vibratory Bending Moment (in.-lb)	Cycles to Failure ($\times 10^6$)	Location of Failure
8	2,000	29,800	20,400	148	0.5	Blade radius (IN 100)
9	1,000	14,900	10,200	74	>10.0	--
			13,600	98.7	>10.0	--
			17,000	123.4	6.2	Blade radius (IN 100)
10	2,000	29,800	6,900	50	>10.0	--
			10,200	74	>10.0	--
			13,600	98.7	>10.0	--
			17,000	123.4	>10.0	--
			20,400	148	1.9	Blade radius (IN 100)
11	2,500	37,300	6,900	50	>10.0	--
			10,200	74	>10.0	--
			13,600	98.7	9.2	Blade radius (IN 100)
12	1,500	22,400	13,600	98.7	10.0	Blade radius (IN 100)

NOTE: Braze coverage of vibratory specimens equal to 85%.

*All tests conducted at room temperature.
**Does not include stress concentration factor.

5.4.2 Failure Analysis

The following conclusions and observations were made as a result of the failure analysis of the brazed specimens:

- All the failures were characteristic of the type of test each represented.
- Room temperature tests yielded failure in the IN 100 blade material (weaker material at room temperature), while the stress rupture failures occurred in the Waspaloy (weaker material at 1400°F).
- All failures occurred in parent metal indicating adequate braze coverage.

5.5 DATA ANALYSIS

The burst margin was determined by comparing the attachment ultimate strength with the calculated centrifugal pull of each design at the location of failure. Table XX presents the results of the calculations. The fir-tree and brazed designs met the 30% design burst margin requirement at the location of failure after including the reduction in ultimate strength at operating temperature. These designs failed at the attachment OD in the IN 100 material, which experienced 1500°F temperatures. The welded design had a burst margin of 21% with failure in the IN 100 heat affected zone of the weld joint that experienced 1200°F temperatures.

Further testing under centrifugal loading to evaluate the attachment ultimate strength would be necessary (i.e., failure at other critical attachment locations) before complete definition of the minimum burst margin for each design could be provided.

The tensile and vibratory test data were combined in the form of a modified Goodman diagram for each of the three attachment schemes to determine their ability to sustain combined static and vibratory loads (Figures 55, 56, and 57). The static load measured at failure from the tensile tests is plotted on the vertical axis. The endurance limit (zero static load) of IN 100 converted into bending moment has been used as the end point on the horizontal axis, since all vibratory failures occurred in the blade portion of the attachments. The curves faired through the fatigue data between these two end points represent the limiting combinations of static load and vibratory bending moment which yield 10^7 cycles for each design. Selecting the theoretical design static load at the location of failure as the critical radial load for each attachment method, the maximum vibratory bending moment yielding design life may be obtained along the horizontal axis. Note that the weld design (in its present state of development) has inferior capability to sustain a vibratory load relative to either the fir-tree or brazed designs.

The stress rupture data for the three attachment methods are plotted in terms of stress at the failure location versus time to failure in Figure 58. Data for specimens that did not achieve a minimum of 5 hours life are not included in the figure. The fir-tree life characteristic (Figure 58a) was drawn favoring the higher points because of clamp yielding, which permitted uneven tooth load distribution in three of the specimens. All but one of the welded specimens had small cracks transverse to the weld in the IN 100 heat-affected zone. Therefore, the higher stress rupture points in Figure 58(b) were favored to represent life for crack-free welds.

TABLE XX. ATTACHMENT BURST MARGIN

Attachment Scheme	Failure Location	Operating Temperature at Failure Location (°F)	Room Temperature Ultimate Load (lb)	Ultimate Load at Operating Temperature (lb)	Centrifugal Pull at Failure Location (lb)	Burst Margin (%)
Fir-Tree	Attachment OD	1,500	13,125	12,050	5,050	54
Welded	Weld Joint	1,200	9,220	9,220*	6,350	21
Brazed	Attachment OD	1,500	8,800	8,000	4,250	37

*Data from good weld specimen; IN 100 experiences no degradation in ultimate strength at 1200°F.

Under actual engine conditions, each attachment would have experienced a large temperature gradient. The blade platform, exposed to gas stream temperature, would operate at approximately 1500°F. However, the disk would be bathed in cooling air and experience 1000° to 1200°F temperature levels near the attachment ID (previously shown in Figure 10). The 1400°F test data were extrapolated to evaluate the attachment concepts at operating temperature conditions. The effects of temperature on stress rupture life are shown by the materials data plotted in Figure 59. For 1000-hr life, the allowable stress level of Waspaloy (PWA 1016) increases 124% when its operating temperature is decreased to 1200°F. The 1000-hr allowable stress of IN 100 (PWA 658) decreases 20.7% when its temperature is raised from 1400° to 1500°F. These percentage changes in allowable stress were applied to the experimental data previously shown in Figure 58. The results are shown for each attachment in Figures 60, 61, and 62 as load versus life; design loads were used to define the requirement for ID (disk) and OD (blade) regions of each attachment.

The life characteristics data summarized in Table XXI indicate that with Waspaloy and IN 100 materials, none of the attachment designs could achieve the 1000-hr design life. The fir-tree life was limited by the IN 100 strength at the 1500°F operating temperature. The welded attachment life was limited by either the weld itself or the IN 100 in the heat-affected zone. The brazed attachment life was limited by the Waspaloy strength at the 1200°F operating temperature. As the IN 100 did not fail in the braze specimens, only the minimum stress that the material could withstand was determined. The minimum IN 100 stress rupture characteristic at the operating temperature, however, fell short of the 1000-hr goal.

Use of the more advanced materials selected in the turbine design would permit increased life from each design. The improvements in allowable stress that could be achieved with directionally solidified SM 200 (PWA 664) as the blade material and Astroloy (PWA 1013) as the disk material are included in the material properties curves of Figure 59. These improvements were applied to the Waspaloy/IN 100 load limit curves of Figures 60, 61, and 62 to define the limits for the improved materials. Assuming that crack-free welds comparable to the Waspaloy/IN 100 combination could be achieved, and that the actual load-carrying capability of the OD section would be somewhat above the minimum strength curve defined for this region, the welded attachment would meet the 1000-hr life requirements with the superior materials. Use of the superior materials in the fir-tree and brazed attachments would clearly meet the required design life. In the brazed attachment, an additional benefit would be expected because the Astroloy disk material is metallurgically more compatible than Waspaloy with the braze cycle and the post-braze heat treatment. Waspaloy undergoes extensive grain growth above 1800°F, which has a detrimental effect on the strength properties of the material.

TABLE XXI. STRESS RUPTURE LIFE OF TASK IV ATTACHMENT SCHEMES

Attachment Scheme	Location	Predicted Operating Temperature (°F)	Material* Life (hr)
Fir-Tree	ID (Waspaloy)	1000	> 1000
	OD (IN 100)	1500	500
Welded	ID (Waspaloy)	1200	> 1000
	Weld Zone	1200	0
	OD (IN 100)	1500	15
Brazed	ID (Waspaloy)	1200	6
	OD (IN 100)	1500	> 70**

*Design life = 1000 hours.
**Actual life indeterminate, only minimum strength defined.

6.0 TASK V - FINAL ATTACHMENT SELECTION AND TEST

OBJECTIVES

The objectives of this task were to (1) select the most promising blade/disk attachment design based on the results of the Task II design analyses and the Task IV screening tests, (2) optimize the design of the selected attachment method through additional uniaxial specimen testing, and (3) proof test the final design by cyclic stress rupture testing of biaxial specimens.

6.1 FINAL ATTACHMENT SELECTION

The data obtained in the Task IV uniaxial tests indicated that the welded design was inferior to either the fir-tree or the brazed design in ability to sustain a vibratory load. In addition, the metallurgical inspection of the weld fractures indicated brittle failures characterized by transgranular cracking. For these reasons, the welded design in its present state of developmer was eliminated from further consideration.

The fir-tree and brazed designs exhibited similar stress rupture lives and vibratory strength. However, when the predicted thermal gradient was analytically applied to the fir-tree design, thermal expansion caused one or more pairs of teeth to unload. Unless very carefully designed and fabricated with critical tolerances controlled, the life of the fir-tree attachment would be limited. In the case of the brazed design, the predicted thermal gradient alleviated in the stress distribution within the fingers, thus extending the life of this attachment. The centrifugal pull of the fir-tree design at the attachment ID was more than twice as great as the brazed design when supporting the same airfoil. This resulted in a much heavier disk and rotor system. Therefore the brazed attachment offered the most potential for small high temperature turbines and was selected for final attachment testing.

It was possible to use Astroloy (PWA 1013) for the disk specimens in this task because surplus raw material became available from another program. This alloy was originally selected for the turbine design and offered the additional benefits in this task of providing (1) a more severe test for the IN 100 blade material and braze joint due to greater disk strength, and (2) superior braze joints due to better resistance of the Astroloy to grain growth during heat treatment compared to WASPALOY$_{TM}$. Thus, the ultimate potential of the brazed attachment could be better defined. The use of directionally solidified SM 200 as the blade material was considered beyond the scope of this program because of material cost and procurement time.

6.2 UNIAXIAL SPECIMEN OPTIMIZATION

Radial and tangential loads were simultaneously applied to photoelastic models of the attachment to simulate both the thermal and radial stress distribution predicted for engine conditions. Three tests were conducted

for different locations of the radii between pairs of fingers. The model stress for each of the three modifications is plotted in Figure 63. Stress patterns of the final modification are shown in Figure 64. Relocation of the disk radii produced a definite minimum stress concentration within the fingers. Relocation of the radius in the blade portion did not indicate a definite minimum, but the largest L_1 dimension produced the highest stress. The larger L_1 dimension would result in a lighter weight attachment, but fatigue life would suffer because of reduced stiffness. The blade radius location was therefore selected as a reasonable compromise between these conflicting factors. The effect of the radii relocations in the final design was to reduce the stress concentrations around the fingers and allow the attachment to achieve a higher average stress level. In addition, the fillet radii external to the fingers of the joint were increased from 0.031 to 0.0625 in. nominal to decrease the stress concentrations in these areas. Figure 65 summarizes the major design changes between the Task IV and Task V specimens.

Redesign of the uniaxial brazed specimens also included refining the dimensional tolerances as applied to the fingers of the attachment. This eliminated the possibility of obtaining an interference fit between mating surfaces as a result of tolerance "stack up."

6.3 UNIAXIAL SPECIMEN FABRICATION

The final uniaxial metallic test specimen design incorporated the design changes resulting from the photoelastic test results. The procedures used to fabricate these specimens and the problems encountered and resolved are described in the following paragraphs:

6.3.1 Machining

- Rough milling to form the fingers
- Electrical discharge machining (EDM) of the 6-deg taper on each finger
- Light grinding operation to remove the thin EDM recast surface material
- Mating in pairs and serializing

6.3.2 Prebrazing Preparation

The surface preparation included depositing 0.0004- to 0.0006-in. nickel plate by the electroless nickel process over mating surfaces of the fingers to prevent the formation of titanium and aluminum oxides which inhibit the flow of the braze material. The specimen cleanliness was controlled by degreasing the test specimen and fixture to remove all contaminants and performing all subsequent handling with white gloves in a "clean room."

6.3.3 Fixturing

A brazing alignment fixture was used to maintain the specimens in the required configuration with a clearance between mating surfaces for the braze. The fixture and specimen setup was accomplished as follows:

- Wall Colmony "green stop-off" applied to specimen shanks to prevent undesired brazing
- Specimens positioned by alternating Astroloy and IN 100 as shown in Figure 66 to reduce effects of thermal expansion
- Shims inserted at selected shank locations to facilitate alignment of mating finger surfaces; prebrazing clearances between all mating surfaces adjusted for 0.001 to 0.0025 in.
- AMS 4779 (Coast Metal 50) braze paste uniformly distributed with a hypodermic syringe and needle to three sides of each mating surface
- Fixture instrumented with two thermocouples spot welded to surface for control of braze thermal cycle

6.3.4 Brazing

The specimens were initially brazed as follows:

- Fixture assembly placed in furnace retort and nitrogen purged
- Retort atmosphere converted to hydrogen with continuous purge
- Retort inserted in heated furnace and held at 2050°F for 18 minutes

Postbraze visual inspection indicated approximately 75% braze, but coverage was very nonuniform. The specimens were subsequently cleaned and rebrazed at 2050°F in a vacuum furnace equipped with a viewport that permitted the braze cycle to be observed. Radiographic inspection indicated 90 to 95% braze coverage which well exceeded the minimum required coverage of 50%.

6.3.5 Postbrazing Heat Treatment

The specimens underwent postbraze heat treatment consisting of:

- 12 hours at 1975°F in hydrogen
- 8 hours at 1600°F in hydrogen
- Cool to 500°F in hydrogen
- 4 hours at 1800°F in hydrogen
- Fast air cool
- 24 hours at 1200°F in air
- 8 hours at 1400°F in air

The first step diffused out the boron and silicon from the braze material, raising the remelt temperature. It also diffused the nickel plate into the parent material to eliminate the interface and create a stronger joint. The diffusion cycle was reduced from 72 to 12 hours to expedite the fabrication and reduce the cost of the Task V uniaxial specimens. The remaining steps in the heat treatment cycle were performed to restrengthen the Astroloy. The specimens are shown in Figure 67.

6.3.6 Problems Encountered and Resolved

The nickel plate required for prebrazing surface preparation was initially deposited by electroplating, which resulted in a variation of plating thickness from 0.0001 to 0.002 in. Visual inspection indicated that the plating produced an interference fit between mating surfaces in some locations. This nickel plate was chemically removed in a nitric acid bath, and nickel was redeposited in a uniform layer by the electroless nickel process.

The 75% braze coverage after the initial brazing attempt produced a joint that had the majority of the void region adjacent to the fixture side of the specimen. It was anticipated that unbalanced loading could result from this void concentration and produce an undesirable stress distribution.

The following cleaning operation was performed prior to rebrazing:

- Hydrogen "scrub" for 1 hour at 1800°F
- Descaling in potassium permanganate
- Oxide removal in inhibited hydrochloric acid
- Completion of oxide removal with hydrofluoric acid rinse
- Nickel plate (electroless nickel process)

Rebrazing in the vacuum furnace permitted the brazing temperature to be controlled from visual observation to obtain a satisfactory braze.

6.4 UNIAXIAL TESTS

6.4.1 Test Procedure and Results

The test procedure was identical to that followed in Task IV. The specimens were subjected to loads ranging from 4500 to 6500 lb, with the specimen temperature maintained at 1400°F. The test data are presented in Table XXII.

The failed specimens are shown in Figures 68 through 72. Close analysis of the specimens indicated that the fracture originated as a result of braze failure on certain fingers. This was concluded by post-test examination of the failed specimens and the observation that rotation of the specimen resulted as the load was shifted following the initial failure of one joint. When two fingers of a specimen experienced failure and caused the joint to be eccentrically loaded, the joint attempted to rotate until

the load was again applied symmetrically. The remaining fingers failed by stress rupture in the parent material. The load carrying capabilities of the IN 100 and Astroloy fingers were essentially equal at the 1400°F test temperature. For the two most highly loaded specimens, the load was sufficient to exceed the stress rupture strength of either material if the load were imposed on three fingers; a similar failure would occur for the other specimens if the total load were imposed on two fingers. Therefore, failure of either or both materials in some specimens could be expected soon after two or three fingers were subjected to the total load.

TABLE XXII. TASK V STRESS RUPTURE TEST DATA*

Specimen	Load (lb)	Stress** (psi)	Life (hr)	Location of Failure
1	6,000	61,000	70.3	2 braze and 2 Astroloy failures
2	6,500	66,000	31.4	2 Astroloy and 2 IN 100 failures
3	5,000	50,900	76.3	2 braze, 1 Astroloy, and 1 IN 100 failure
4	5,500	56,000	58.0	1 braze and 3 Astroloy failures
5	4,500	45,800	93.2	2 braze, 1 Astroloy, and 1 IN 100 failure

*All tests conducted at 1400°F.

Specimen materials were IN 100 (PWA 658) for the blade segment and Astroloy (PWA 1013) for the disk segment.

**Radial stress generated at the base of the Astroloy fingers not including a stress concentration factor.

6.4.2 Data Analysis

A stress rupture plot comparing Task IV and Task V data is presented in Figure 73; the plot shows that four of the five Task V specimens exhibited improved strength relative to IN 100-Waspaloy specimens tested in Task IV. The Task V specimens yielded greater data scatter that was attributed to the difficulty in obtaining a satisfactory braze. Nonuniformity in the braze strength among the four mating surfaces caused premature failure of some specimens. This dissimilarity in braze strength was attributed to the combined effect of excessive thickness of braze material, variation of braze coverage, and incomplete diffusion of boron and silicon from the

braze material. The thicker braze between the mating surfaces resulted from a deflection of the fingers that occurred during the brazing cycle. The specimens apparently heated faster than the brazing fixture, and the differential thermal growth forced the tips of the fingers to engage the adjacent radius and deflect away from the mating surface.

Four of the Task V specimens achieved a 70 to 1000% increased life relative to the failure line established by the Task IV specimens. The remaining specimen (No. 5) experienced a 42% decrease in life. Visual inspection of the failure of the latter specimen indicated a severe lack of braze coverage (less than 30%) on one finger that was not detected by the pretest X-ray inspection. Therefore, this point received little weight in establishing the Task V failure line. The point from this specimen was plotted as the small square in Figure 73. The Task V failure line was drawn parallel to the previously established slope of the Task IV failure line because the stress rupture curves of Astroloy and Waspaloy are similar, and the Task IV data contained less scatter.

In Figure 74, the Task V failure line for the IN 100-Astroloy was correlated with the design stress rupture life of directionally solidified SM 200 (PWA 664), as the blade material, and Astroloy (PWA 1013), as the disk material, by the method previously applied in Task IV. That is, the percentage increase or decrease in stress rupture strength that would be experienced with the respective material at its operating temperature was applied to the Task V failure line. At 1000 hours of life, the directionally solidified SM 200 blades should have a load-carrying capability in excess of the OD design load plotted on the right of Figure 74; similarly, the Astroloy disk load-carrying capability should exceed the ID design load. Thus, the correlation indicated that the design life of 1000 hours could be fulfilled by using these materials in the brazed attachment.

6.4.3 Metallurgical Evaluation

A metallurgical examination of the test specimens was conducted to determine the mode of failure. The specimens were sectioned and subjected to optical and electron microscopic examination. Examination of photomicrographs of the failures indicated the presence of a grain boundary film within the Astroloy material. The film was primarily composed of grain boundary carbides that formed a network which promoted embrittlement, thus reducing ductility and shortening the stress rupture life of the Astroloy. However, the test results indicated that the stress rupture properties of the Astroloy were not substantially reduced by the carbide film. The load-carrying capabilities of both the IN 100 and Astroloy fingers were essentially equal at the 1400°F test temperature when both materials met specification properties. The specimens contained failures by intergranular cracking in both parent materials. All of the parent material failures would most likely have occurred in the Astroloy if it had been significantly affected by the carbide film in the grain boundaries.

The sequence of the failures could not be determined from the metallurgical examination of the specimens; however, the structural analysis of the

failed specimens appears to be valid. The analysis indicated that the fracture originated as a result of braze failure on certain fingers and the load was shifted to the remaining fingers, which were subsequently overstressed to failure.

6.4.4 Braze and Heat Treatment Study

The nonuniformity in braze strength of these specimens relative to the Task IV specimens raised questions concerning the reduced diffusion cycle time (72 to 12 hours) and the effectiveness of the nickel plate in preventing titanium and aluminum oxide formation on the brazing surface. Therefore, additional braze samples were fabricated for metallurgical examination to evaluate the plating method and diffusion cycle. Braze samples with two types of nickel plating (electroless and electrolytic 0.001 in. thick) were prepared to determine if Astroloy was affected by the plating method. Following vacuum brazing, specimens with both types of nickel plating were subjected to the two different diffusion heat treatments. The planned 72-hour cycle was terminated after 60 hours following a burn-out of the furnace heater. Optical and electron microscopic examination showed that the 60-hour diffusion cycle caused the original braze material to diffuse into the base metals, eliminating the braze interface, as intended, and producing a nickel-rich layer with no secondary phases between the IN 100 and Astroloy. The 12-hour diffusion cycle produced a similar structure of agglomerate nickel in the braze fillet, but it did not completely remove the original braze interface between the two parent materials. The program scope did not permit additional trials with intermediate diffusion cycle times. Therefore, the 72-hour cycle was considered to be necessary. No discernible metallurgical difference was detected between specimens that contained electrolytic and electroless nickel plate. As a result, the final Task V fabrication procedure included 0.001 in. electroless nickel plating and a 72-hour diffusion heat treatment following the vacuum braze cycle.

6.5 BIAXIAL PROOF EVALUATION

Biaxial specimens were used for the final proof test of the brazed attachment to evaluate the combined effect of cyclic radial and tangential loads on the life of the attachment. The stress condition of the attachment in the engine environment was established by the centrifugal load and the thermal gradient through the attachment. The centrifugal load produces a radial tensile stress and a resulting tangential (hoop) stress that is normally tensile. However, in the brazed attachment, the disk live rim extended into the circumferential fingers, and the thermal gradient produced a compressive stress, which was higher at the OD than the ID. Superposition of the hoop stress on the thermal stress created a tangential stress variation with radius as shown in Figure 75. The tangential stress, which was a maximum at the OD rim (87,400 psi compressive), rapidly decreased to zero, reversed sign, and remained tensile as the bore of the disk was approached. After engine shutdown, the residual tangential stresses at the rim were tensile (25,700 psi at the OD), while the stress in the interior of the disk was compressive. The radial load would vary from blade centrifugal pull during engine operation to zero at shutdown.

The uniaxial brazed specimen data represent the durability that could be achieved with a discontinuous rim with slots between blades. These slots would require a separate seal, possibly a ductile material brazed over the opening. A continuous disk rim would provide a simpler integral air seal with lower attachment weight and improved access for inspection. Although the tangential stresses calculated at the continuous live rim were quite severe and created high effective stresses (radial plus tangential), there were insufficient data available for an accurate analysis. The space between blade fingers forms an unknown notch effect that would be a function of the braze coverage and fillet geometry. Also, the maximum and mean stress (during an engine cycle) were compressive, and Astroloy stress rupture data were available only for tensile stresses. Therefore, to test the feasibility of the continuous rim configuration, this feature was retained in the biaxial specimen design.

6.6 BIAXIAL SPECIMEN DESIGN

Since the biaxial specimens were to be tested under isothermal conditions, it was necessary to define an isothermal stress distribution equivalent to the engine condition. As shown in Figure 75, the equivalent compressive rated cruise stress (94,000 psi) at the attachment OD was higher than the engine stress (87,400 psi) because the test temperature (1400°F) was below that in the engine (1500°F). Similarly, the equivalent OD residual stress (20,700 psi) was lower than the engine stress (25,700 psi) because the test temperature exceeded that in the engine (70°F). The ID equivalent cruise and residual stresses were also obtained by considering the disparity between the test and engine temperatures. In the absence of centrifugal or thermal loading effects, the static, isothermal test specimen could only be subjected to a linear stress distribution (lines A and B in Figure 75). Therefore, the biaxial specimen was designed to duplicate the critical maximum stress at the attachment OD (highest stress-temperature combination, point C), and to produce a tangential stress gradient that simulated the stress reversal to tension outside of the attachment ID (point D). Simulating the tangential stress reversal was desirable to evaluate crack propagation in the event a crack were to occur in the disk finger. It was anticipated that for a crack initiating at the attachment OD (maximum stress region), radial propagation inward would terminate in the region of low tangential stress near the neutral axis.

The basic design of the biaxial test specimen is shown in Figure 76. Three simulated attachments were joined to a disk specimen model to produce a final test article. The two side attachments ("slaves") served to create the correct stress distribution in the tangential direction for the center test attachment. The initial joint configuration of the three attachments conformed identically to that evaluated in the Task V uniaxial tests. However, an error in the biaxial design required modification of the specimen to achieve the correct stress distribution within the test zone (see Figure 77) and to avoid overstressed areas outside the test zone. The platform weights had been neglected during the calculation of the applied radial load to each blade specimen. The revised radial load to the entire specimen (three blades) was 12,735 lb as opposed to the 6,180-lb original

design load. Since specimen and load linkage fabrication had already been initiated, the most expedient modifications to the specimen design to achieve the correct attachment stress levels were (1) removal of the center two fingers from each of the simulated blade specimens, (2) brazing of additional supports to the simulated disk specimen, and (3) relocation of the disk specimen load application point.

Removal of the center two fingers from the blade specimen retained the validity of biaxial testing since the two remaining fingers still experienced biaxial stresses as generated in an engine environment. To provide lateral support and eliminate buckling of these sections, a plug was designed to fit into the slot formed by the two unbrazed middle fingers of the disk specimen. The plug (Figure 78) was slotted to maintain the section modulus at the critical test zone areas (see Figure 79). Small wedges were used to provide lateral stiffening to the outer fingers of the disk and to remove the notch effect at the outer edges of the slave blades. The point of load application to the disk specimen was altered to apply the correct radial and tangential loads to the disk specimen with the single ram loading arrangement illustrated in Figure 80.

All three specimen modifications were required to reduce the applied load by 50% and eliminate the overstressed condition in the load linkage.

The small size of the prototype attachment specimen required a relatively small and complex loading fixture to uniformly distribute the radial load to the three blade attachments. This was accomplished by the linkage arrangement shown in Figure 81. Waspaloy was selected as the fixture material to provide reasonable fixture life with a compact linkage arrangement. The fixture design stress level was set at 25,000 psi to produce a stress rupture life at 1400°F, well in excess of the cumulative life of the five test specimens.

The brazing fixture was designed to support each biaxial specimen assembly individually during the brazing operation (see Figure 82). The design incorporated alignment pins, precisely located for proper installation of the mating parts. The fixture material (Inconel 600) and thickness were selected to minimize the steady-state and transient differential thermal expansion between the specimen and the fixture.

6.7 BIAXIAL SPECIMEN FABRICATION

6.7.1 Machining

Electrical discharge machining (EDM) was initially used to form the fingers on both the simulated blades (IN 100) and simulated disk (Astroloy) pieces. The mating surfaces were ground to the final dimensions; however, a rough EDM surface was left on the nonmating side of each finger (see Figures 83 and 84). Metallurgical examination indicated (see Figure 85) that the depth of the affected material was between 1.0 and 1.5 mils on the Astroloy, thus reducing the available load supporting area. Visual

inspection indicated similar penetration of the IN 100 pieces. The specimen load was adjusted to reflect the reduction in load carrying area resulting from the EDM surface conditions. Removal of the center fingers of the blade specimens as a result of redesign was accomplished by precision grinding at a slow rate to avoid distortion in the part.

The specimens were serialized, arranged together in matched sets (see Figure 86), and dimensionally inspected. The clearance between mating surfaces was measured to be between 0.5 and 2.0 mils. The recommended clearance to allow plating both surfaces and flowing of the braze material was 3 mils; however, insufficient material remained to machine the fingers to the proper clearance. Therefore, the specimens were mechanically adjusted by cold-working the fingers of both the IN 100 and Astroloy pieces to develop the recommended clearance. Limited cold-working of both materials could be performed without detrimental effects on the material properties.

6.7.2 Brazing

Dimensional inspection following cold-working of the specimen fingers indicated that a 0.003- to 0.005-in. clearance existed between mating surfaces prior to depositing a 0.001 in. nickel plate over the mating surfaces of the fingers. The center plug (Astroloy) was also electroless nickel plated; the wedges (Inconel 600) did not require plating since the material constituents did not restrict wetting of the braze. The disk specimen and supports are shown before and after brazing in Figures 87 and 88, respectively. AMS 4779 filler material was used to braze the supports to the disk specimen. The braze operation was conducted in a vacuum of less than 2 microns of Hg at 2050°F for 15 minutes.

Postbraze visual inspection indicated that the simulated disk specimen fingers experienced some stress relief due to prior cold-working to align the mating fingers (see Figure 88). Readjustment of these fingers was required before brazing on the simulated blades. In addition, all disk specimens experienced some distortion so that the distance between the bottom pair of holes ("A" in Figure 79) decreased 0.004 to 0.025 in. The specimens were realigned prior to brazing on the blade specimens.

The five biaxial test specimens were prepared for the final braze cycle by plating the simulated blades (IN 100) with 0.0005- to 0.001-in. nickel deposited by the electroless process. The simulated disk specimens (Astroloy) were replated with an additional 0.005 in. of electroless nickel to assure good wetting of the braze, since the initial plating had been cycled through the vacuum furnace during the specimen modification. The specimens were cleaned with acetone and assembled on fixtures (Figure 89). Braze material (AMS 4779) was applied to the outside edge of each finger (but not within the 6 to 10 mil space between the test blade and the slave blade fingers) by means of a hypodermic syringe.

The specimens were brazed in a vacuum of less than 2 microns of Hg at a temperature of 2040°F. No remelt of the braze previously performed to install the supports for specimen modification was observed. Postbraze visual inspection indicated that the new braze material had been drawn into the areas between the IN 100 and Astroloy by capillary action, leaving no apparent voids. Good flow of the braze material was indicated by the presence of braze along the entire length of the slots between slave and test blade fingers.

6.7.3 Heat Treatment

Postbraze heat treatment of the biaxial specimens included the following steps:

1. Diffusion
   a. 1800°F - 1 hr
   b. 1900°F - 3 hr
   c. 1975°F - 68 hr
   d. Cool at 40°F/min to 1000°F or below
2. Stabilization
   a. 1600°F - 8 hr
   b. Cool to 500°F
   c. 1800°F - 4 hr
   d. Fast air cool
3. Precipitation
   a. 1200°F - 24 hr
   b. 1400°F - 8 hr

All of steps 1 and 2 (except where noted) were performed in a hydrogen atmosphere, while step 3 was entirely in air. Step 1 was designed to raise the remelt temperature of the braze by diffusing out the boron and silicon and to remove the braze joint interface by diffusing the nickel base braze material into the two parent materials (Astroloy and IN 100), producing a homogeneous microstructure. Steps 2 and 3 were designed to restrengthen the Astroloy.

6.7.4 Nondestructive Inspection

Visual inspection of the biaxial specimens following completion of the heat treatment cycle indicated the possible presence of certain void areas between the Astroloy and IN 100. An attempt was made to accurately define and record the imperfections of each specimen. Detailed photographs of the test zones of each were taken and are presented in Figure 90. Several specimens had the appearance of hairline crack formations, both in the IN 100 parent metal and in the braze material around the edges of the fingers. Zyglo inspection of the attachment fingers proved these formations to be superficial and were apparently the result of the melting point depressors (boron and silicon) present in the braze material. This effect is metallurgically referred to as "rivering", and is frequently observed in brazing. Radiographic examination of the biaxial specimen verified that the apparent hairline cracks were superficial, corroborating the results of the Zyglo inspection. The radiographic examination provided no conclusive information concerning the extent of braze coverage due to the specimen geometric restriction that prevented in-plane viewing of the braze junction.

The evaluation of braxe imperfections by nondestructive inspection included an experimental thermal test using "temperature indicating liquid crystals". The liquid crystals are derivatives of cholesterol and exhibit the optical properties of a crystal by scattering light selectively (i.e., white light is reflected as colored light). A change in temperature causes a shift in molecular structure so that a different color is reflected. For this test, a liquid crystal was selected with sufficient sensitivity to display the entire visible spectrum from red to violet, with a 4°F temperature change. The specimens were prepared for examination by spraying the liquid crystal film over the specimen attachment zone. The inspection technique was based on the theory that a homogeneous braze joint would readily and uniformly conduct heat from one material into the other. Thus, when a cooled specimen was heated from one side, the surface adjacent to a homogeneous braze would have a slower and more uniform thermal response than a surface adjacent to a void in the braze. The specimens were cooled on one side by a water bath and heated on the opposite side with two photoflood lamps focused on the test zone. Areas that exhibited a rapid color transient represented low conductivity and were classified as voids and recorded by color photography. Precise measurement of void size and shape was not possible. However, qualitative judgment was used to estimate the extent of braze voids. If the entire test zone heated uniformly, it displayed a uniform color that was interpreted as indicating a continuous braze

coverage. Figure 91 shows the typical color pattern obtained from specimens that indicate good braze coverage.

Two specimens were found to contain voids in the braze. Specimen SN 216 contained a void as shown in Figure 92. Specimen SN 219 contained a larger void and is discussed later. The voids exhibited by the "temperature indicating liquid crystals" were corroborated by visual inspection of the parts; however, the minimum void size that could be detected by this technique was not determined. The test indicated that three of the five biaxial test specimens (215, 217, and 218) were well brazed and that specimen SN 216 was marginal with respect to meeting the design criterion of 50% coverage. Specimen SN 219 (shown in Figure 93) appeared to have less than the required braze coverage (estimated 75% unbrazed on one finger). It was anticipated that this incomplete braze joint would fail in shear and result in premature failure of the remaining finger.

Mechanical impedance tests of the brazed blade fingers were conducted on two specimens to determine if this inspection method could be used to define the extent of braze coverage by determining spring rate and harmonic frequency. High spring rate and high frequency would correspond to high stiffness and good braze coverage, while low spring rate and low frequency would indicate low stiffness due to voids in the braze joint. The results of the mechanical impedance tests are presented in Table XXIII. Only one side of each specimen was studied because of limited time. Both the resonant frequency and spring rate of one finger of specimen (SN 219) show a marked reduction relative to the remaining fingers, corroborating the liquid crystal tests. One finger of specimen SN 217 indicated a shift in the high resonant frequency that did not correspond to liquid crystal tests. Specimen SN 217 was damaged as it was removed from the impedance test fixture. An attempt was made to repair the specimen by machining a 0.040-in.-diameter hole in the Astroloy to delay crack propagation. The part was also strained back toward original alignment, but the entire deformation could not be removed. However, the specimen was included in the test program to provide additional data.

Preliminary laser holographic inspection of the biaxial specimen indicated that good fringe patterns could be obtained and recorded by double exposure interferometric holograms, with the specimen excited from either a heat source or a vibrational loading. However, no significant correlation could be detected between the quality of the braze joint (based on the other NDT results) and the recorded fringe patterns. The development of the holographic inspection technique was beyond the scope of this program. Additional trials on joints of known quality would be required to establish the feasibility of using holography.

TABLE XXIII. MECHANICAL IMPEDANCE DATA

		Resonant Frequency (Hz) Low	High	Spring Rate (lb/in.)
	Slave	1393	2400	65,000
SN 217	Test	1386	3098	65,000
	Slave	1395	3101	65,000
	Slave	1425	3162	65,000
SN 219	Test	1415	3135	70,000
	Slave	1118	1425	30,000

6.8 BIAXIAL TESTS AND RESULTS

6.8.1 Test Rig

The test rig consisted of a single-ram loading arrangement as previously depicted in Figure 80. The vertical (radial) and horizontal (tangential) components of this load were applied to the disk specimen by accurate control of the angle of the load linkage. The ram was actuated hydraulically and controlled by a meter relay receiving the load cell output (see Figure 94). Dwell time at the maximum load was controlled, and the number of load cycles was recorded automatically. A pressure-sensing limit switch was used in the system to prevent overloading of the test part, and the rig was designed to automatically shut down after failure of the specimen. Heat was supplied to the specimen through a small resistance oven fabricated to fit over the test zone. Fibrefrax insulation was required to maintain 1400°F test temperature (Figure 95).

6.8.2 Test Cycle

During one-half of each load cycle, engine cruise stresses were simulated by application of the ram load to the specimen. The calculated stress level at the simulated disk live rim was 94,000 psi compression within the sections between the test and slave blades. The remainder of the cycle represented the residual stress in the disk after engine shutdown and was calculated to be 20,700 psi tension at the simulated live rim between blades. This stress was generated by a vertical dead load acting on the specimen for the load cycle indicated in Figure 96.

The test cycles were chosen to define the cyclic life characteristics of the brazed attachment design, which depend on cumulative (creep) damage resulting from a combination of cyclic and steady-state loads. Definition of the entire relation between the extremes of pure cycling and steady-state failure was beyond the scope of this program because of the large number of specimens and long test times required. However, tests over a short range of cycle times near the pure cyclic strain end of the

curve would define the departure from a linear cumulative damage law in this region; therefore, cycles with zero, one minute, and three minute dwell were selected.

6.8.3 Test Procedure and Results

Preliminary check-out of the test rig, heating oven, and associated equipment was performed with a "dummy" specimen installed in the load fixture.

Strain gage data of the first test specimen (No. 215) were taken from ambient temperature tests at 20, 40, and 80% of design load. The instrumentation is shown in Figure 97, and the specimen is shown installed in the test frame in Figure 98. Radial stress levels varied between the front and back fingers of each simulated blade, which indicated that the fingers were experiencing an additional bending load due to small radial misalignment of the blades. This misalignment resulted in a corresponding distortion in the Astroloy disk that was indicated by a variation in the tangential stress distribution from blade to blade. Increasing the applied load did not produce a linear increase in stresses, denoting a redistribution of load as the specimen was strained into alignment. Two additional specimens (SN 218 and 216), instrumented with a minimum number of strain gages, also exhibited a similar strain pattern when subjected to ambient temperature loads. Analysis of the strain gage data gave qualitative agreement with theoretical calculations; however, actual values ranged from 25% above to as much as 50% less than predicted. This was generally attributed to misalignment in the brazed junction and was considered indicative of the fabrication difficulties associated with this design. For this reason, no further strain gage measurements were taken, and the test rig was calibrated to apply the theoretical radial and tangential loads to the specimen.

The first specimen (215) was prepared for cyclic testing by removing the strain gages and tack welding thermocouples to the IN 100 fingers for measuring specimen temperature. The test was initiated by heating the specimen gradually to 1400°F prior to applying the cyclic load. The specimen was cyclically loaded at a rate of 2.5 cycles per minute with zero dwell time for 4700 cycles. Catastrophic failure had not occurred; however, cracks were found in the region between the test and slave blades leading from the disk OD toward the disk center into the live rim on both sides of the specimen (see Figure 99). Complete failure of the specimen (Figure 100) occurred after an additional 54 cycles.

The second specimen (218) was similarly prepared and tested with a load cycle that included three minutes dwell at the high load level to evaluate the effect of cumulative damage. Visual and Zyglo inspection after 2192 cycles revealed no surface cracks; however, radiographic inspection indicated internal cracks in the disk OD fingers radiating toward the live rim similar to the first test specimen. The specimen completed 413 additional cycles prior to total failure (Figure 101).

Specimen (SN 216) was cyclically tested with one minute dwell time for 30 cycles prior to complete failure (see Figure 102). Shearing of one braze joint promoted failure (primarily IN 100) by overloading the remaining joints. Visual inspection indicated a lack of braze coverage (< 50%) over the sheared joint. This area was not detected by nondestructive inspection. The area that was detected by NDT did not fail in shear.

The fourth specimen (SN 219) contained the large void apparent from visual and nondestructive inspection and failed at 80% of the initial load (Figure 103). The entire front side of the specimen had less than 50% braze coverage; however, only one finger had been detected as containing a void by nondestructive inspection.

The last specimen (SN 217) had been previously distorted. It sustained 319 cycles with zero dwell time prior to failure of the IN 100 blade fingers. No braze failures occurred (see Figure 104).

The biaxial test data are presented in Table XXIV.

TABLE XXIV. TASK V BIAXIAL TEST DATA*

Specimen No.	Test Cycle	Accumulated Cycles to Failure	Creep (hr)	Location of Initial Failure
215	Pure Fatigue	4754	< 10	Astroloy
216**	Fatigue + 1 min Dwell	30	< 1	Braze
217***	Pure Fatigue	319	< 1	IN100
218	Fatigue + 3 min Dwell	2605	< 134	Astroloy
219**	Pure Fatigue	Failed at 80% - Initial Load	--	Braze

*All tests conducted at 1400°F.

**Braze voids detected by pretest nondestructive inspection.

***Damaged specimen.

6.8.4 Metallurgical Evaluation

Failure analysis of the test specimens indicated that the failure mode was primarily stress rupture with slight evidence of fatigue. These results are typical of elevated temperature low cycle fatigue tests where the test specimen fracture faces rub out the lines of fatigue.

Microstructural examination showed fractures in both parent materials to be intergranular and heavily oxidized. Areas failing in overstress, which normally are only slightly oxidized after elevated temperature tests, could not be identified due to the oxidation. Precise metallurgical definition of the order of failure was not always possible, but by using all information available, the most probable sequence of failure has been established. The IN 100 fracture faces were extremely granular due to the coarse grains typical of a cast material. In general, the Astroloy failures were smooth due to the very fine grained microstructure (ASTM 7-8). However, within the thin fingers of the Astroloy, the effects of braze alloying were found to have caused grain growth to ASTM 0-1. This was believed to be caused by diffusing the boron and silicon from the braze into the parent material. No severe grain growth was noted within the IN 100 microstructure, but photomicrographs showed grain boundary deposits (see Figure 105). Material hardness was not affected by the braze alloying.

Failure of the first test specimen (SN 215) originated in the Astroloy and was visually apparent at the intermediate inspection prior to testing to failure (as previously shown in Figure 99). Propagation of the fatigue crack continued through the Astroloy and promoted catastrophic failure of the specimen. Subsequent to the Astroloy fracturing, the blade segments were subjected to a tangential bending moment that overstressed the attachment fingers. This failure occurred primarily in the IN 100 fingers, and the metallurgical analysis revealed no evidence of secondary cracking (indicative of stress rupture), tending to verify this sequence of failure (see Figure 106). Braze coverage was estimated at 75 to 80%.

Cracking of the Astroloy fingers also initiated failure of the second test specimen (SN 218); however, the blade segments (IN 100) failed prior to complete Astroloy fracture. The presence of secondary cracking within the IN 100 (Figure 107) indicated a stress rupture type failure. Microstructural examination of the failed attachment area revealed a drastic alteration of the Astroloy matrix (Figure 108). Grain size grew to ASTM 0-1, grain boundaries were filled with microconstituents, and a needlelike phase appeared in the matrix. These phenomena were attributed to braze alloying as a result of diffusing the boron and silicon into the parent material. Astroloy material specifications normally included 0.03% boron, while the AMS 4779 (Coast Metals 50) braze material contained 3% of this element. It was not determined whether this modification in material microstructure degraded the material life. Braze coverage was estimated to be 95 to 100%.

The third specimen (SN 216) tested with one minute of creep at high load per cycle failed after 30 load cycles. Failure was due to a lack of braze coverage (less than 50%) over one finger of a slave blade (previously shown in Figure 102). Fracture of the remaining attachment fingers occurred immediately thereafter due to overstress. Nondestructive inspection techniques were unsuccessful in revealing this braze void. The void area that was detected prior to testing did not fail.

Detailed radiographic and metallurgical evaluation of sections taken from the failed specimen revealed 65 to 70% braze coverage for the finger with the void area previously detected by nondestructive inspection (Figure 109).

Analysis of the fourth specimen failure (SN 219) revealed approximately 30 to 35% braze coverage on the front side of the specimen (previously illustrated in Figure 103). This area was previously found to be deficient in braze coverage both by visual and nondestructive inspection; the braze failed in shear as anticipated. Subsequent failure occurred on the back side of the specimen without shearing the braze that exceeded 50% coverage.

The damaged test specimen (SN 217) failed through the IN 100 parent material (previously illustrated in Figure 104). The fracture face was oxidized and granular; microscopic inspection showed the failure to be intergranular. No secondary cracking was apparent, indicating that failure was by overstress. Sections through the attachment area revealed 95 to 100% braze coverage. Apparently the fingers were overstressed as the specimen was strained into alignment during each loading cycle due to the pretest damage that promoted excessive deflection.

6.8.5 Data Analysis

A general conclusion from the biaxial specimen test data is that, with sound braze joints, the brazed attachment can develop reasonable cyclic life. The limited amount of data obtained did not permit a definition of low cycle fatigue and creep interaction as originally intended. However, the well-brazed fingers performed satisfactorily, and the failures initiated in the highly stressed disk rim between fingers. As previously discussed under specimen design, this rim was continuous to provide a positive seal between attachments.

The cyclic life developed by specimen 215 (4754 cycles with zero dwell) and specimen 218 (2605 cycles with 3 minute dwell) should represent the minimum capability of the brazed attachment design in the engine environment. The specimen tests were actually more severe than engine conditions because of two factors: (1) specimen temperature was constant at 1400°F for the entire cycle, which would tend to accumulate more creep damage than the varying temperature engine cycle; and (2) the specimens were loaded to the same level, each cycle producing an increase in tangential stress for a crack propagating from the disk rim, whereas a crack in the engine disk rim should have limited propagation. Because the cool and massive portion of the engine disk below the attachment should exert a controlling influence on the stress distribution in the attachment region, the position of the neutral axis (zero stress) would be relatively unaffected by a crack at the disk rim. Therefore, a crack initiated at the disk rim should experience stress relief and limited growth in the radial direction.

Nondestructive inspection using temperature-indicating liquid crystals and mechanical impedance provided a qualitative indication of the braze coverage that was subsequently verified by the metallurgical evaluation following the destructive testing of the specimens. The void in the braze of specimen SN 216 was confirmed; this void covered less than 50% of the braze surface as anticipated from the liquid crystal testing. Also, the large void detected in specimen SN 219 covered more than 50% of the braze surface as expected. However, on the back side of specimen SN 216, one finger contained an inferior braze joint that failed during cyclic testing; this defect in the braze had not been detected by the liquid crystal method.

The general characteristics of the biaxial specimen failures were directly related to the quality of the braze joint. Specimens that contained good braze coverage exhibited no tendency to fail in the junction area. Failure in these specimens was in the disk material and corresponded to combined fatigue and stress rupture characteristics of Astroloy. Specimens that contained less than 50% braze coverage on any one finger exhibited a braze failure on that finger that subsequently overstressed the remaining fingers and resulted in premature failure of the complete specimen. This emphasized the importance of developing suitable nondestructive inspection techniques for the brazed joints.

There are several areas of potential improvement in the brazed specimen design and fabrication that should increase the durability. A redesign to a two-finger attachment (rather than four) would increase the OD-to-ID length and reduce the thermal gradient that was the predominant factor contributing to the critical disk rim stress. Additional benefits may be possible through modified fabrication procedures that would minimize rough surface effects (such as produced by the EDM process used to form the fingers) and undesirable alloying of braze constituents (boron and silicon melting point depressors) with the base metals. This would require testing additional specimens to determine the effect of these factors on material strength.

7.0 CONCLUSIONS

The objective of the turbine blade/disk attachment program was to evaluate attachment methods suitable for 2- to 5-lb/sec gas turbine engines. Based on a preliminary ranking, six attachment methods were selected for analytical evaluation: (1) Standard Fir-Tree, (2) Welded, (3) Brazed, (4) Integral Cast, (5) Inverted Fir-Tree, and (6) Pinned. In subsequent analyses the first three attachments were selected for experimental evaluation through uniaxial specimen testing to determine their strength and vibrational capabilities. Based on the results of uniaxial tests, the brazed attachment was selected as the most suitable blade/disk attachment method and was subjected to final proof testing.

As a result of this program the following conclusions were reached:

1. The brazed attachment design combines a lightweight rotor system, good potential for coolant air sealing, and good resistance to fatigue. Analyses of uniaxial test results indicated that this attachment with directionally solidified SM 200 blades and Astroloy disk could meet study engine requirements for stress rupture life. The biaxial LCF tests indicated that brazed attachments could be cycled between engine maximum rated power and shutdown for more than 4000 cycles without failure demonstrating good cyclic life characteristics under test conditions more severe than the engine would impose. However, creep effects on low cycle fatigue life could not be determined from the limited data. Improvements in the brazed attachment should be possible through design modifications to reduce high disk rim stresses, fabrication techniques that minimize rough surface effects, and braze/heat treatment refinements that minimize undesirable alloying.

   Nondestructive inspection of assembled rotors using the four-finger design would be very difficult with present techniques. However, the use of a two-finger configuration simplifies the attachment inspection sufficiently that several NDT methods could be developed.

2. The welded attachment provides the lightest overall rotor system, requiring only a 0.3-in. disk thickness at the live rim. However, this attachment did not develop adequate strength due to weld cracking and brittle failures at the IN 100 fusion line. This attachment technique has excellent potential for small engine application if acceptable super alloy weldments and suitable nondestructive inspection methods can be developed.

3. The fir-tree is the only one of the mechanical attachments studied that indicated sufficient joint efficiency to meet the study turbine requirements; uniaxial specimen testing revealed that this attachment could attain the study engine requirement for stress rupture life by using advanced materials (directionally solidified SM 200 blades and Astroloy disk). This attachment

requires critical control of tooth dimensions to maintain load distribution, but inspection is much simpler than for either the brazed or welded configurations. However, the fir-tree attachment requires a disk and rotor system that is four times as heavy as the welded type.

4. Integrally cast blade/disk assemblies suffer from a compromise in disk material properties that results in a heavy and bulky rotor system. In addition, formation of the required airfoil cooling passages by existing fabrication processes presents a formidable problem.

5. Preliminary assessment of the bicasting process indicates that parent metal strength can be obtained. Ultimate stress, creep life, and elongation exceeded IN 100 material specifications in specimens free of casting shrinkage. It is concluded, therefore, that satisfactory bicast attachments can be fabricated with proper control of the casting parameters. See Appendix II for bicast discussion.

8.0 RECOMMENDATIONS

This program demonstrated for small high tip speed gas turbines that only the brazed and welded attachments offered significant weight advantages relative to the fir-tree attachment and that other conventional mechanical attachments did not satisfy the strength requirements. The application of the brazed and welded attachments will require additional development that was beyond the scope of this program. The recommendations for further work on these attachment concepts follow.

The brazing process should be further refined by conducting an experimental investigation with simple uniaxial specimens to produce consistently reliable joints that exceed 80% braze coverage. Factors requiring further definition include: (1) braze material, (2) specimen preparation, (3) braze cycle, (4) postbraze heat treatment, and (5) effect on parent material constituents and strength. Particular emphasis should be directed to determining the factors that promote the flow of the braze material and improve braze coverage, and the effect on strength of the alloying of braze constituents with the parent materials. Nondestructive inspection techniques should be developed to provide a reliable evaluation of brazed rotor assemblies. Techniques which appear to be potentially suitable for prediction of braze soundness are: (1) holography, (2) mechanical impedance, (3) temperature indicating liquid crystal film, and (4) ultrasonics. The results of the braze process improvements and nondestructive inspection development should subsequently be applied in a program for the design, fabrication, and hot turbine rig demonstration of a complete rotor.

In view of the welded attachment's attractive light weight and simplicity, a weld development program is recommended to eliminate weld cracking and subsequent brittle failures. Suitable blade and disk materials joined by electron beam, inertia, and diffusion welding should be evaluated with respect to the effects of material constituents, grain size, and heat treatment on joint strength. The program should include the development of a nondestructive inspection technique to evaluate the quality of weldments.

Although the bicast joint showed potential for developing parent metal strength, the use of a cast disk material would result in a relatively heavy rotor similar to the integral casting. Therefore, it is recommended that "bimetal" casting using a forged disk material with the blade airfoils cast-on be investigated. This would permit selection of optimum materials for blades and disk. This effort should include selection of candidate alloys through simple specimen casting trials and metallurgical examination, refinement of casting parameters for the best material combination including strength tests, and development of nondestructive testing methods suitable for this type of joint.

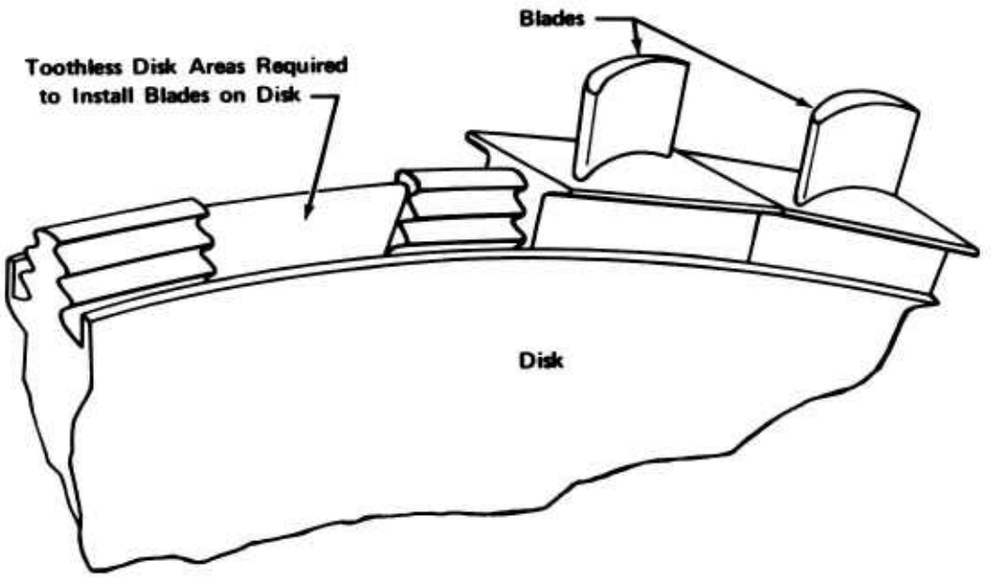

Figure 1. Typical Inverted Circumferential Fir-Tree Design.

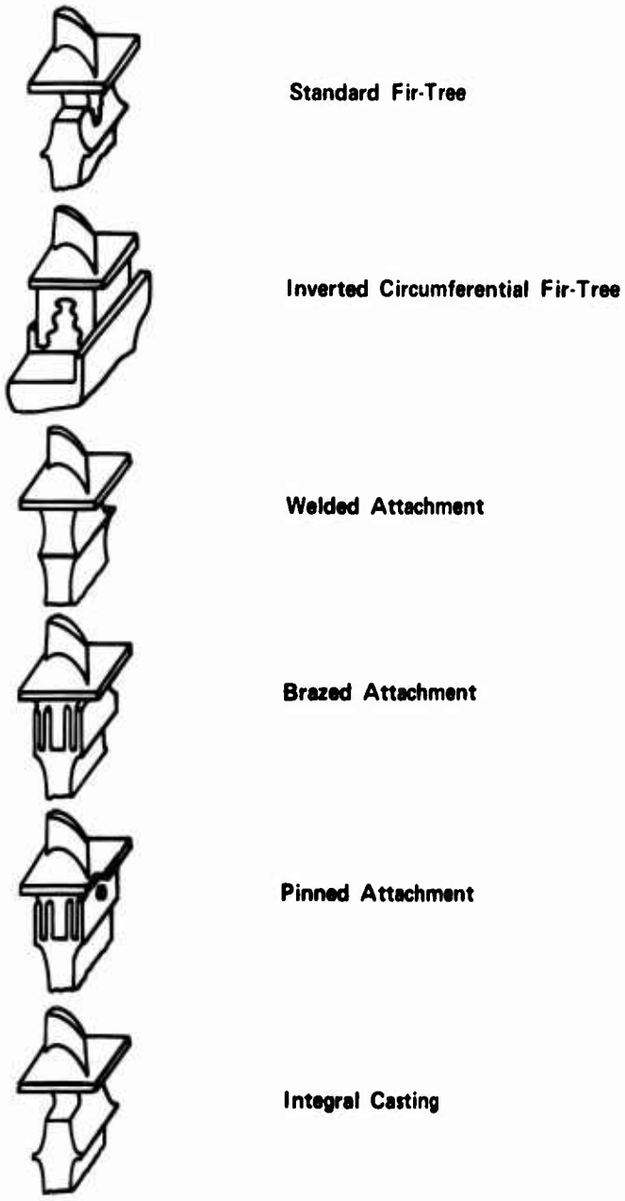

Figure 2. Attachment Methods Selected for Analyses.

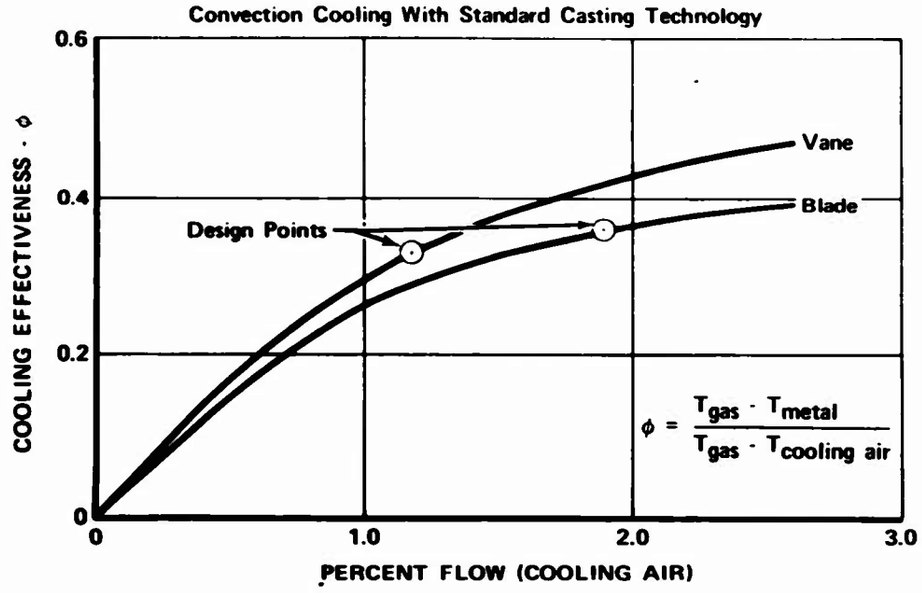

Figure 3. First-Stage Vane and Blade Cooling Requirements.

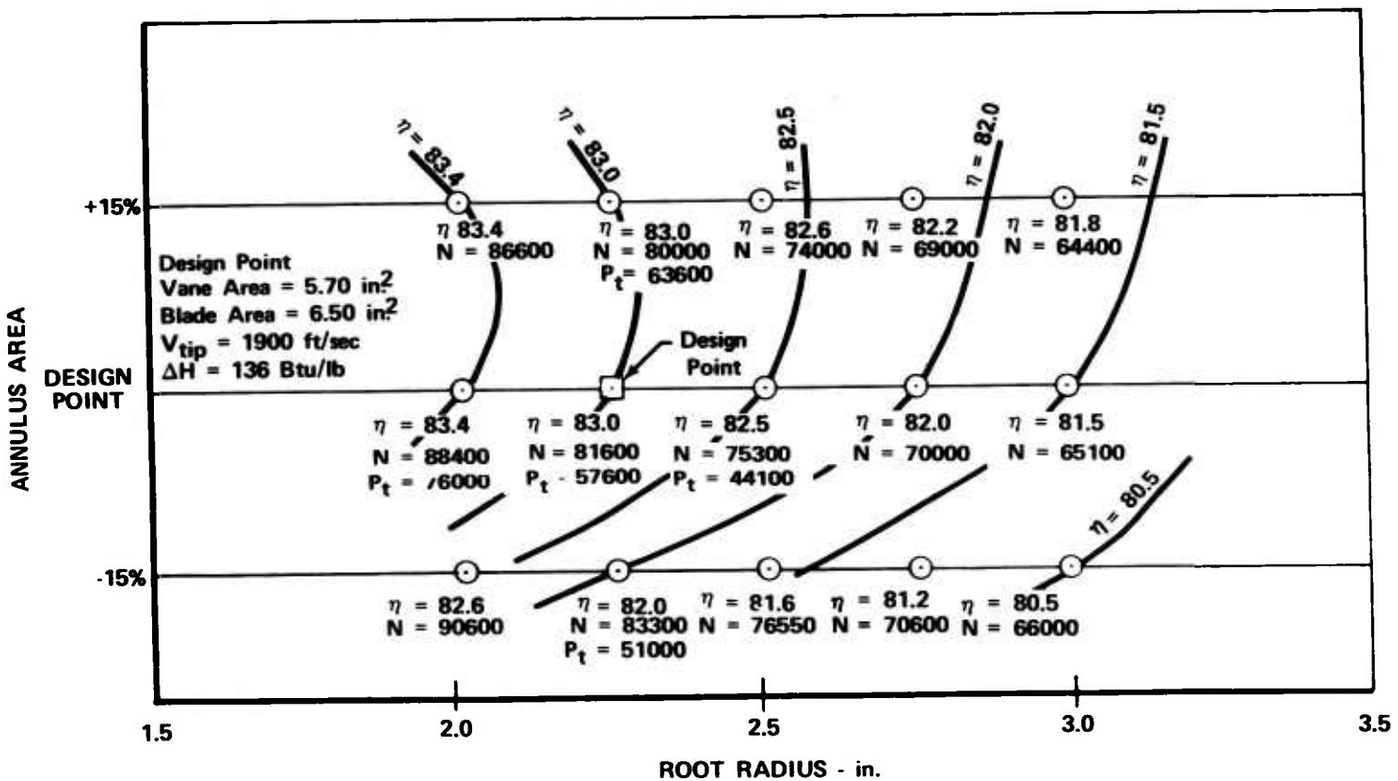

Figure 4. Turbine Mean Line Design Optimization.

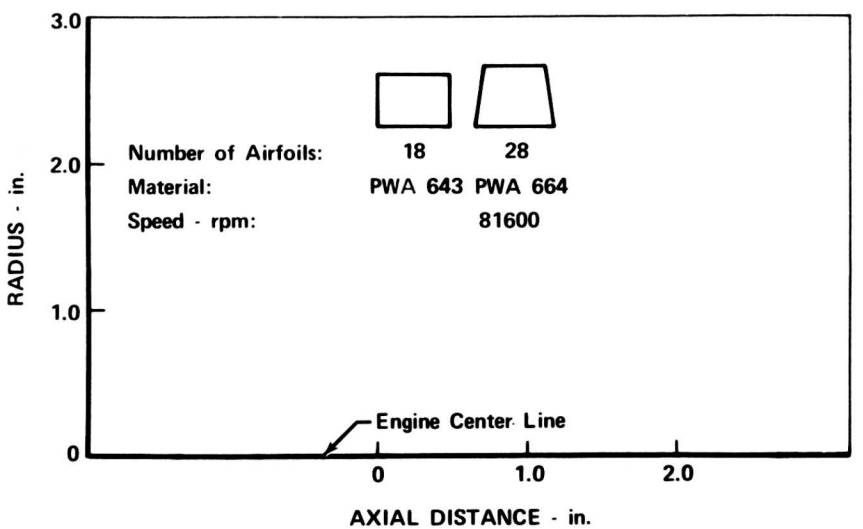

Figure 5. Turbine Elevation.

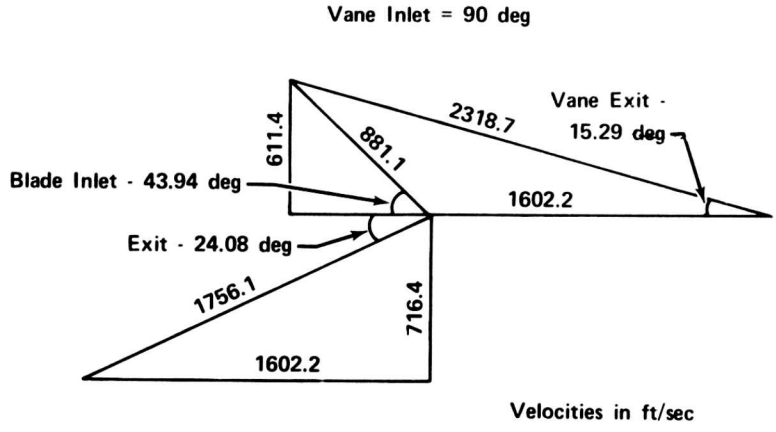

a. Root Section

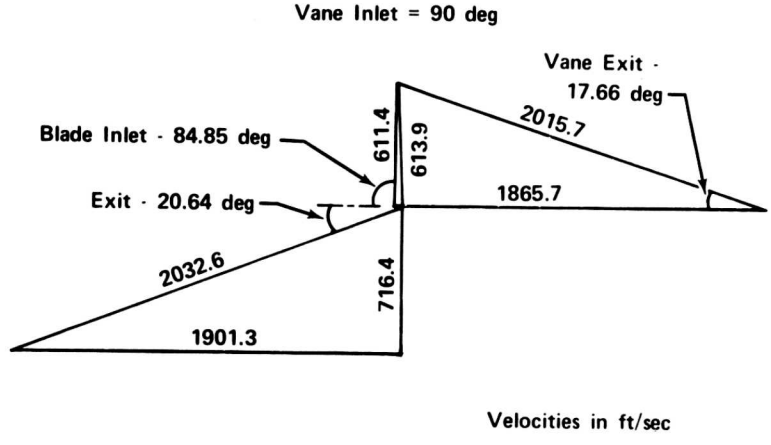

b. Tip Section

Figure 6. Velocity Triangles.

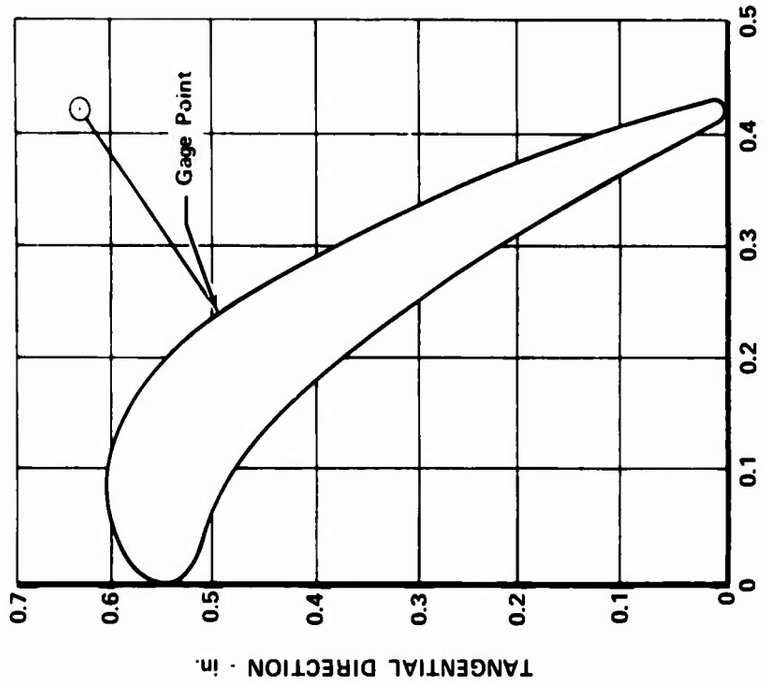

Figure 8. Turbine Blade Tip Contour.

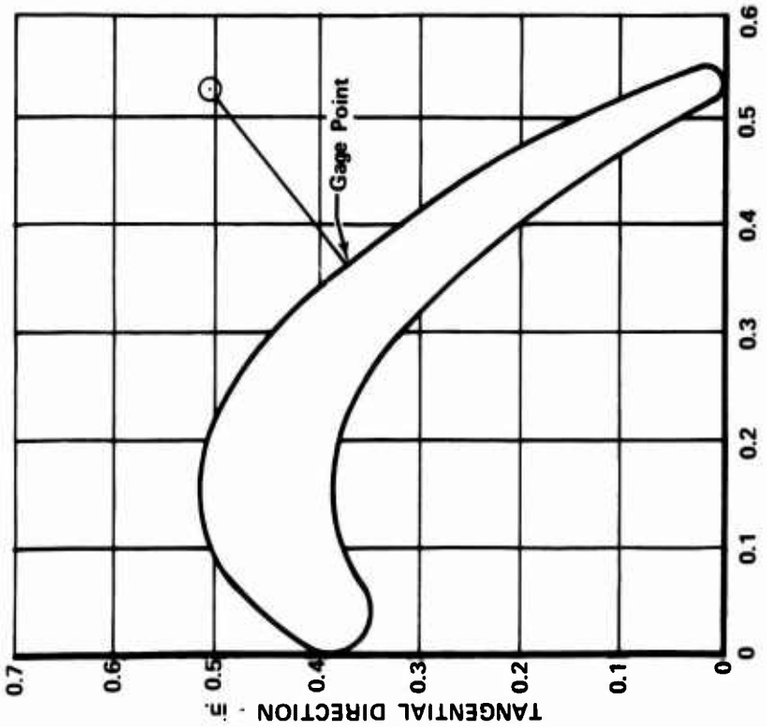

Figure 7. Turbine Blade Root Contour.

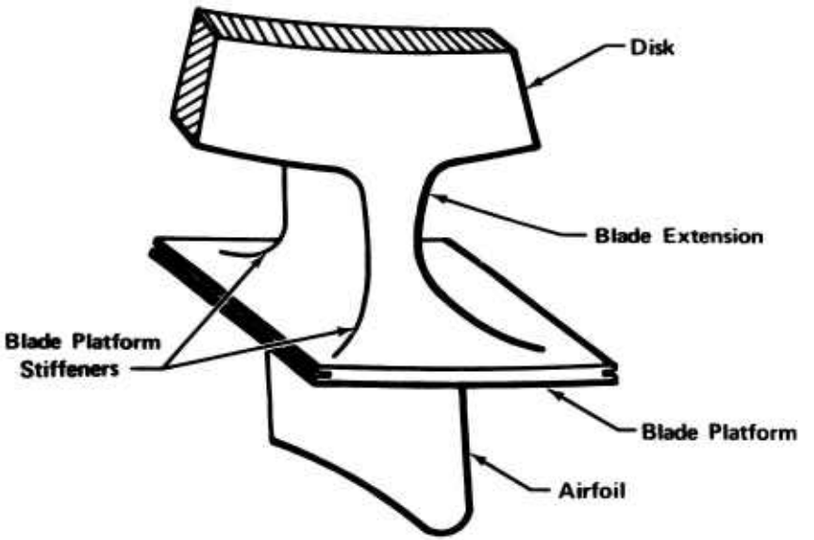

Figure 9. Modified Blade Platform Design.

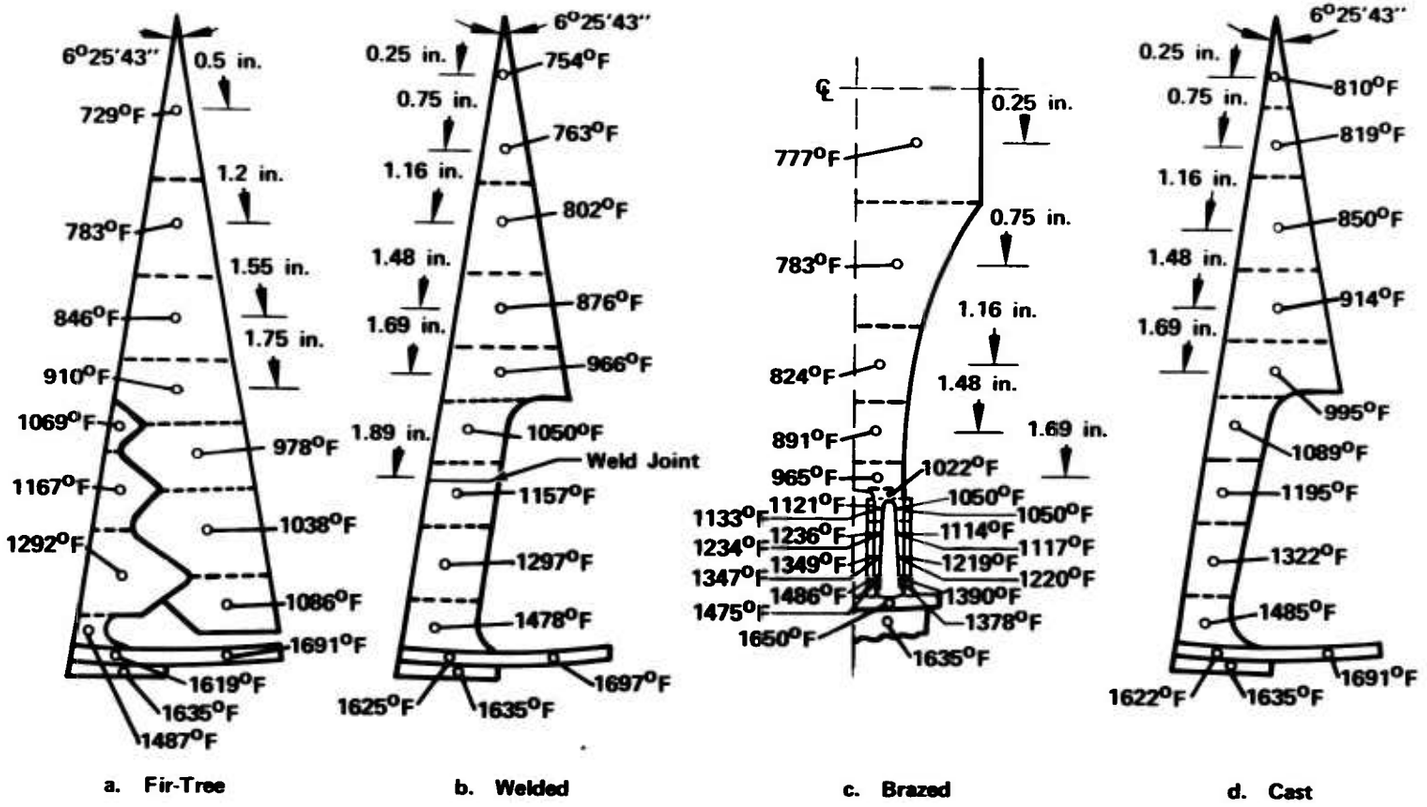

Figure 10. Attachment Thermal Maps.

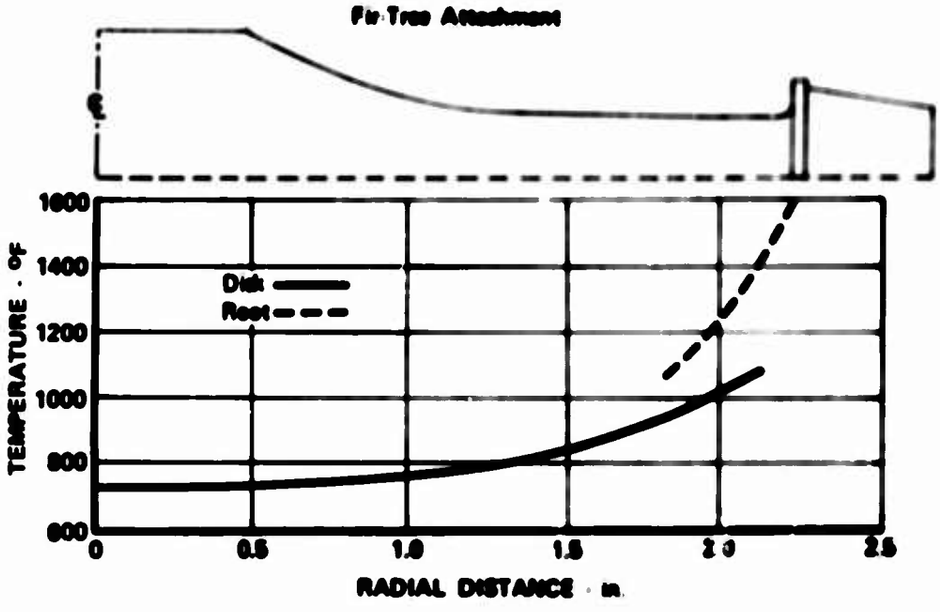

Figure 11. Disk and Blade Root Temperature Profile.

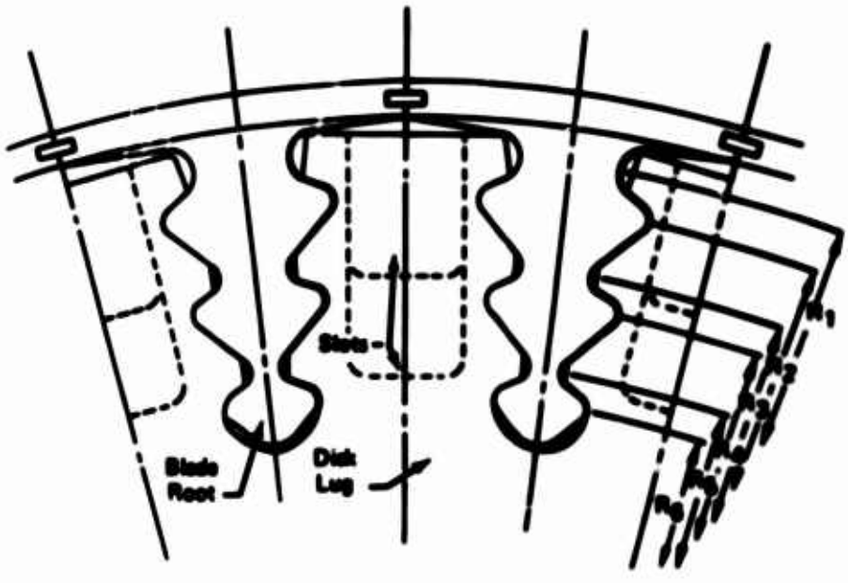

Figure 12. Fir-Tree Slotted Disk.

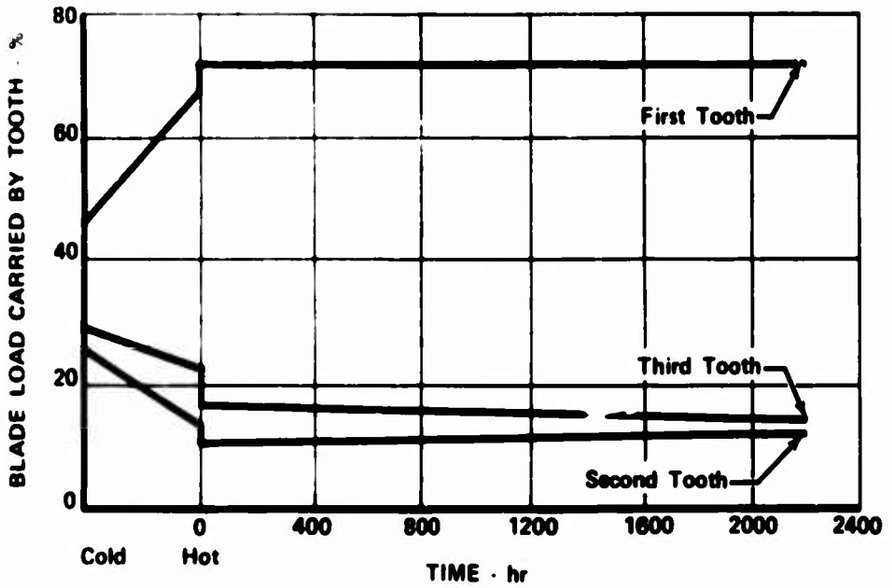

Figure 13. Fir-Tree Load Distribution.

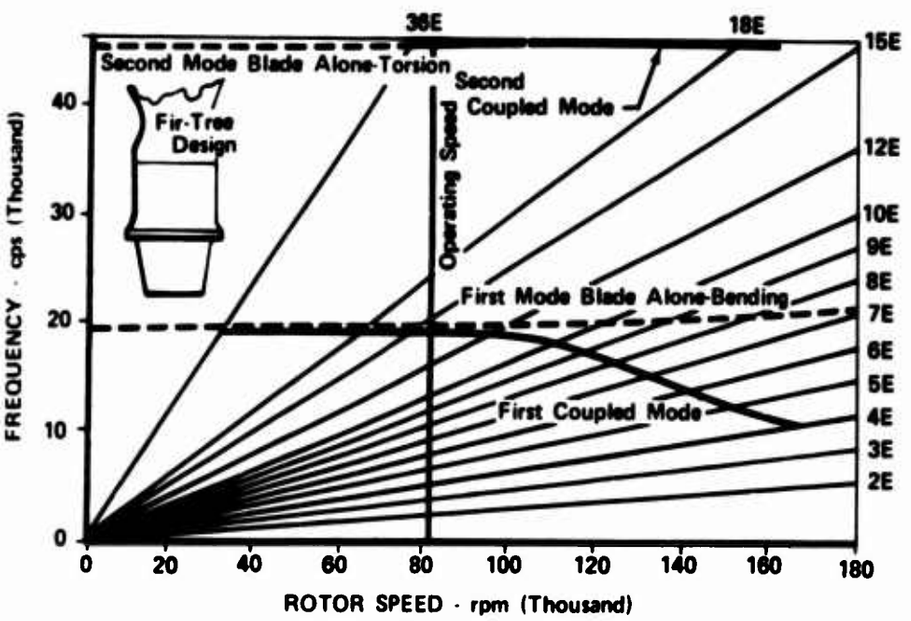

Figure 14. Vibration Analysis of Fir-Tree Design.

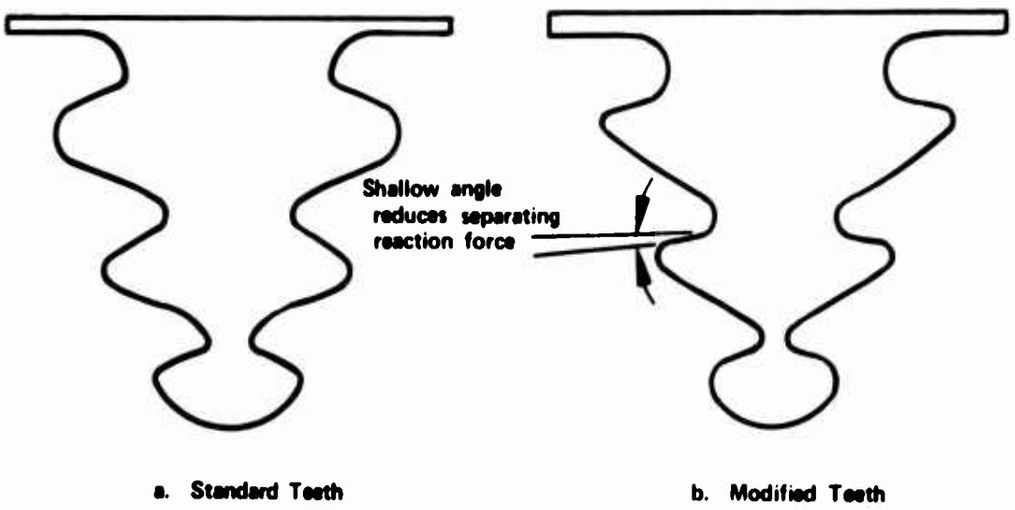

Figure 15. Fir-Tree Tooth Design for Split Disk.

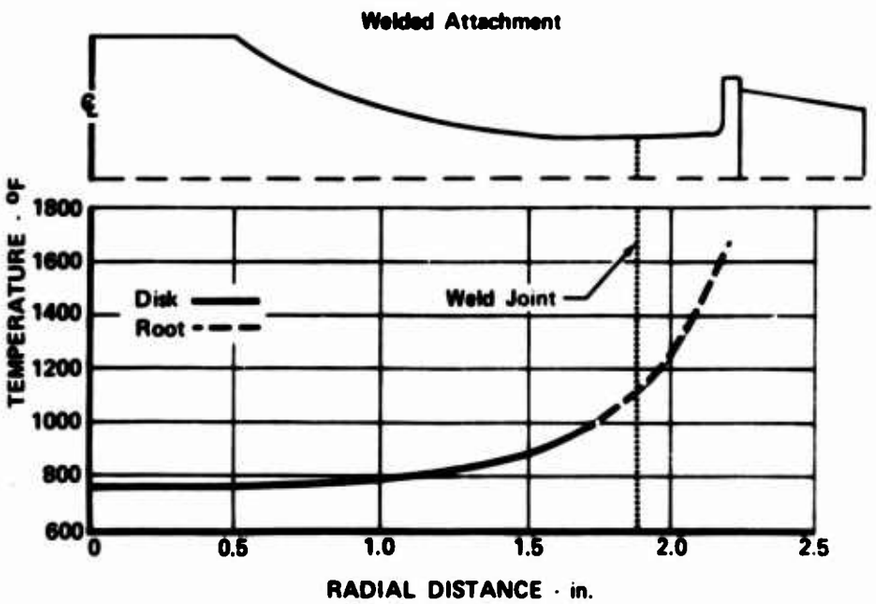

Figure 16. Disk and Blade Root Temperature Profile.

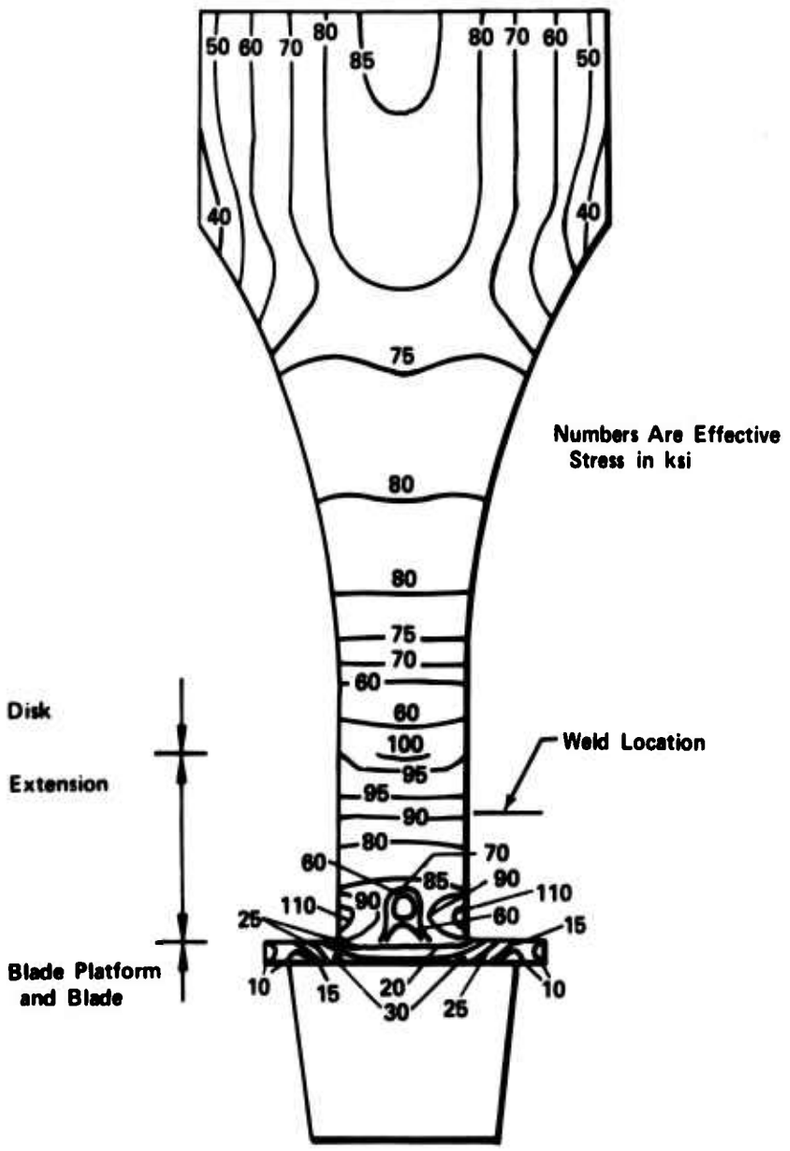

Figure 17. Welded Design.

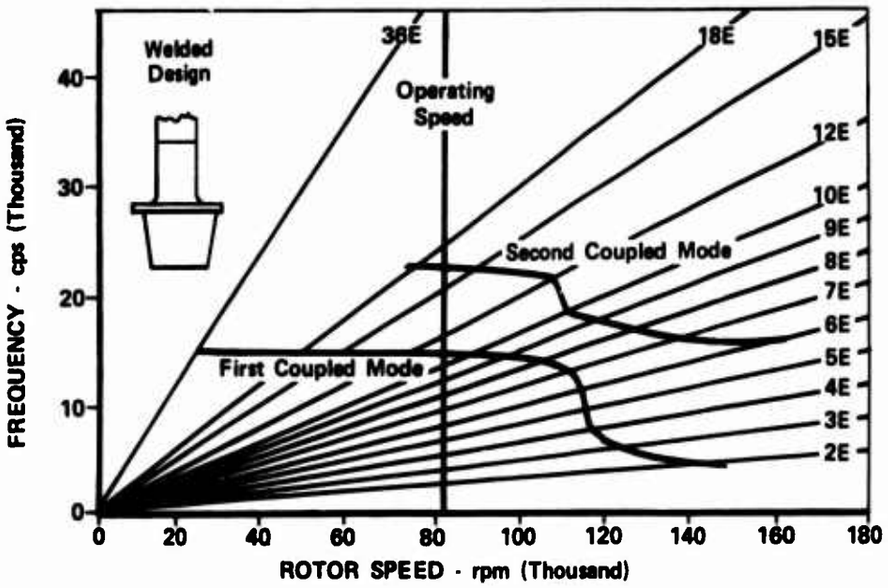

Figure 18. Vibration Analysis of Welded Design.

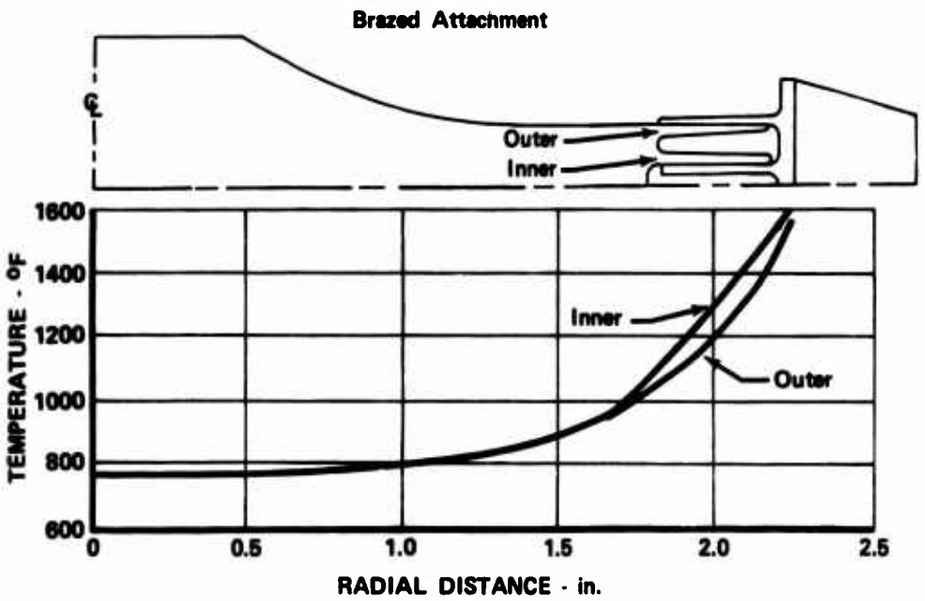

Figure 19. Disk and Blade Root Temperature Profile.

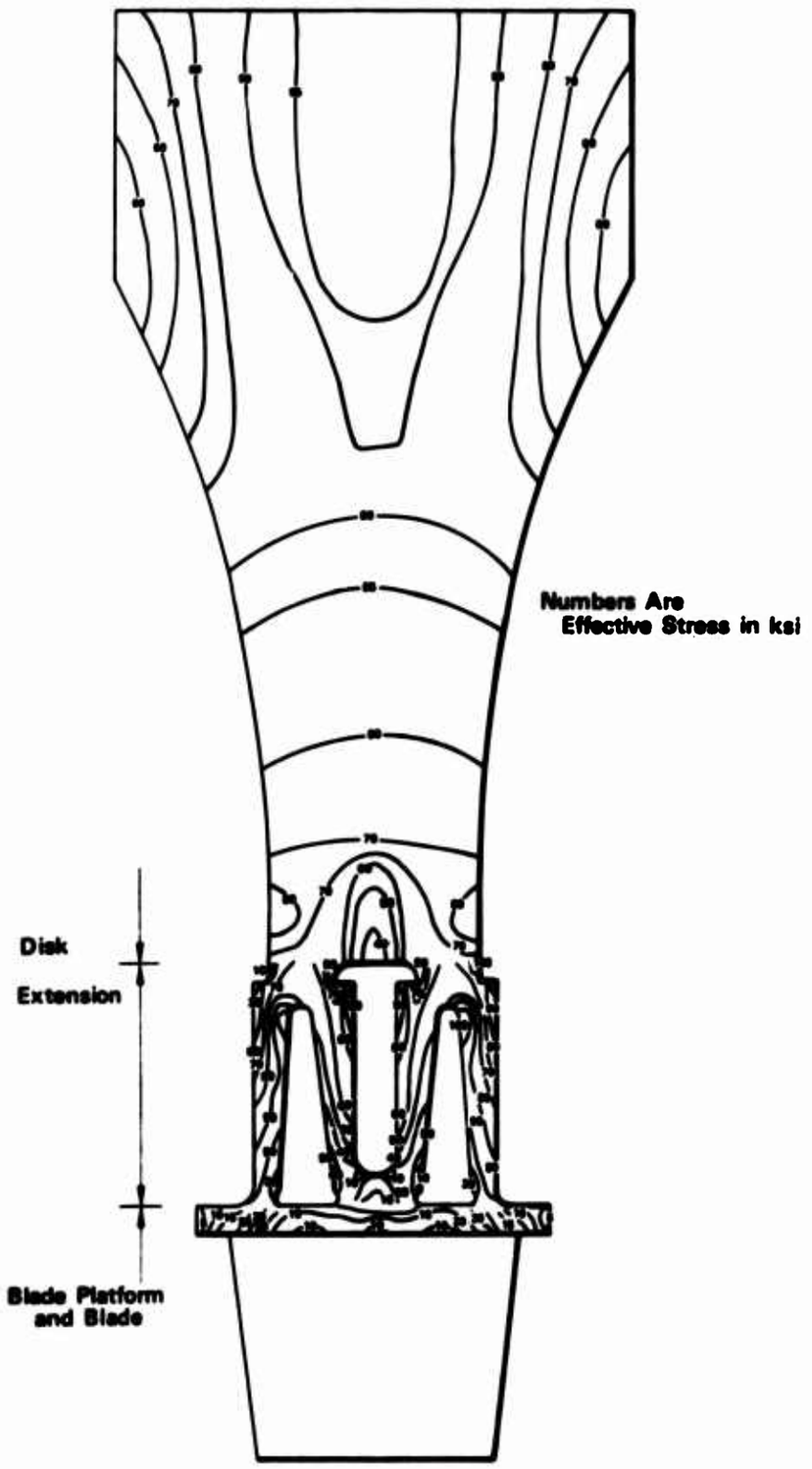

Figure 20. Brazed Design.

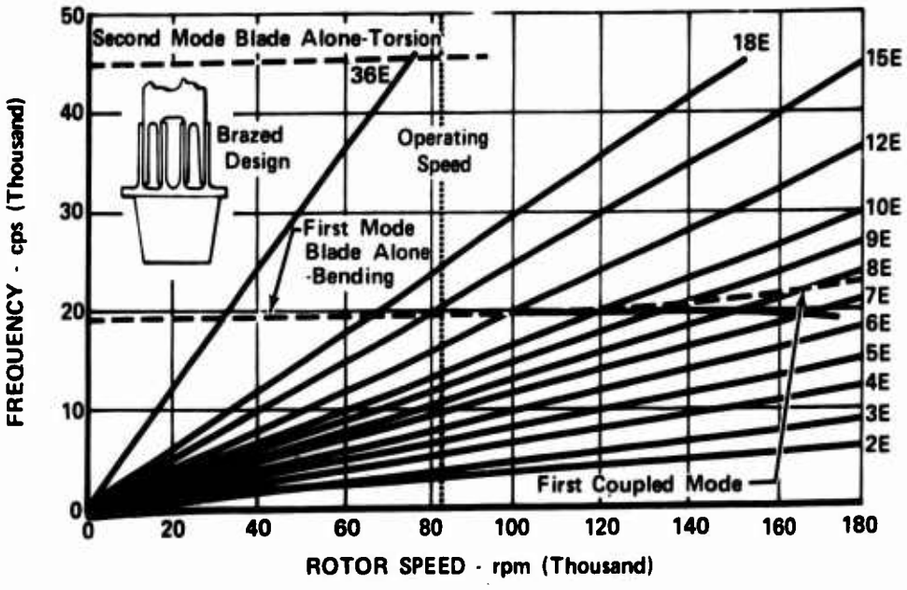

Figure 21. Vibration Analysis of Brazed Design.

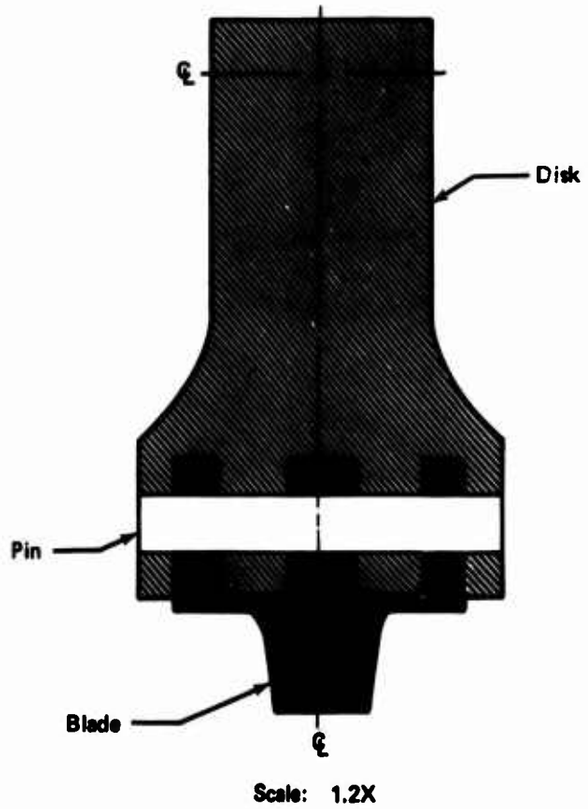

Figure 22. Pinned Root Attachment.

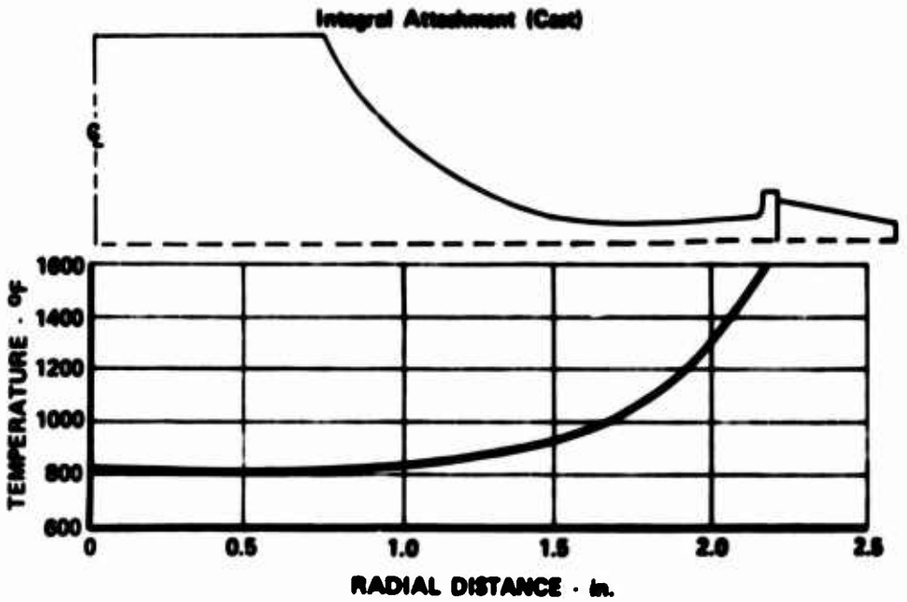

Figure 23. Disk and Blade Root Temperature Profile.

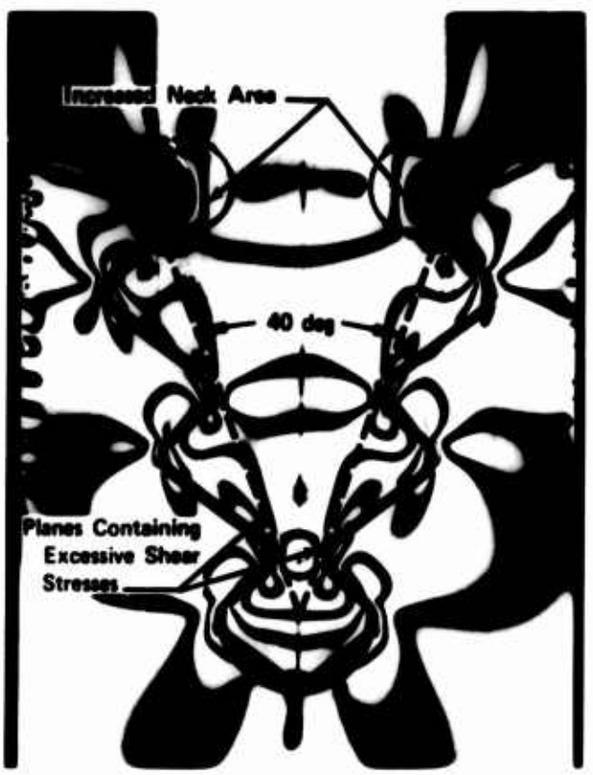

Figure 24. Photoelastic Analysis of Fir-Tree With 40-Degree Root.

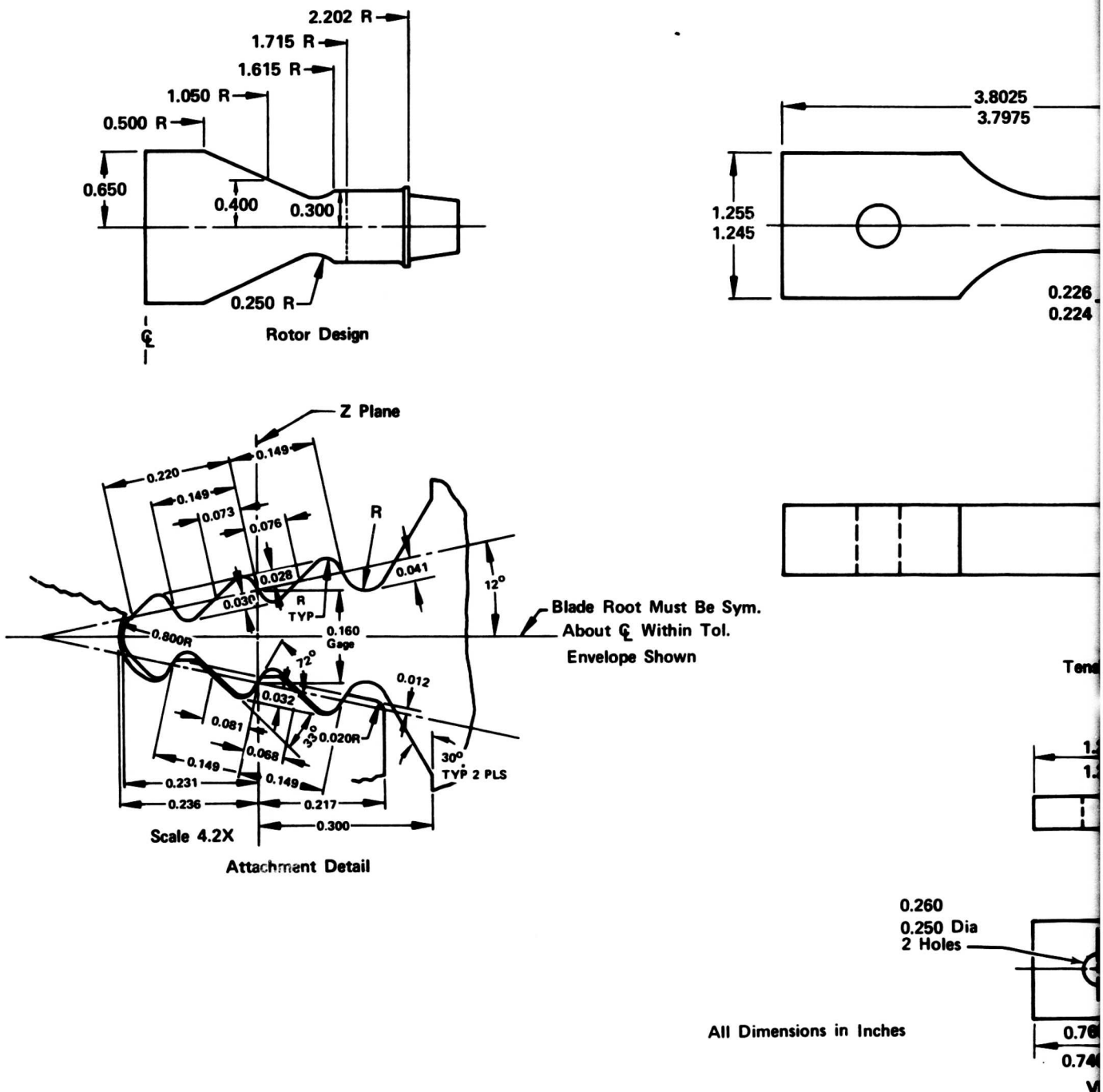

Figure 25. Fir-Tree Attachment Design.

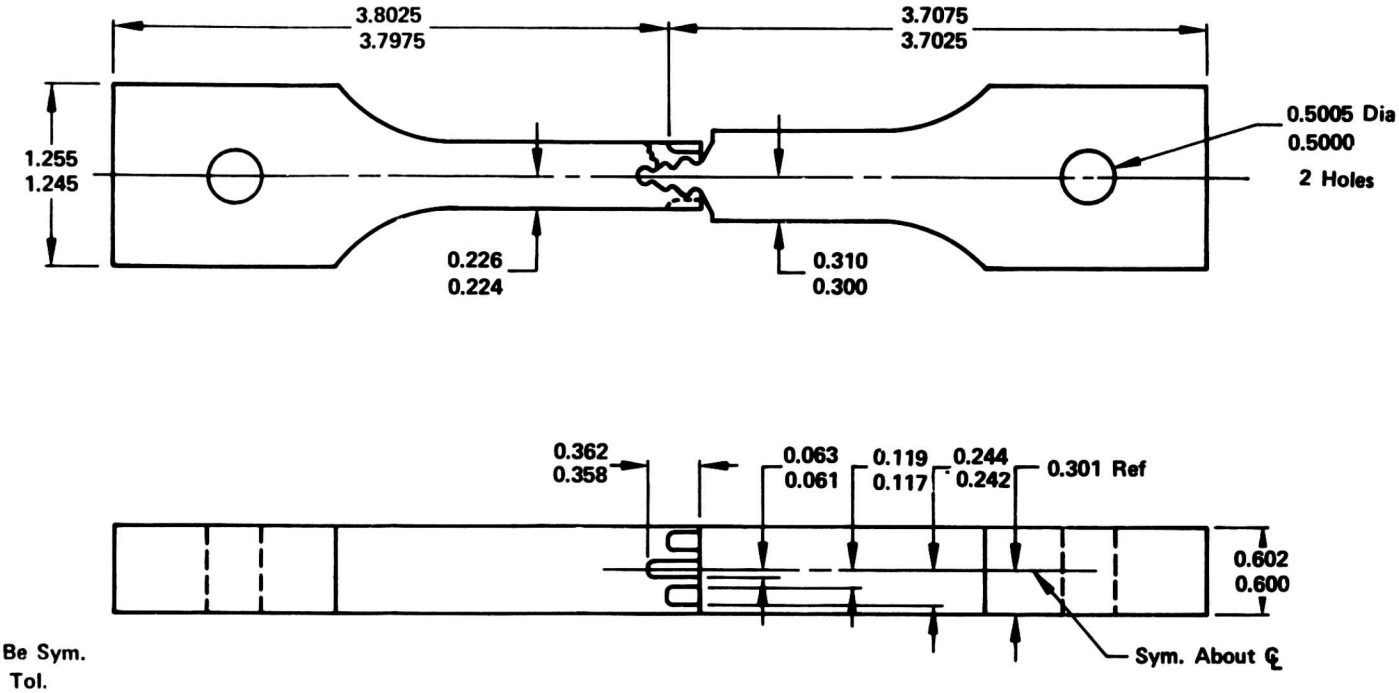

Must Be Sym.
Within Tol.
Shown

Tensile/Stress Rupture Specimen

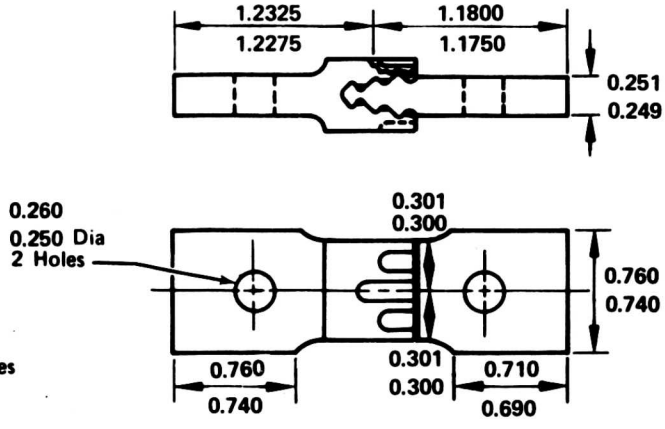

All Dimensions in Inches

Vibratory Fatigue Specimen

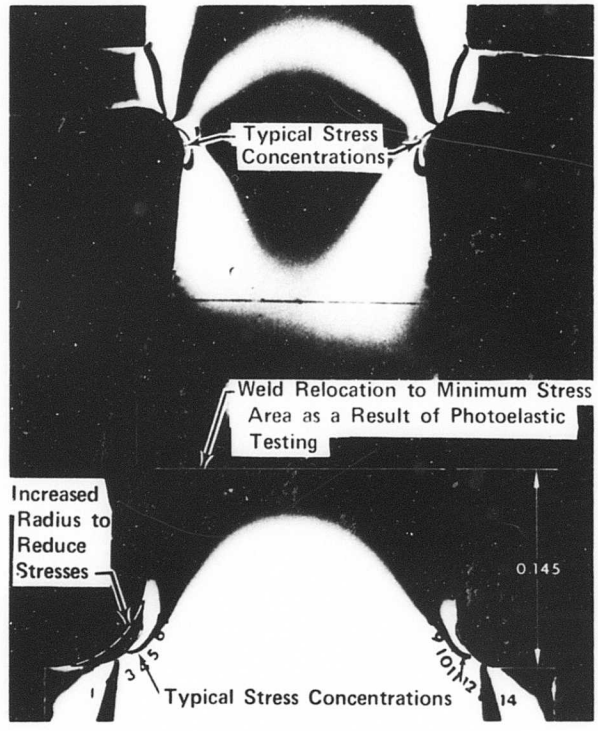

Figure 26. Photoelastic Model of Welded Attachment Design.

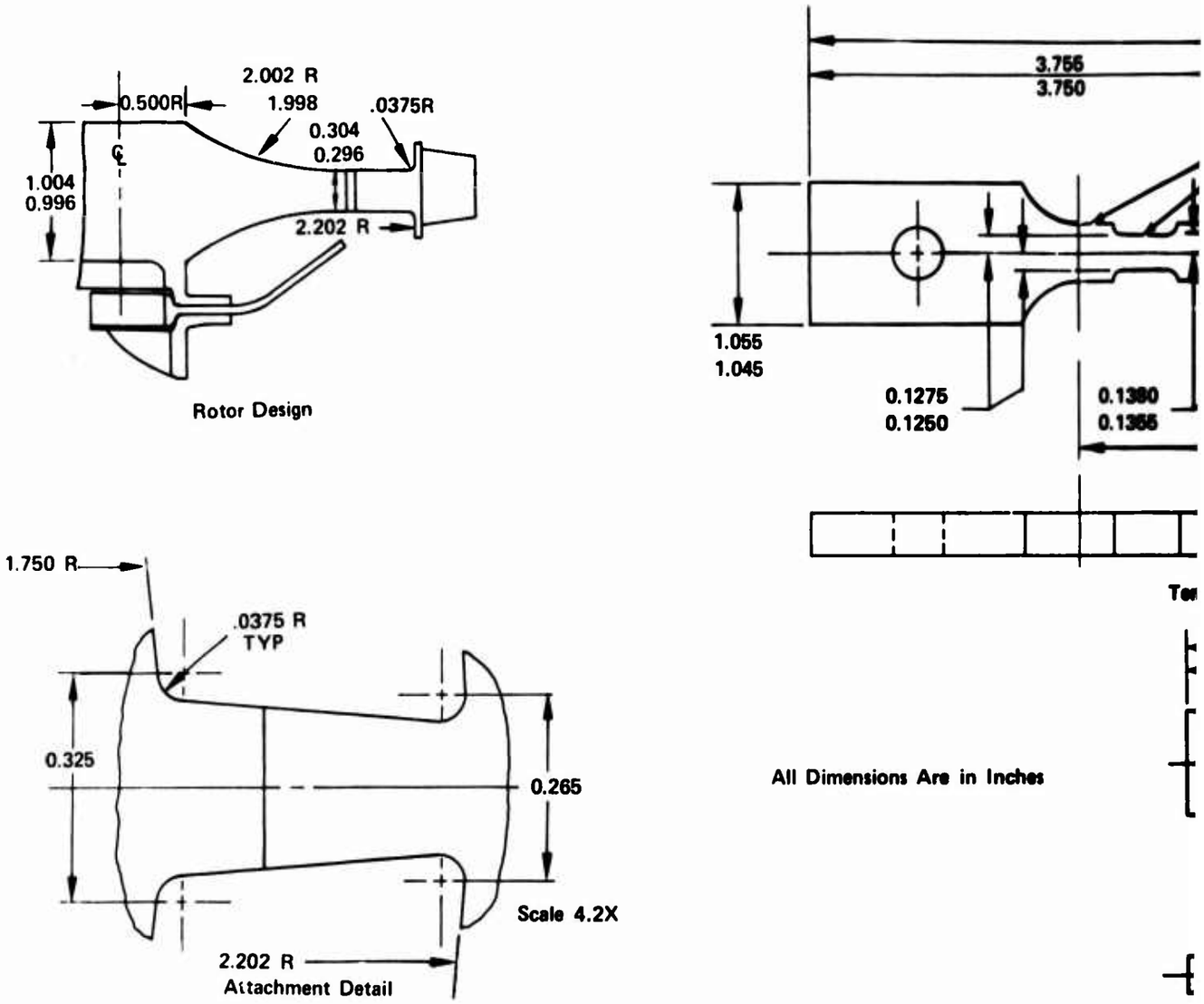

Figure 27. Welded Attachment Design.

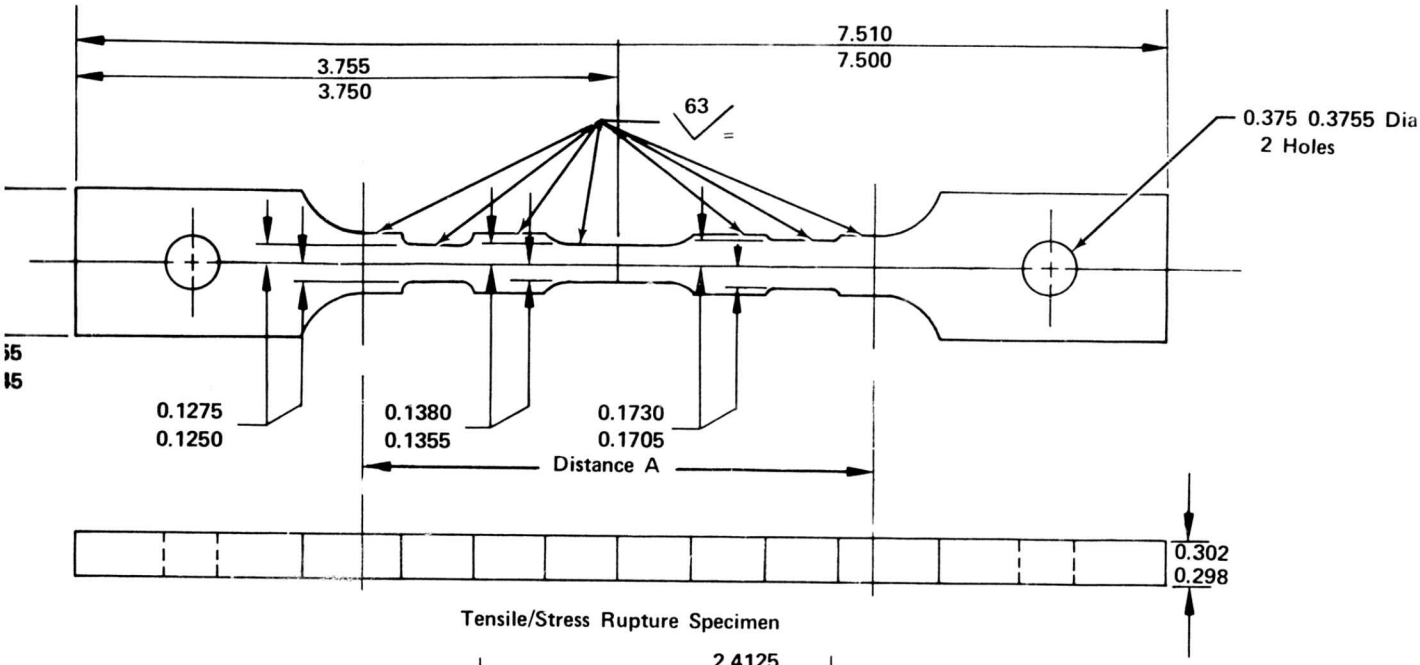

Tensile/Stress Rupture Specimen

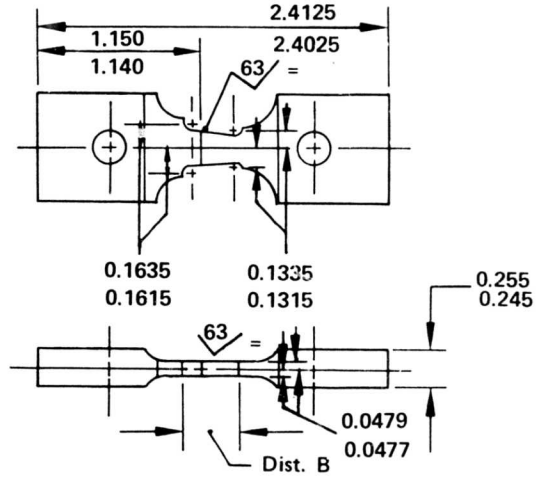

Vibratory Fatigue Specimen

All Dimensions Are in Inches

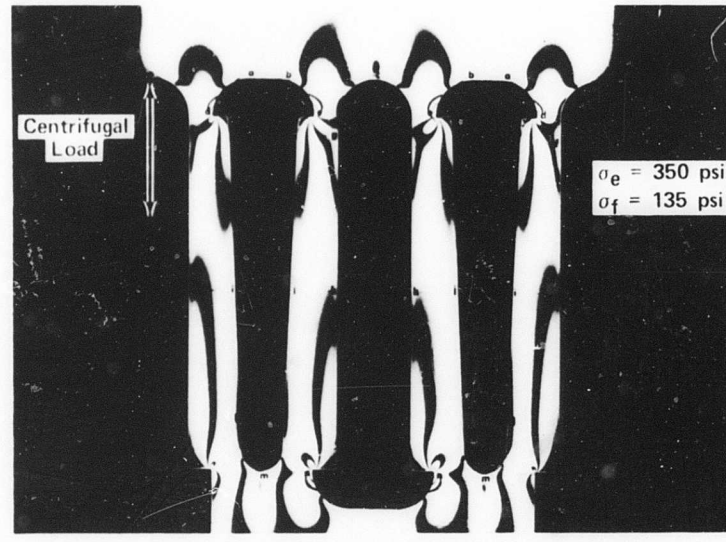

a. Under Simulated Centrifugal Load

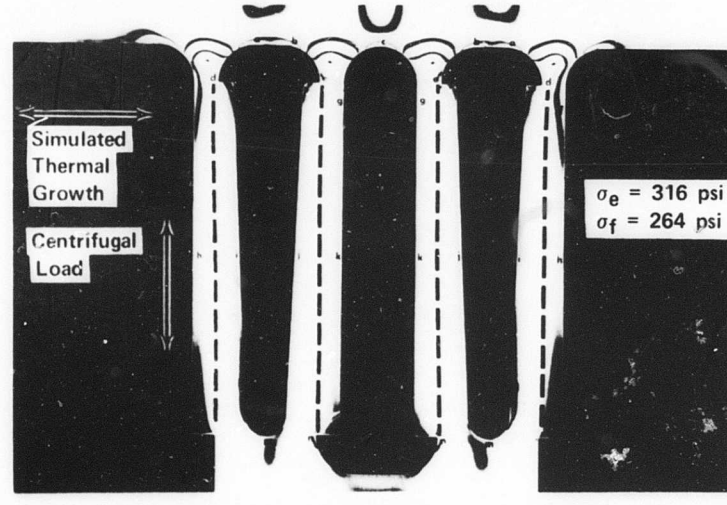

b. Under Simulated Centrifugal Load and Blade Thermal Growth (Combined Load)

Figure 28. Photoelastic Model of Original Brazed Attachment Design.

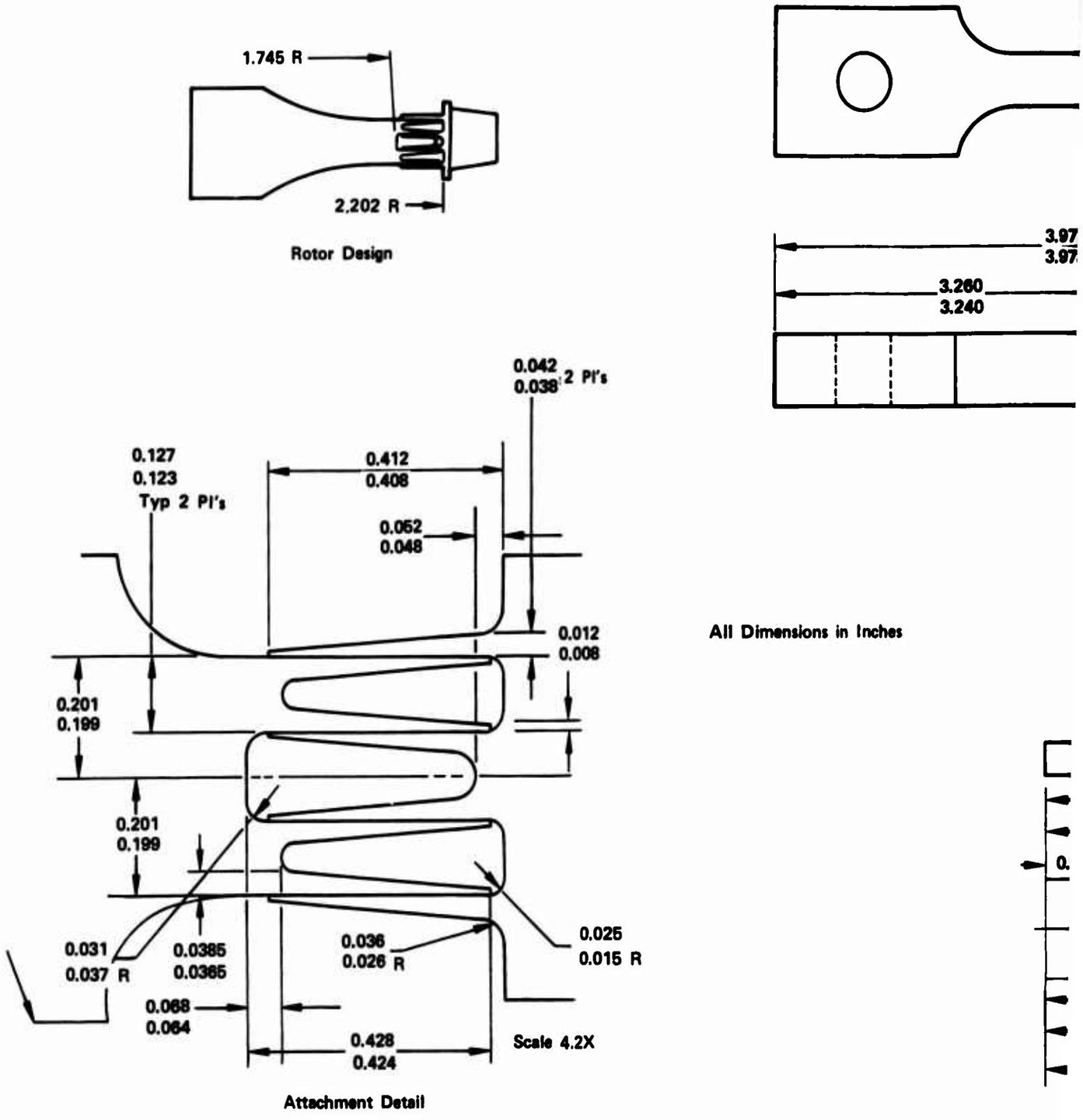

Figure 30. Brazed Attachment Design.

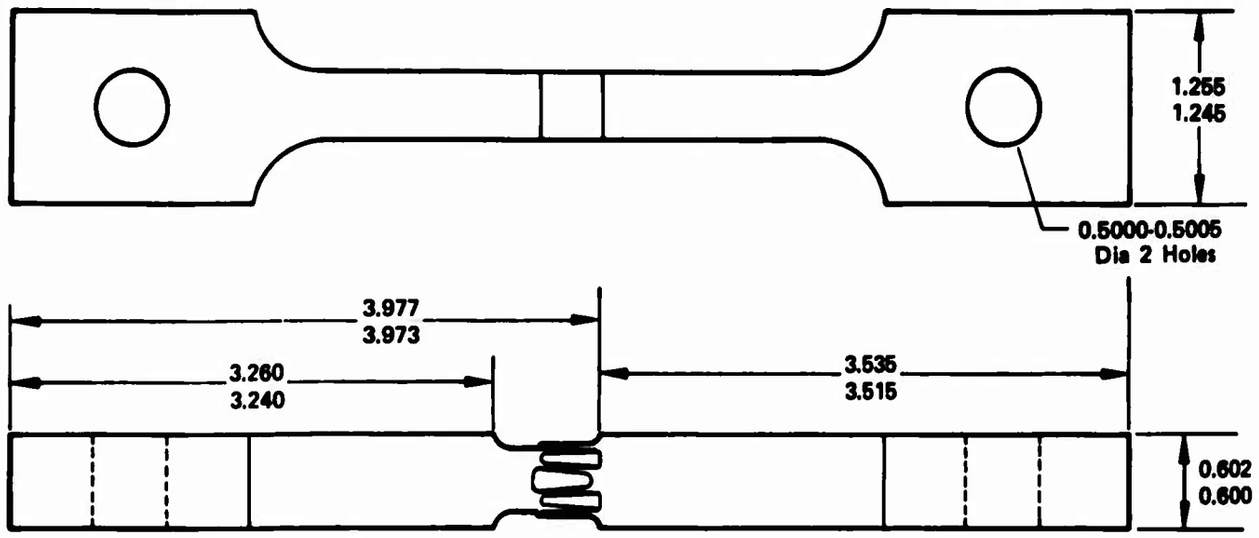

Tensile/Stress Rupture Specimen

All Dimensions in Inches

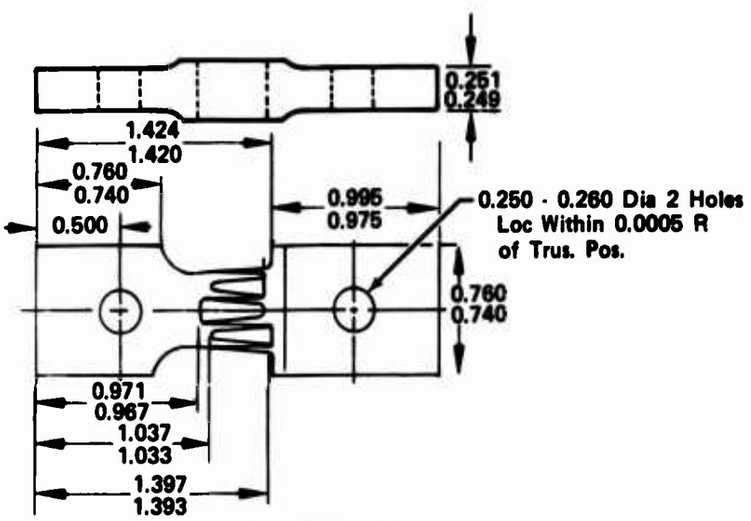

Vibratory/Fatigue Specimen

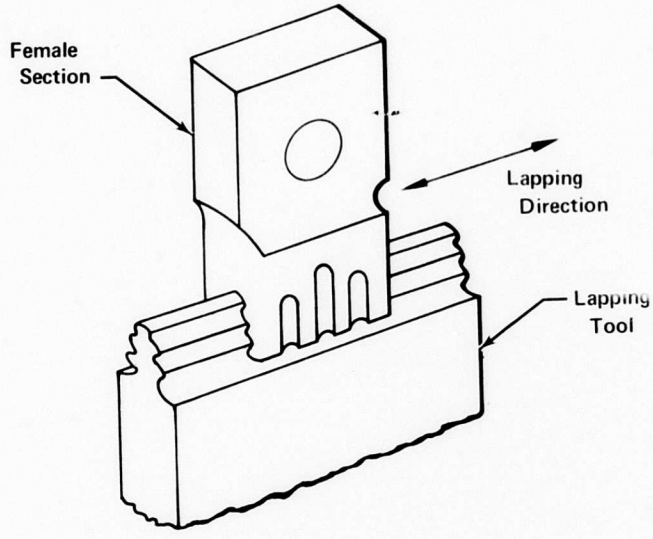

Figure 31. Fir-Tree Lapping Operation.

Figure 32. Fir-Tree Tensile and Stress Rupture Specimens.

Figure 33. Fir-Tree Fatigue Specimens.

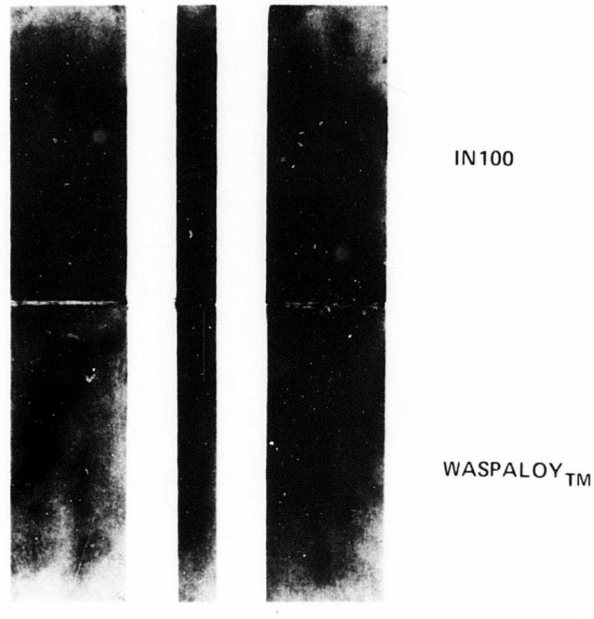

Figure 34. Electron Beam Welded Bars.

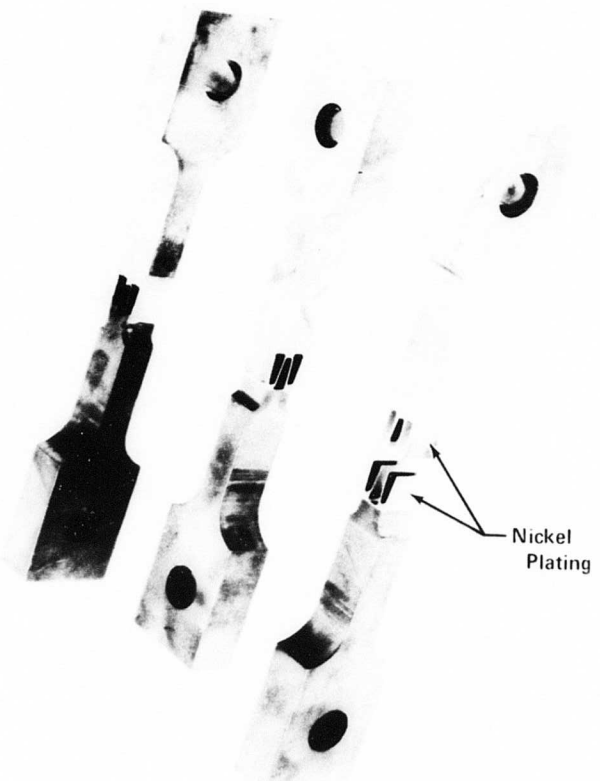

Figure 35. Brazed Tensile and Stress Rupture Specimens.

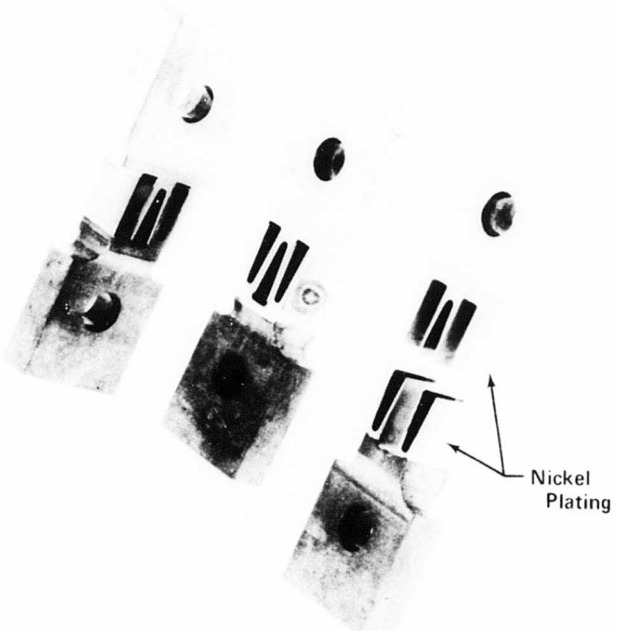

Figure 36. Brazed Fatigue Specimens.

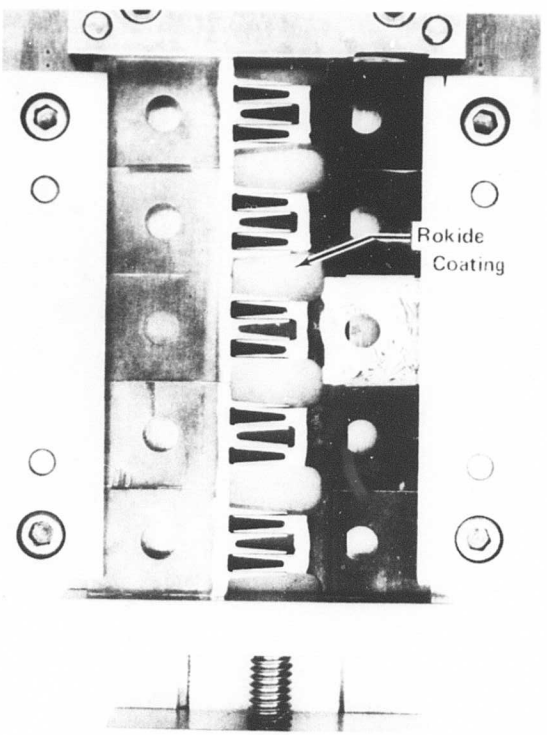

Figure 37. Fatigue Specimen Braze Fixture.

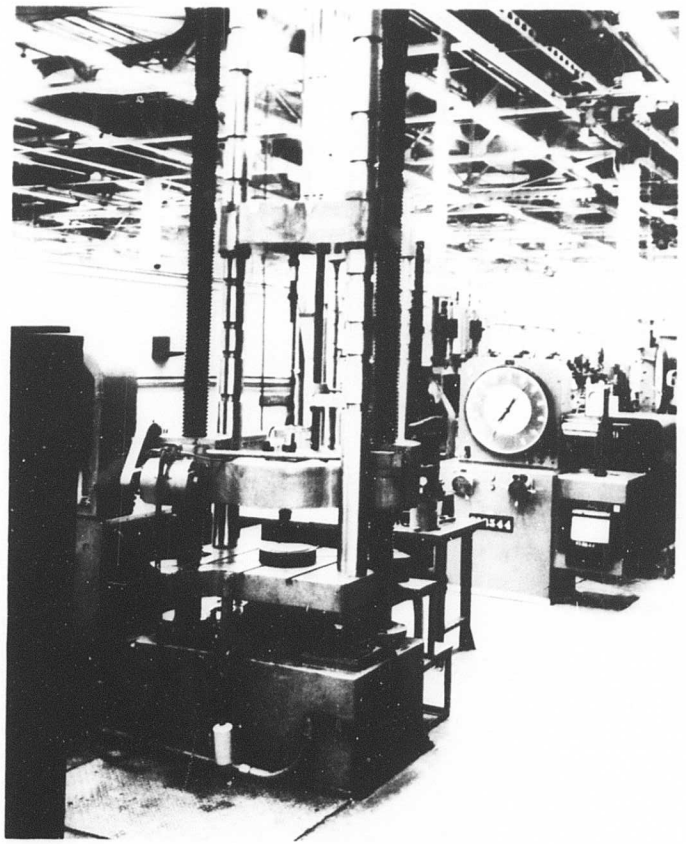

Figure 38. Tinius Olsen Tensile Testing Equipment.

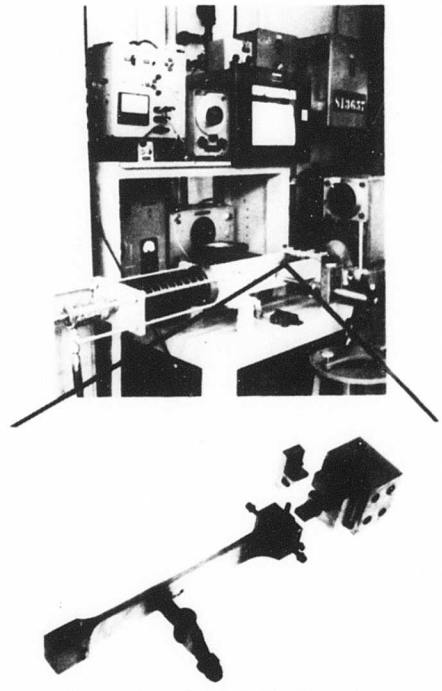

Resonating Beam With Brazed
Fatigue Specimen

Figure 39. Resonating Beam Rig.

Figure 40. Arc Weld Manufacturing Co. Stress Rupture Machines.

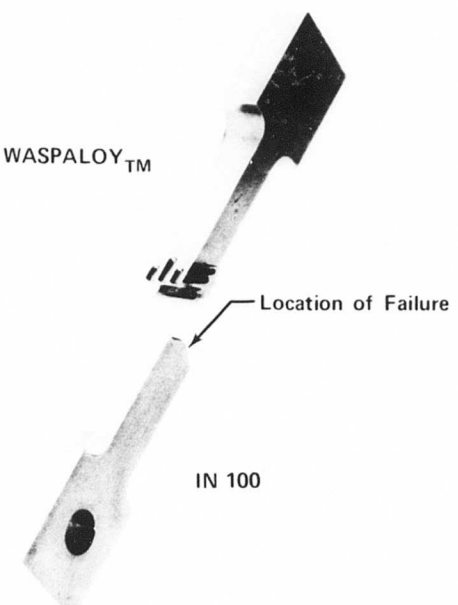

Figure 41. Typical Fir-Tree Tensile Test Failure.

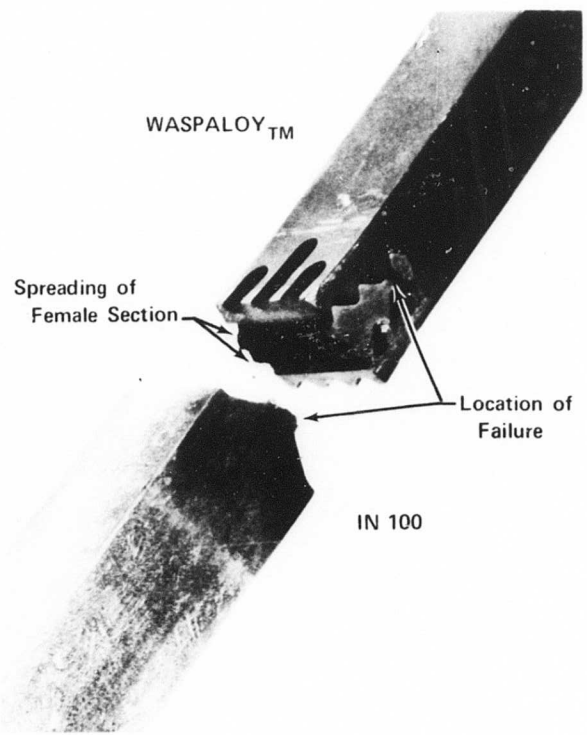

Figure 42. Typical Fir-Tree Stress Rupture Failure Prior to Clamp Modification.

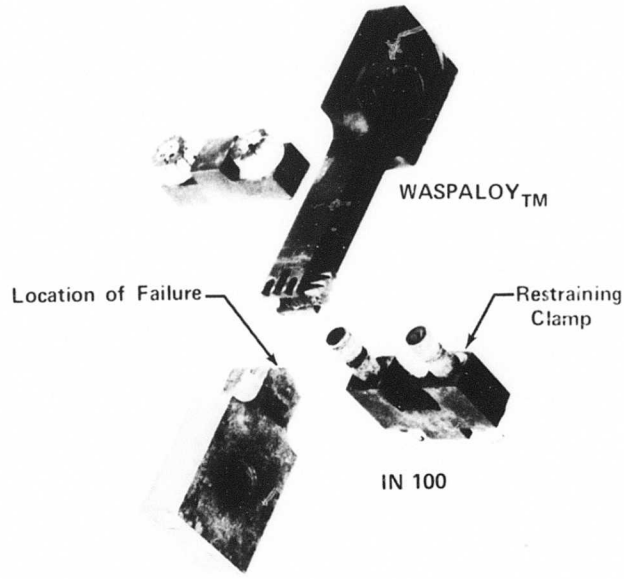

Figure 43. Typical Fir-Tree Stress Rupture Failure After Clamp Modification.

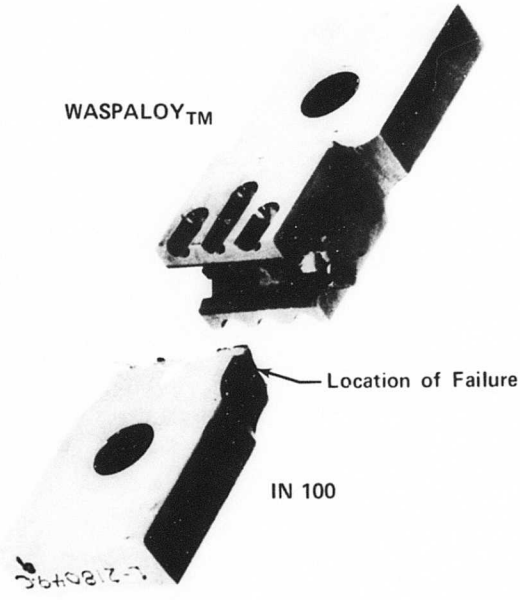

Figure 44. Typical Fir-Tree Vibratory Test Failure.

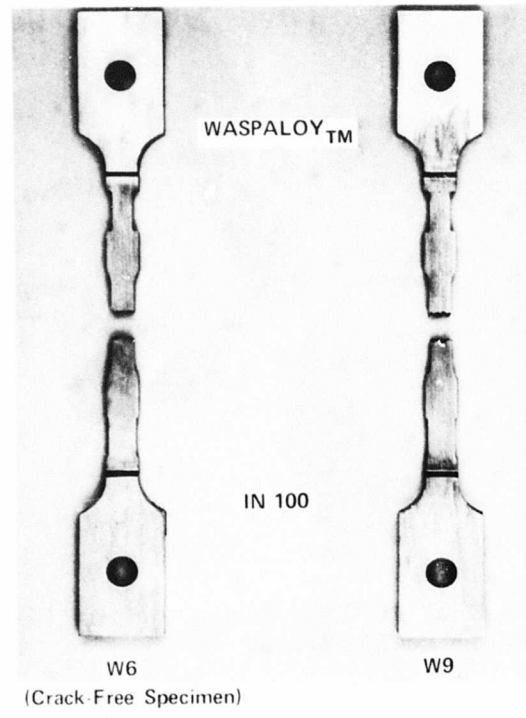

Figure 45. Welded Attachment Tensile Test Specimens.

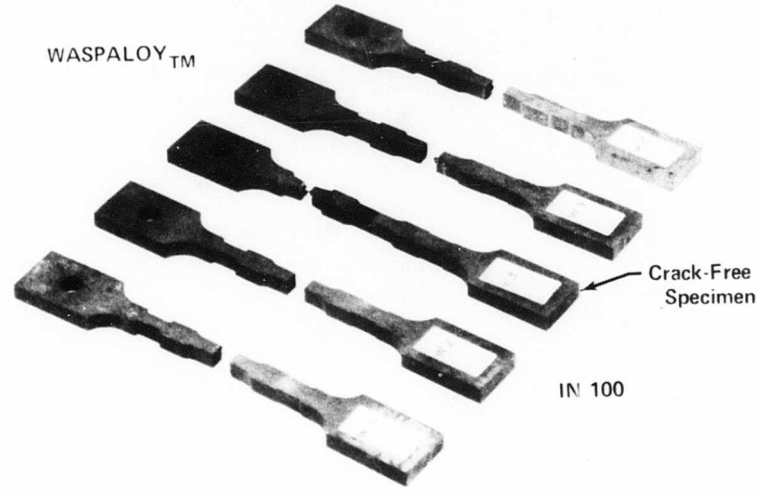

Figure 46. Welded Attachment Stress Rupture Test Specimens.

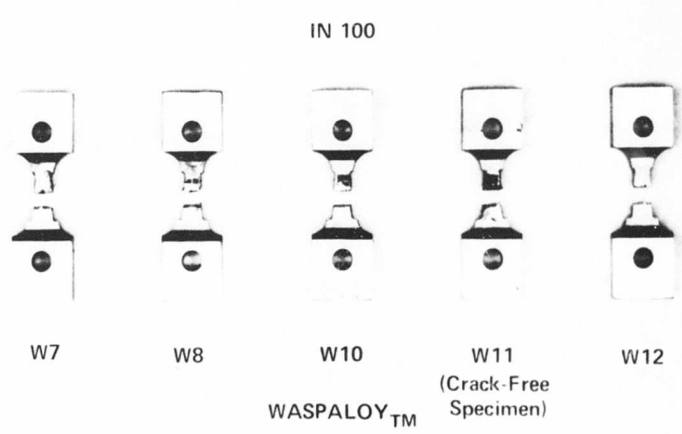

Figure 47. Welded Attachment Vibratory Test Specimens.

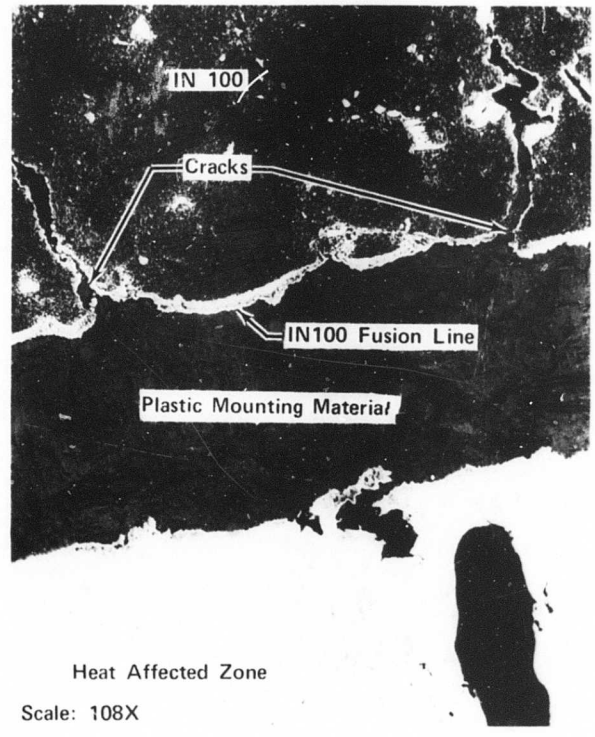

Figure 48. Photomicrograph of IN 100 Cracks.

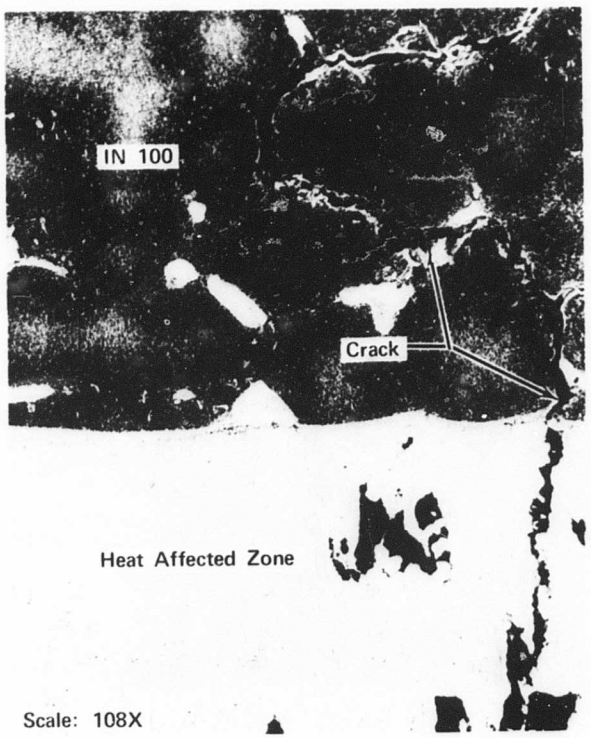

Figure 49. Photomicrograph of IN 100 Cracks.

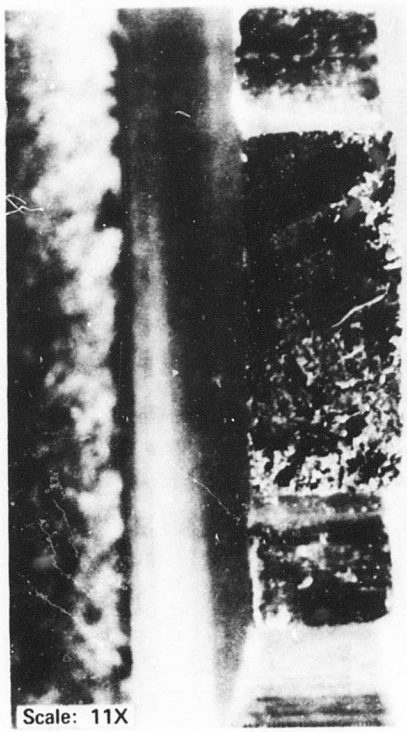

Figure 50. End View of Fatigue Specimen Fracture Face.

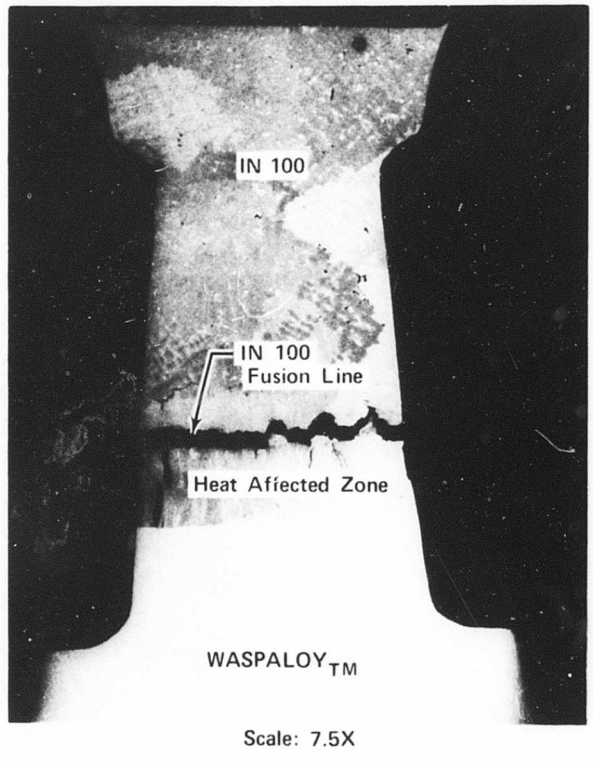

Figure 51. Fatigue Specimen Failure.

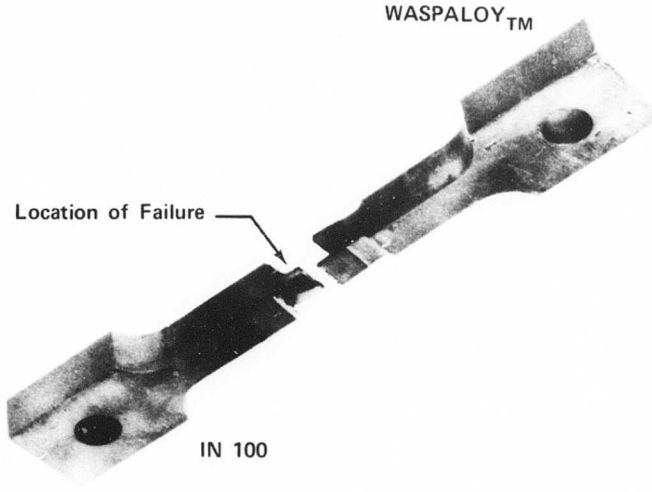

Figure 52. Typical Brazed Tensile Test Failure.

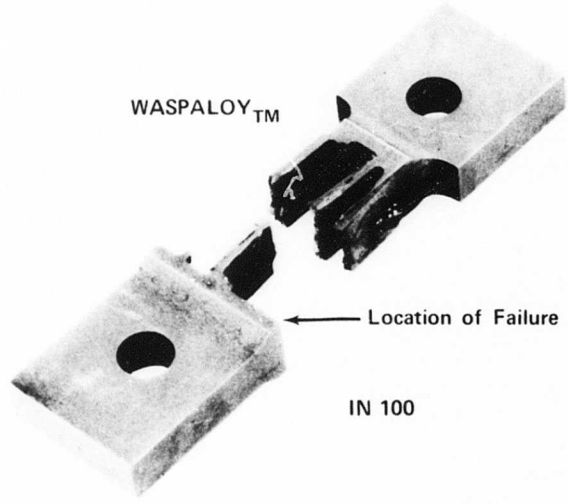

Figure 53. Typical Brazed Vibratory Test Failure.

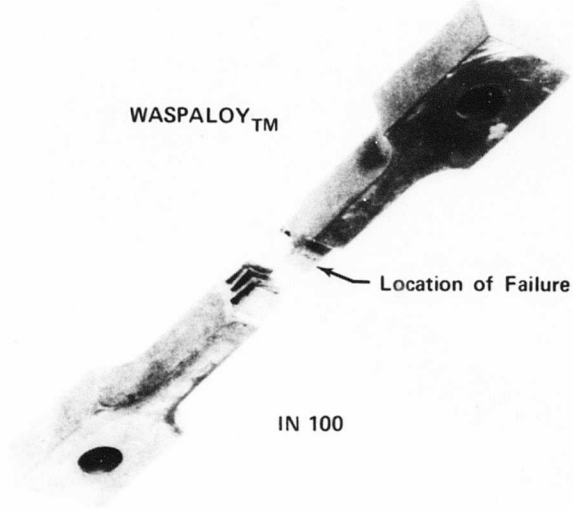

Figure 54. Typical Brazed Stress Rupture Failure.

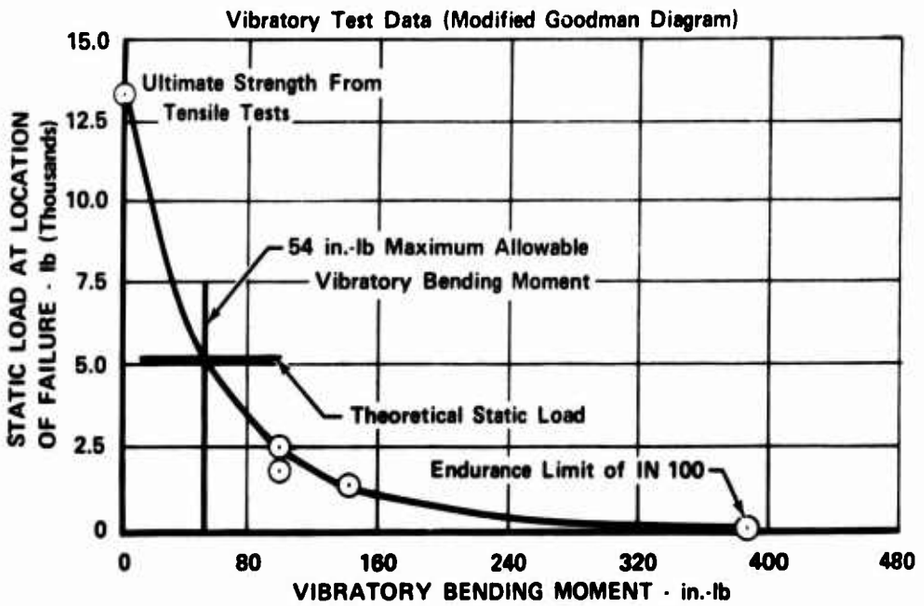

Figure 55. Fir-Tree Design.

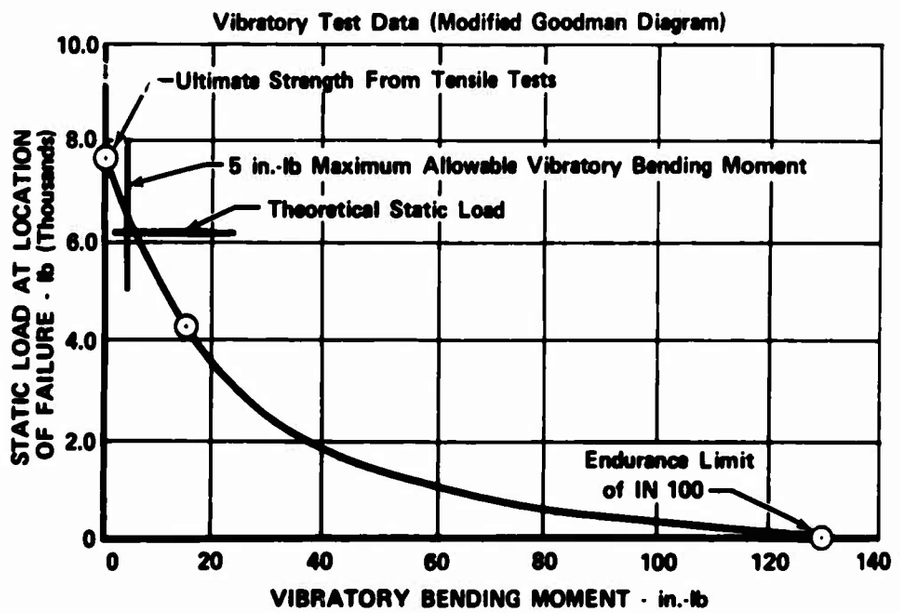

Figure 56. Welded Design.

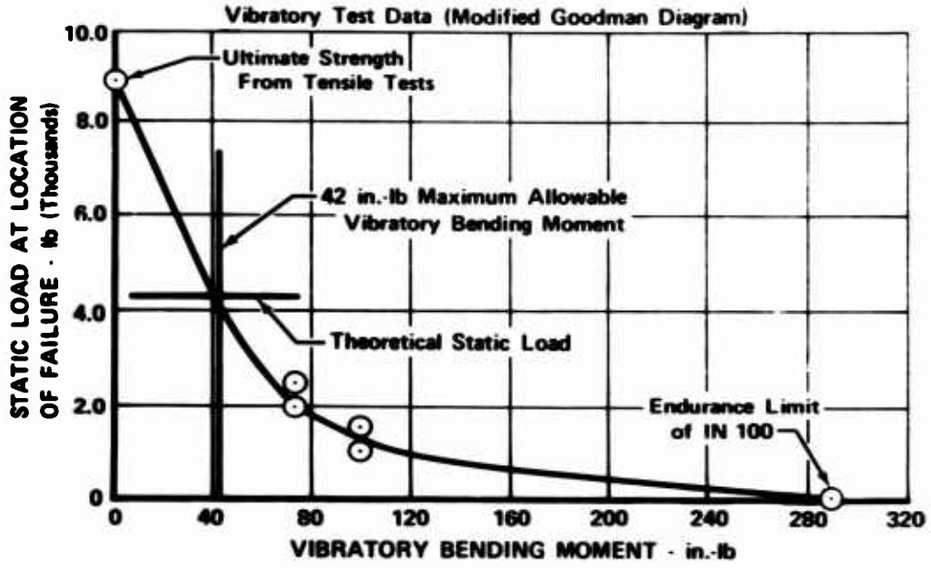

Figure 57. Brazed Design.

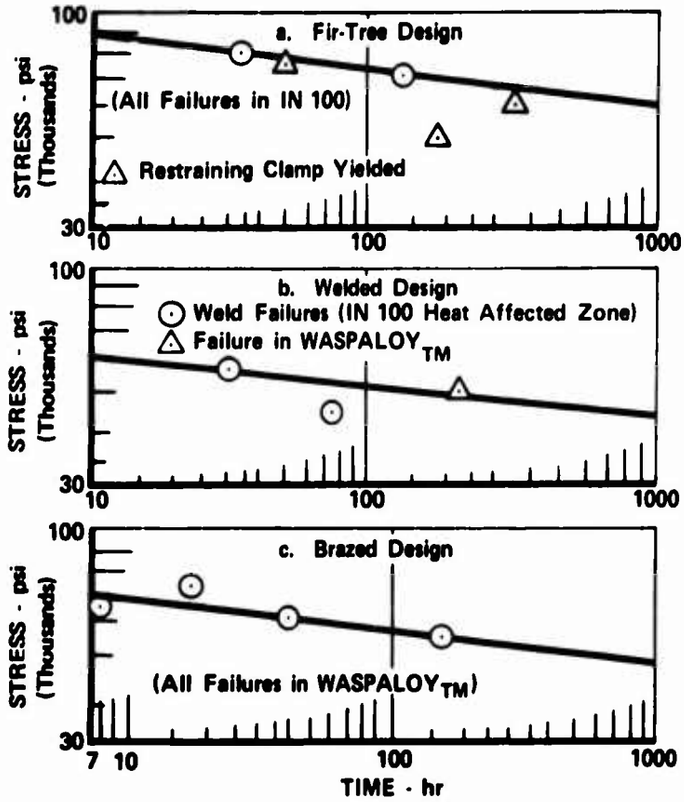

Figure 58. Stress Rupture Life of Task IV Attachment Schemes.

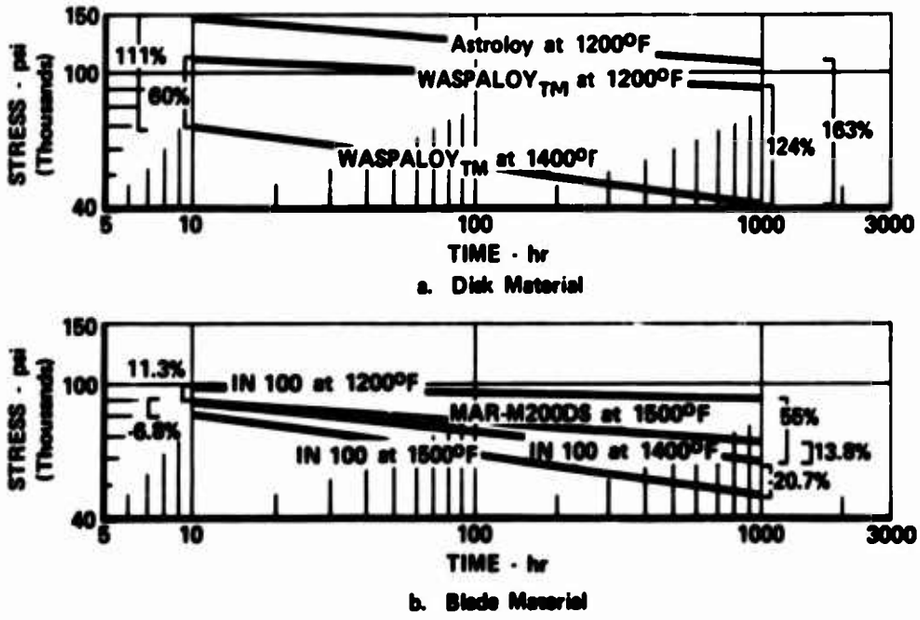

Figure 59. Material Stress Rupture Life.

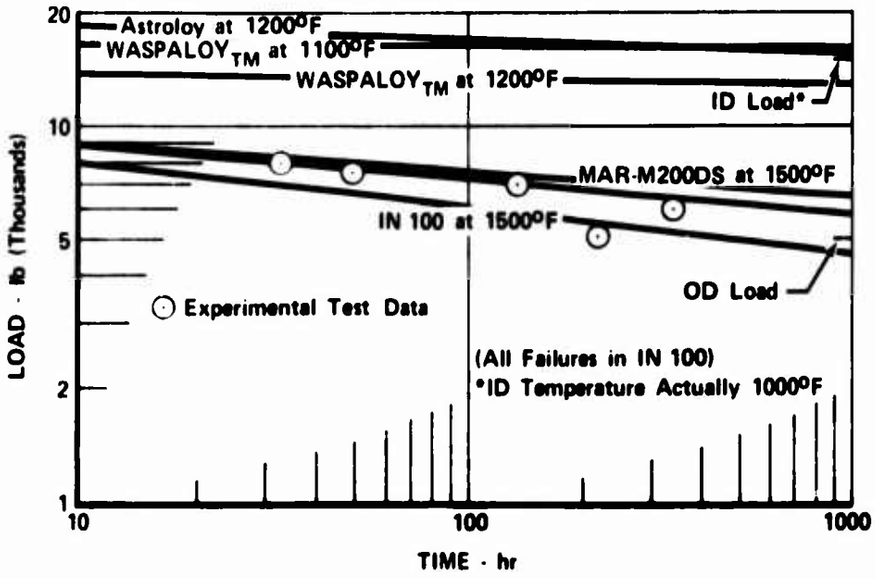

Figure 60. Fir-Tree Design Stress Rupture Data.

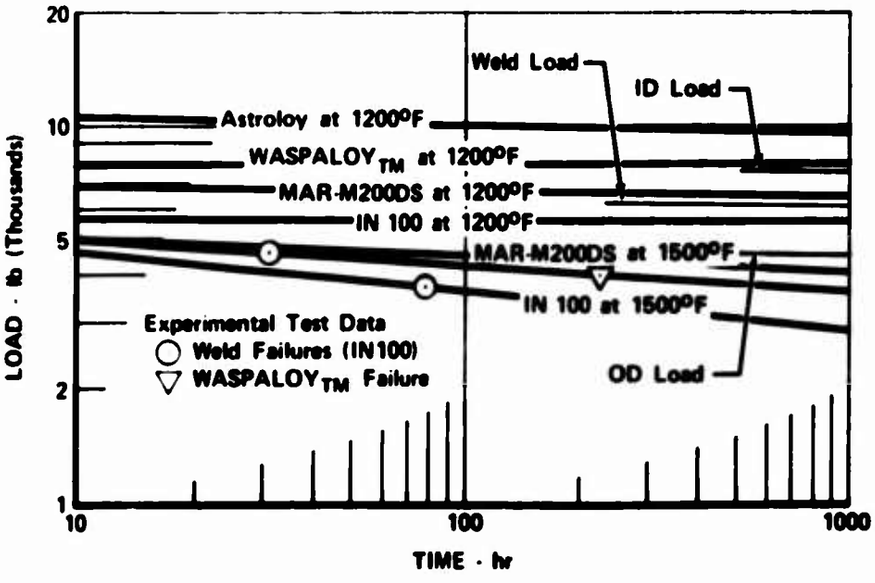

Figure 61. Welded Design Stress Rupture Data.

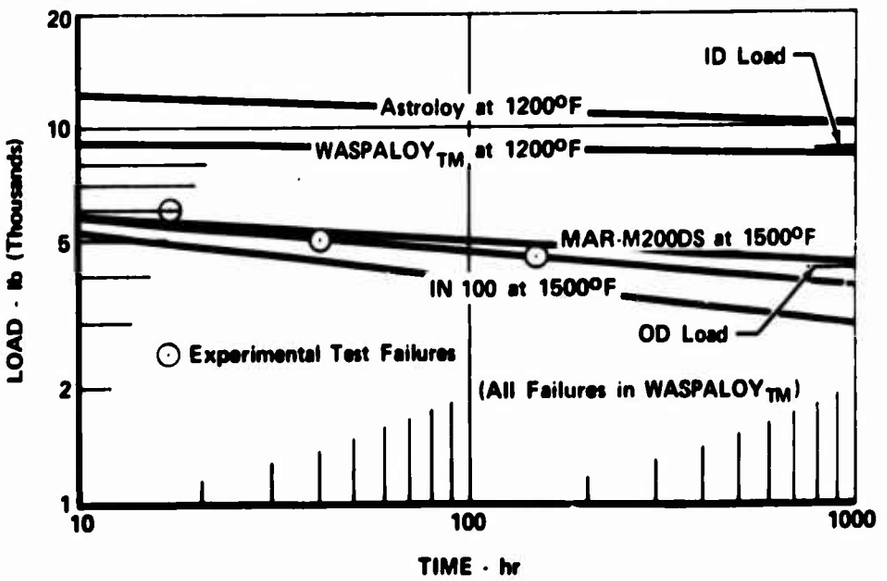

Figure 62. Brazed Design Stress Rupture Data.

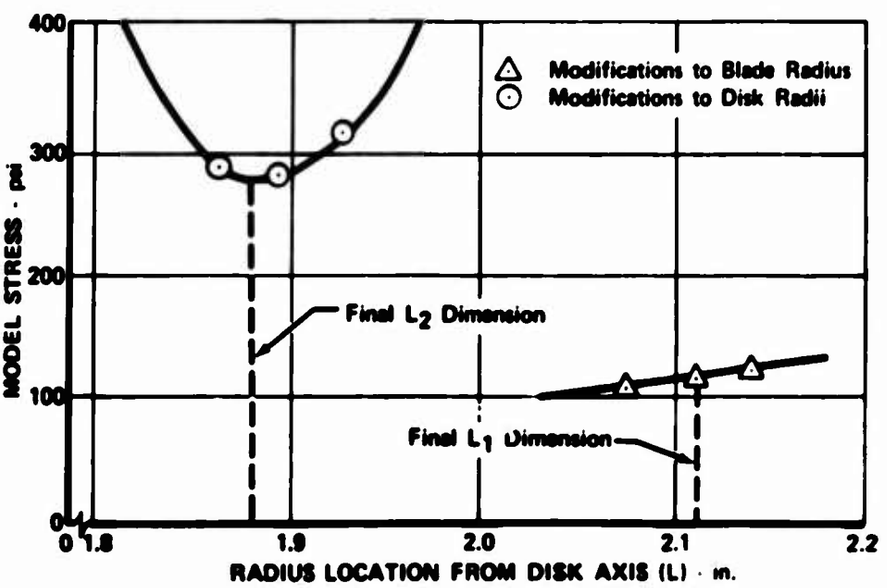

Figure 63. Photoelastic Model Test Results.

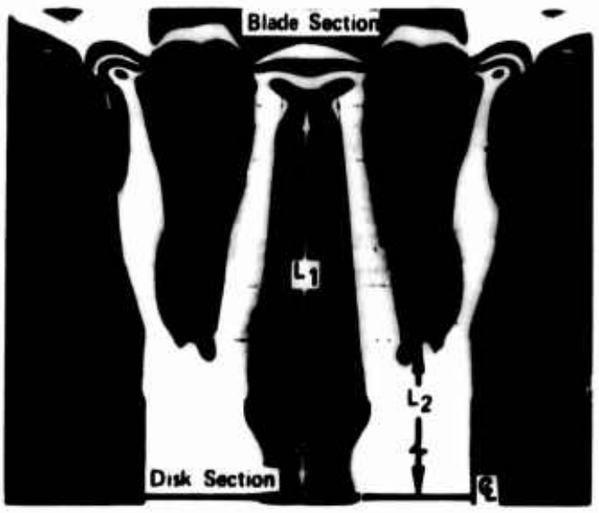

Figure 64. Photoelastic Model of Final Brazed Design Subjected to Radial Load and Simulated Thermal Growth.

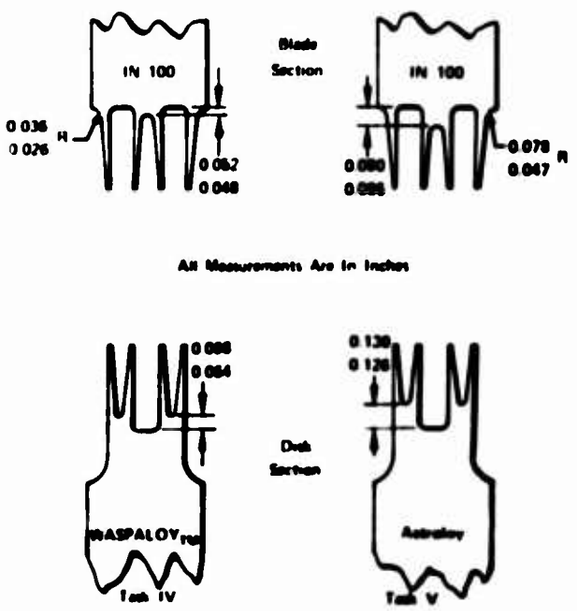

Figure 65. Comparison of Brazed Uniaxial Test Specimen Geometry.

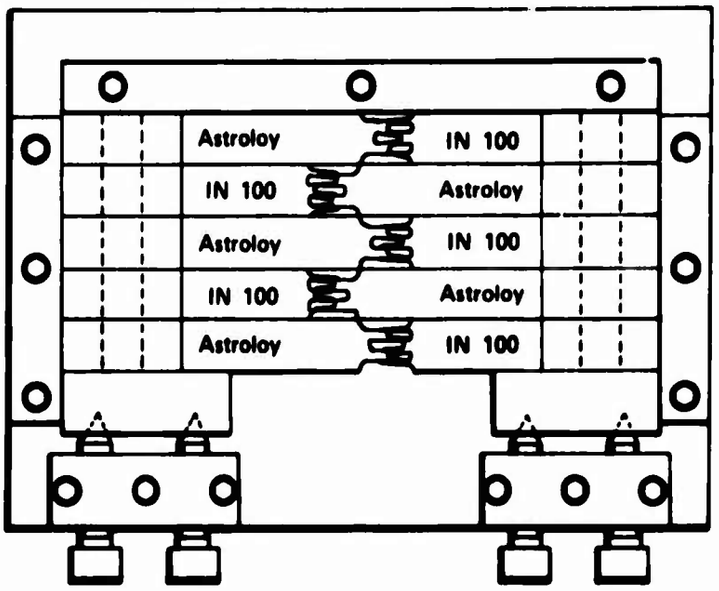

Figure 66. Uniaxial Specimen Brazing Fixture.

Figure 67. Task V Uniaxial Test Specimens.

Figure 68. Uniaxial Stress Rupture Failure (Specimen No. 1).

Figure 69. Uniaxial Stress Rupture Failure (Specimen No. 2).

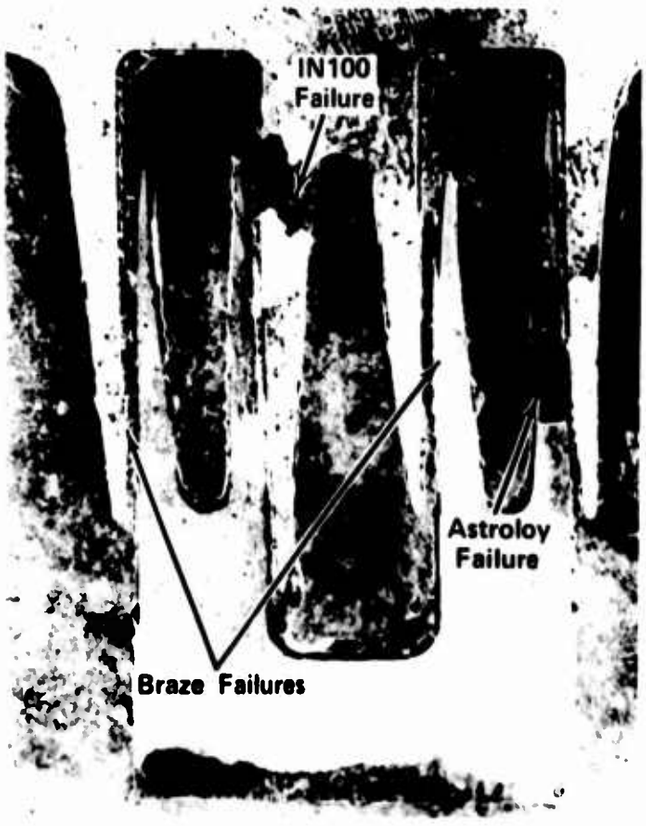

Figure 70. Uniaxial Stress Rupture Failure (Specimen No. 3).

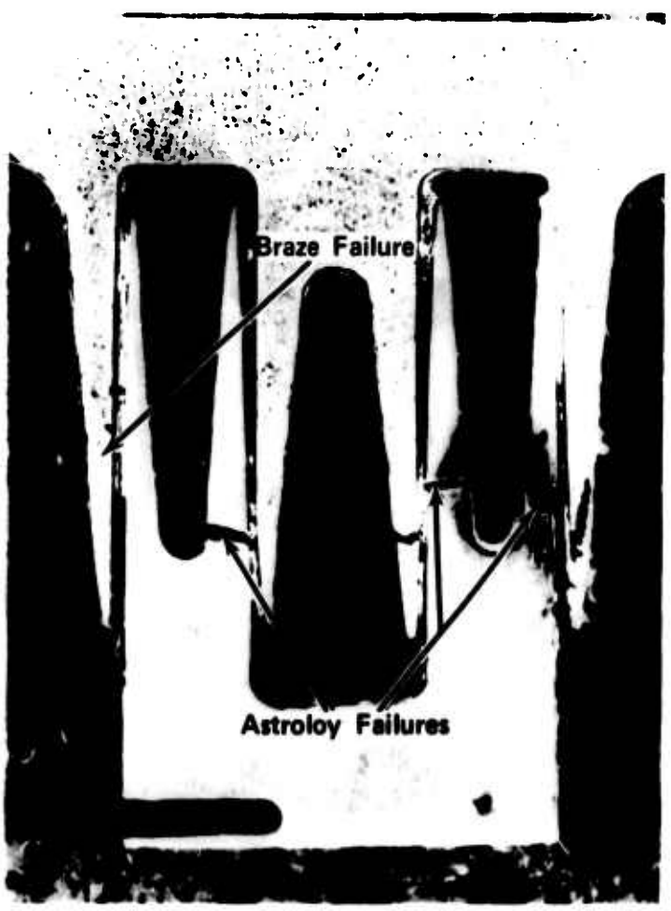

Figure 71. Uniaxial Stress Rupture Failure (Specimen No. 4).

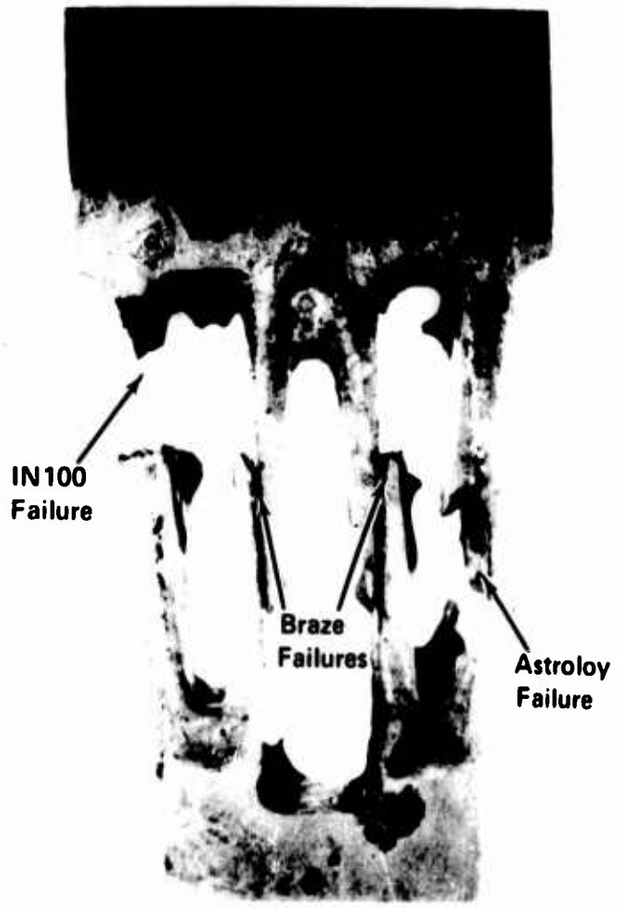

Figure 72. Uniaxial Stress Rupture Failure (Specimen No. 5).

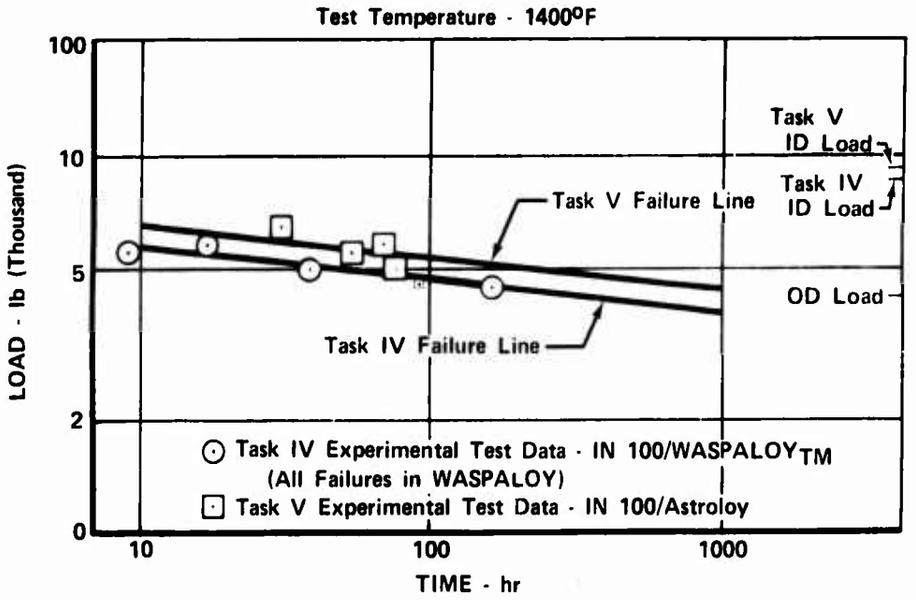

Figure 73. Brazed Design Stress Rupture Data.

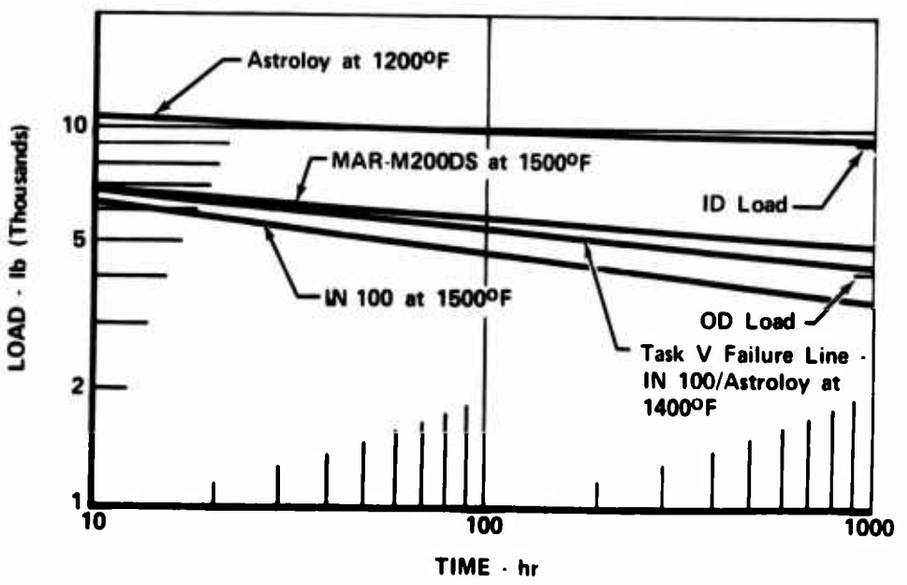

Figure 74. Task V Brazed Design Stress Rupture Life.

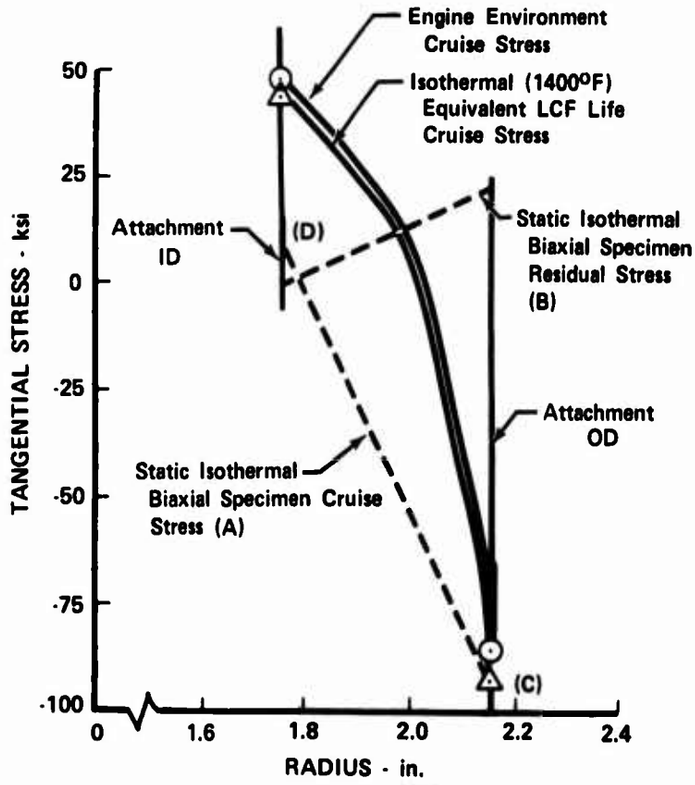

Figure 75. Attachment Stress Distribution.

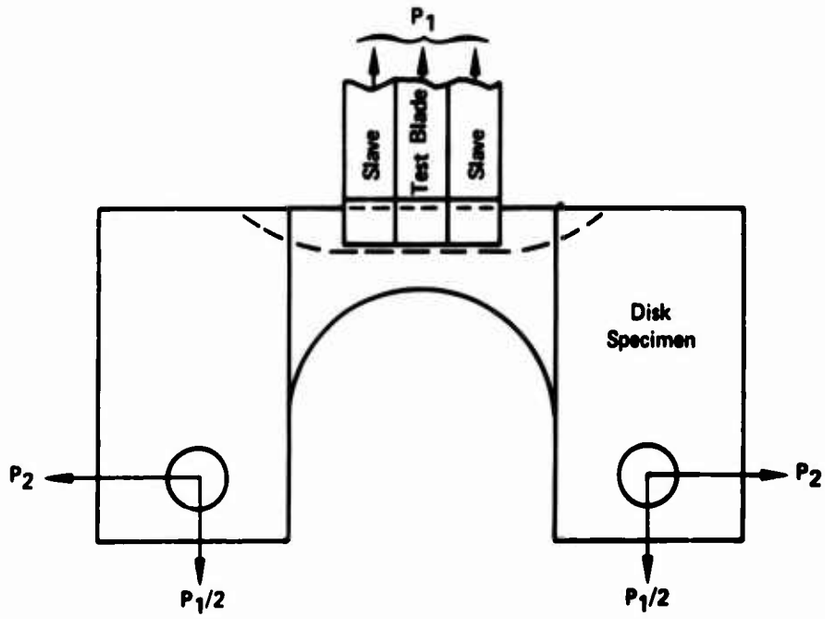

Figure 76. Brazed Biaxial Test Specimen.

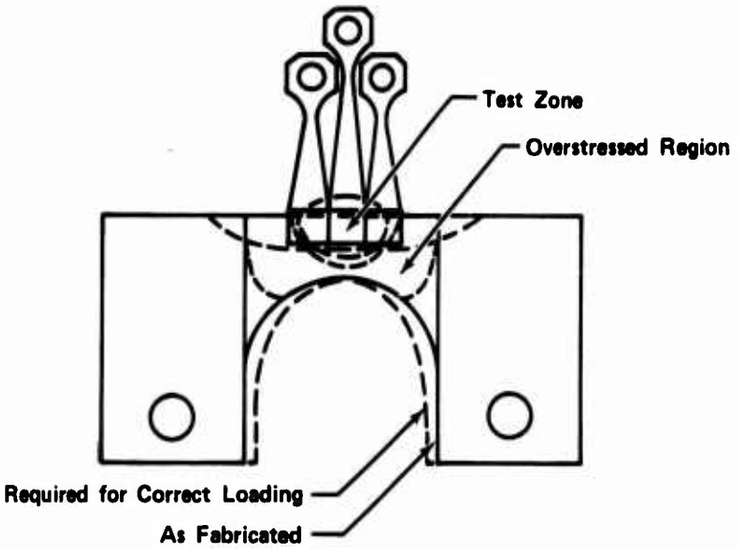

Figure 77. Biaxial Specimen.

Figure 78. Biaxial Specimen Center Support Plug.

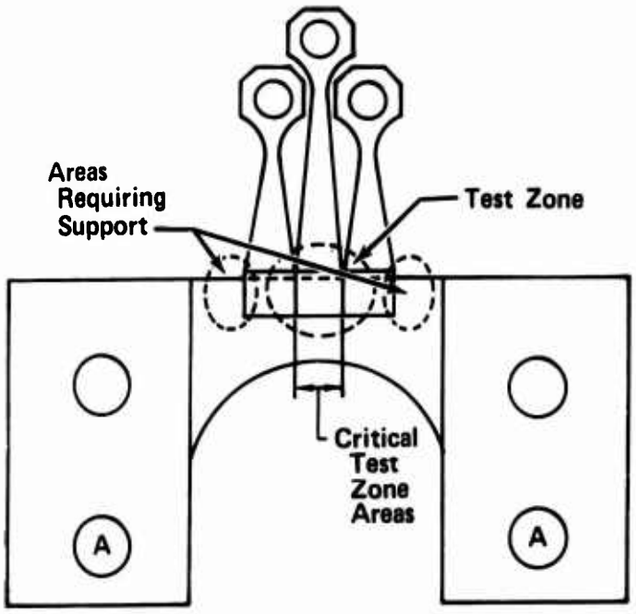

Figure 79. Biaxial Specimen.

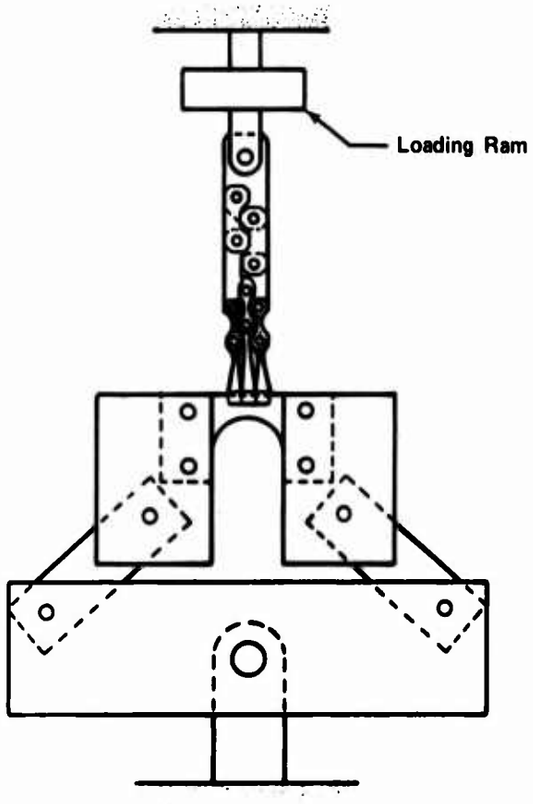

Figure 80. Single Ram Loading Arrangement.

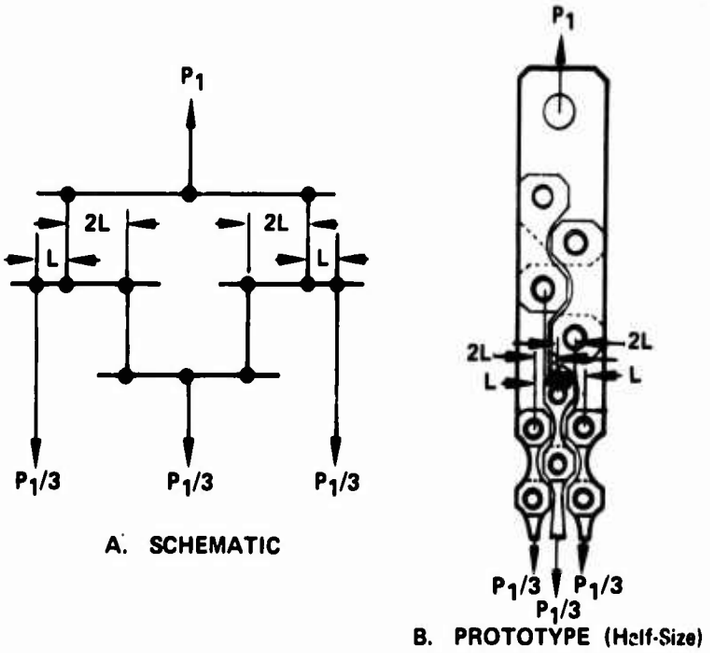

Figure 81. Loading Fixture for Biaxial Specimen.

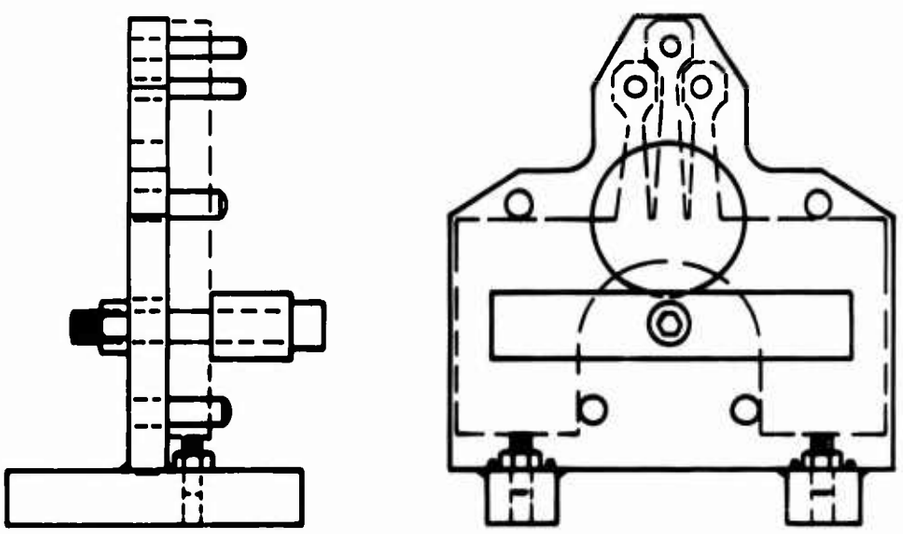

Figure 82. Brazed Specimen Support Fixture.

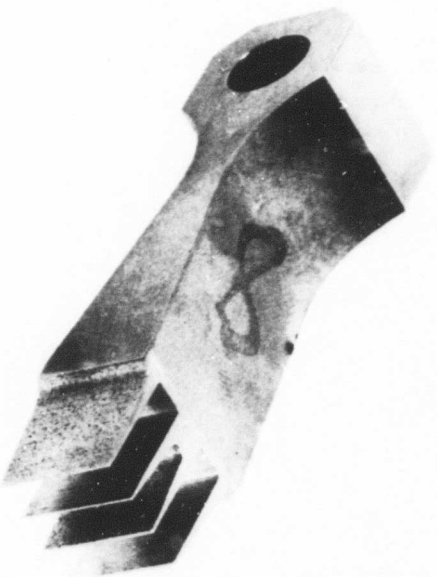

Figure 83. Surface Condition of IN 100 Simulated Blade Attachment Fingers.

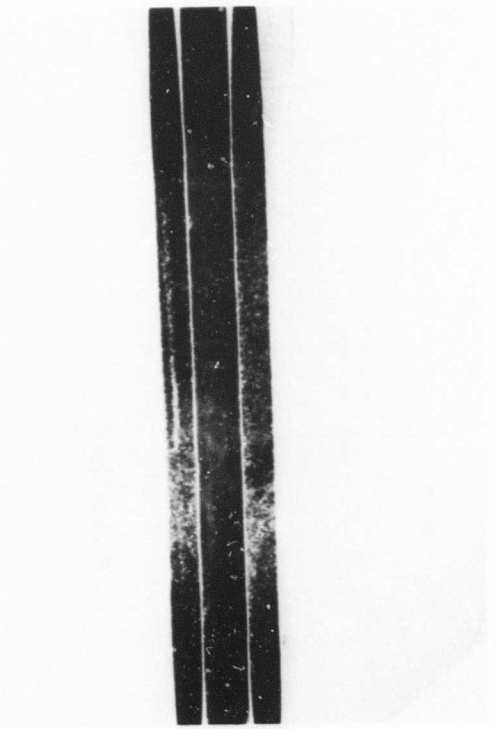

Figure 84. Surface Condition of Astroloy Simulated Disk Attachment Fingers.

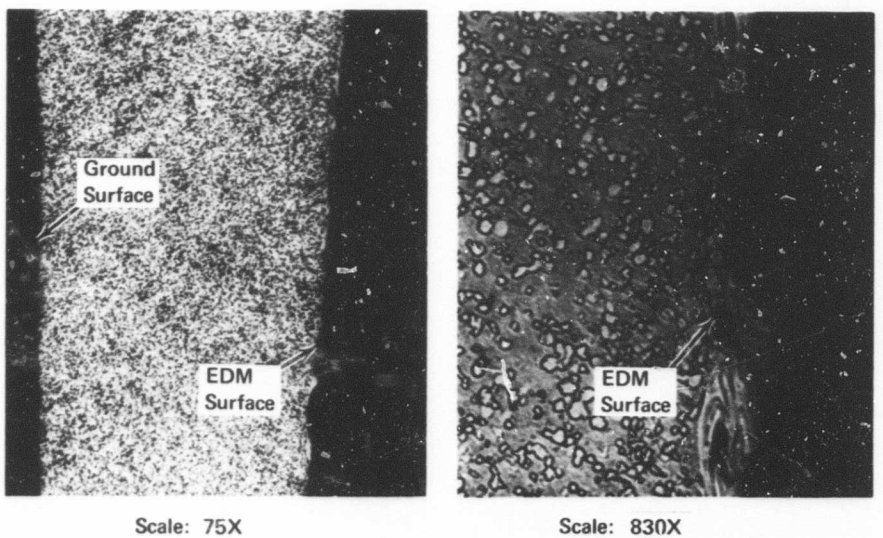

Figure 85. Microphotographs of Astroloy Simulated Disk Attachment Fingers.

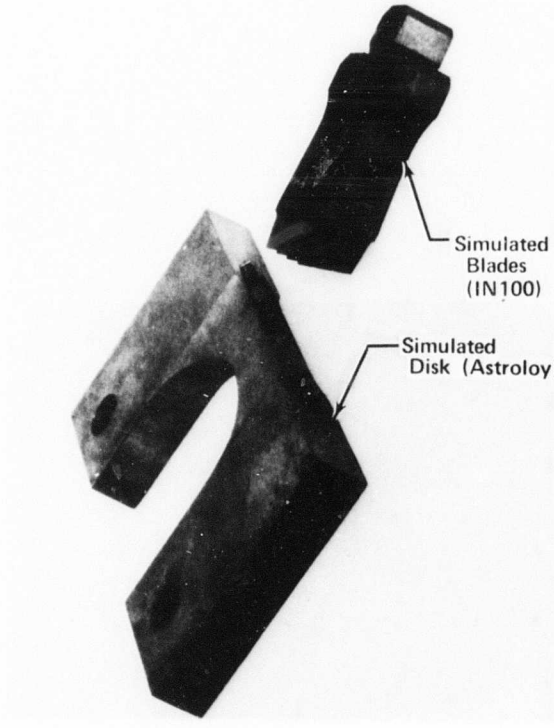

Figure 86. Assembly of Biaxial Test Specimens Prior to Redesign.

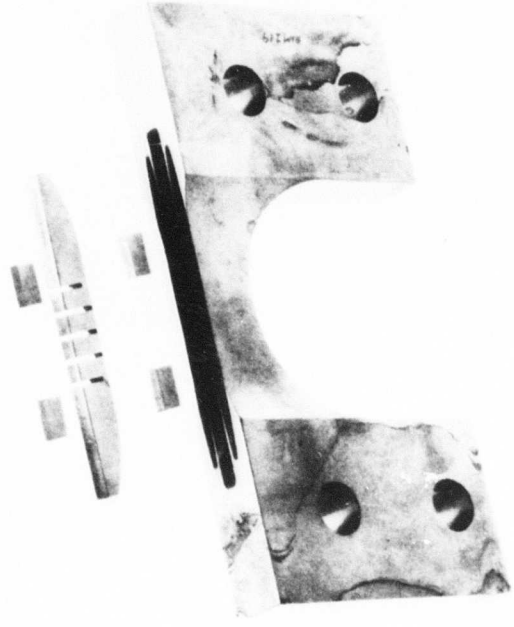

Figure 87. Simulated Disk Specimen With Supports.

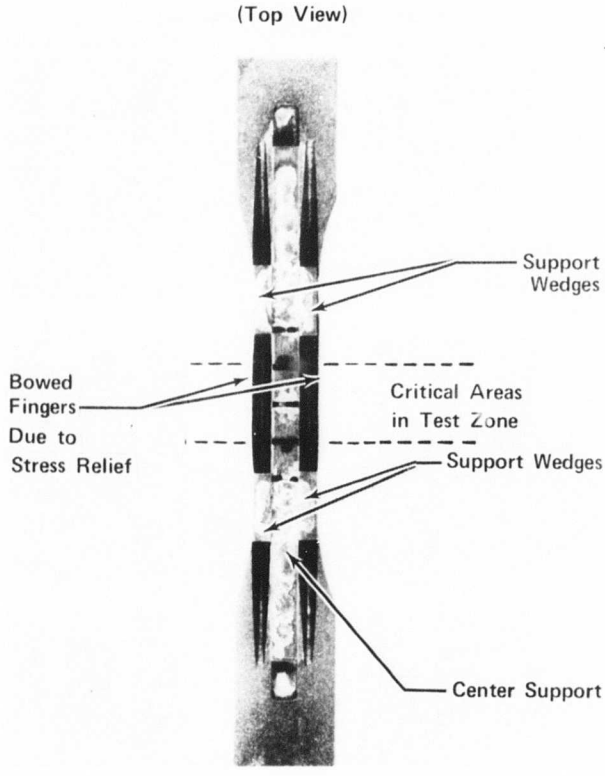

Figure 88. Modified Disk Specimen.

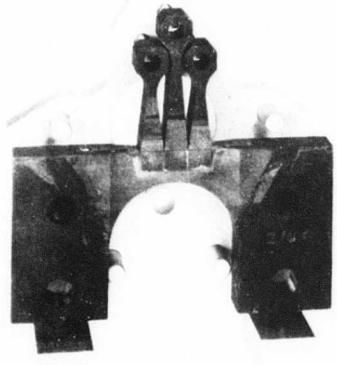

Figure 89. Biaxial Specimen Braze Fixture.

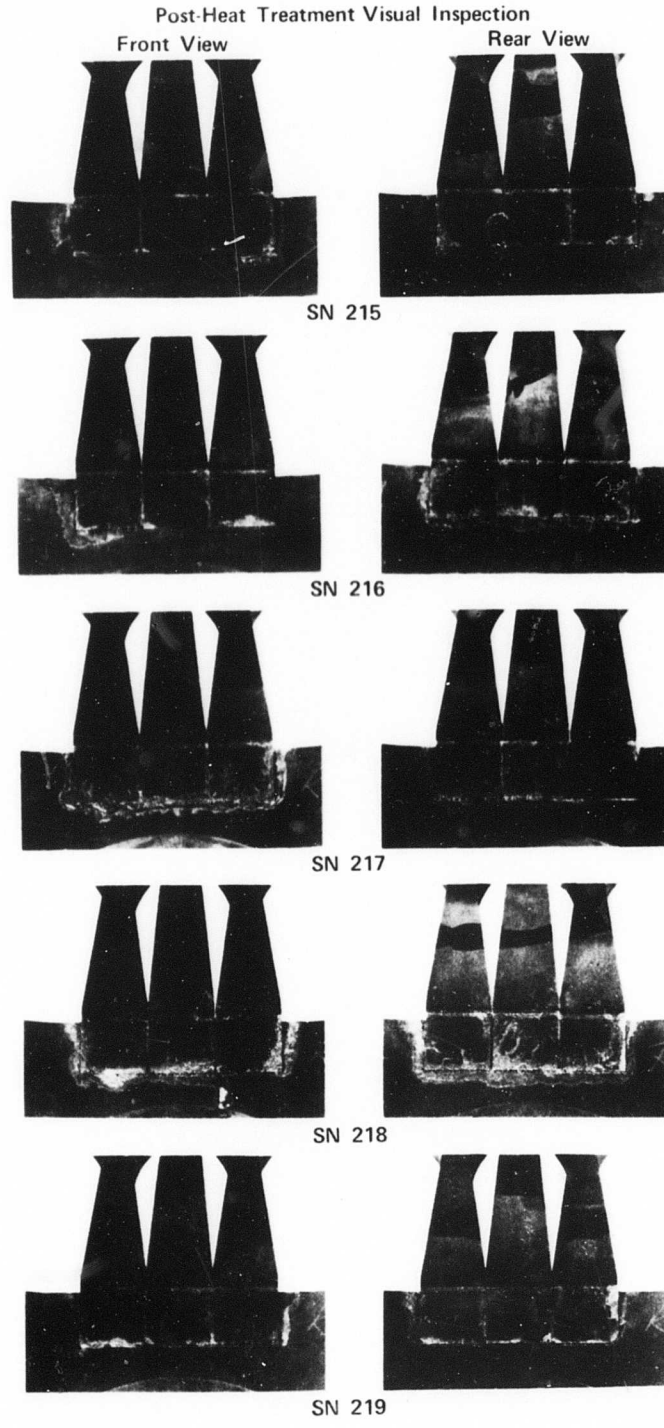

Figure 90. Biaxial Specimen Brazed Attachment.

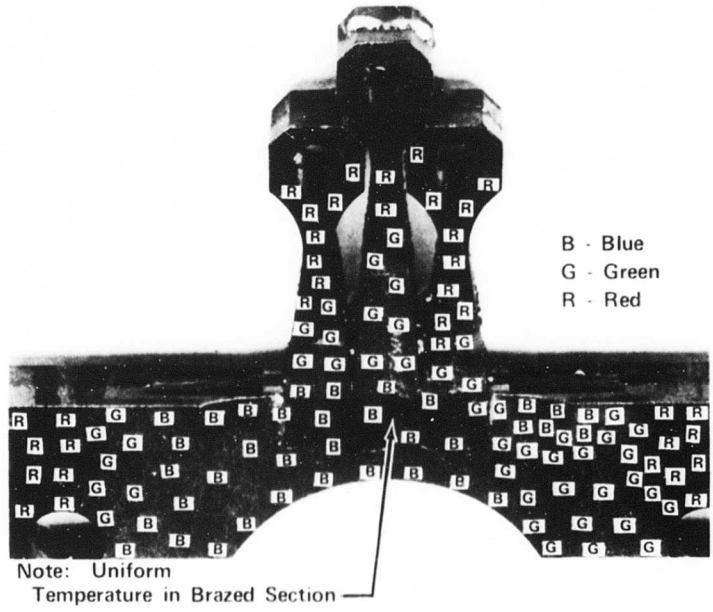

Figure 91. Typical Test Specimen Thermal Response Displaying Good Attachment Braze Coverage.

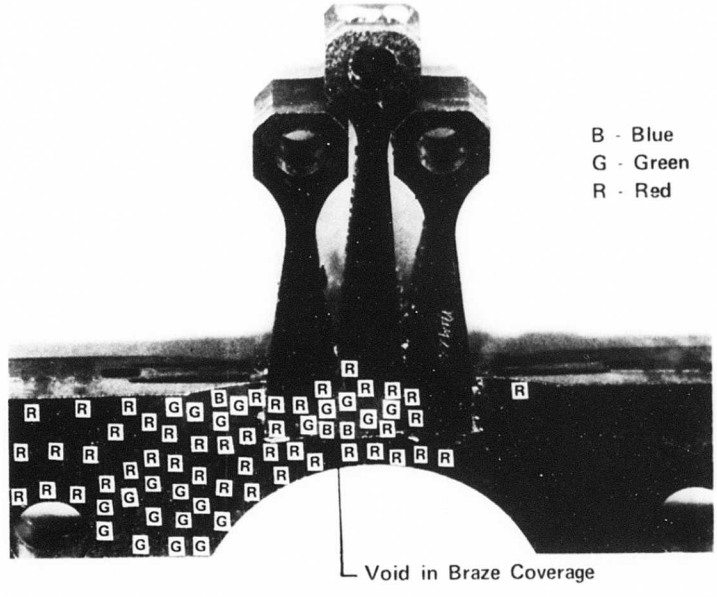

Figure 92. Specimen SN 216 Displaying Small Void in Braze.

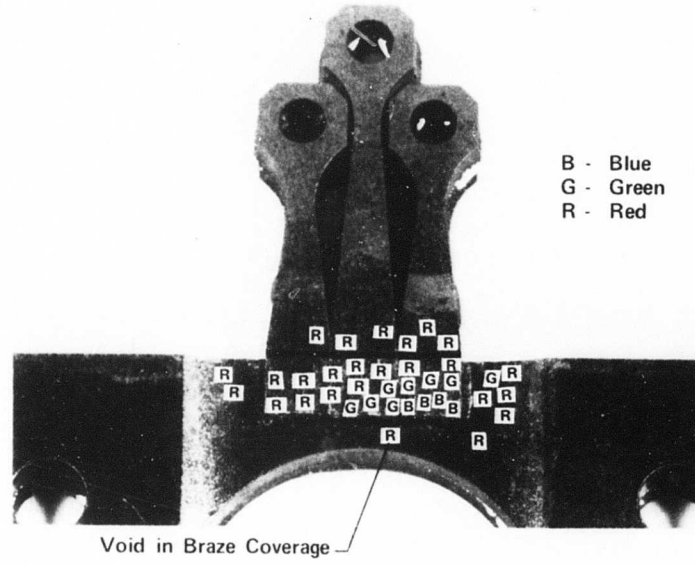

Figure 93. Specimen SN 219 Displaying Large Void in Braze.

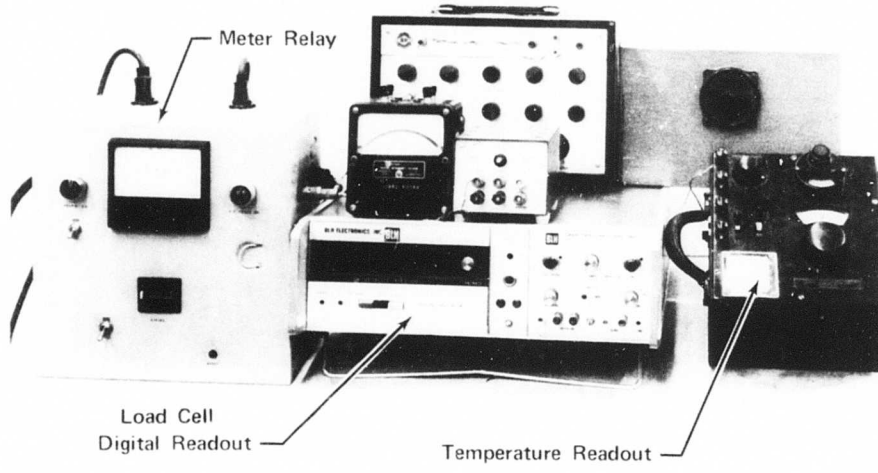

Figure 94. Test Equipment.

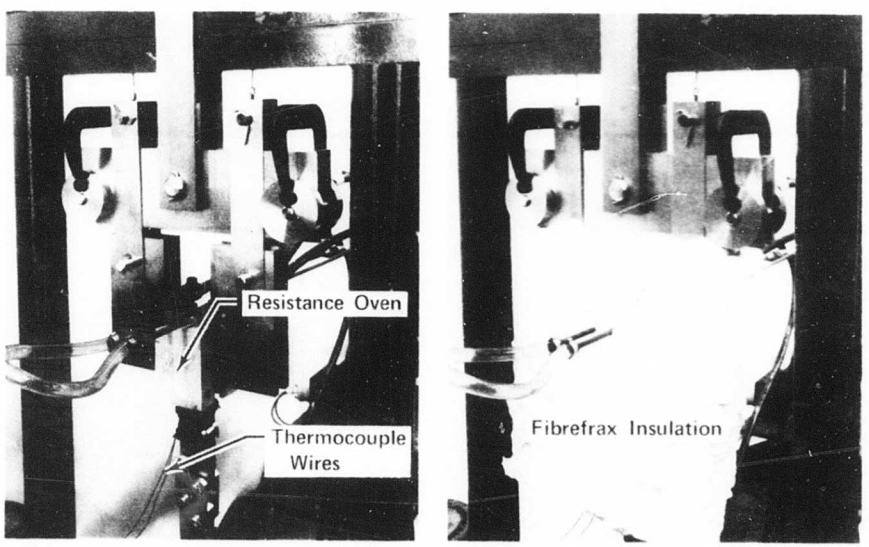

Figure 95. Biaxial Specimen Heater.

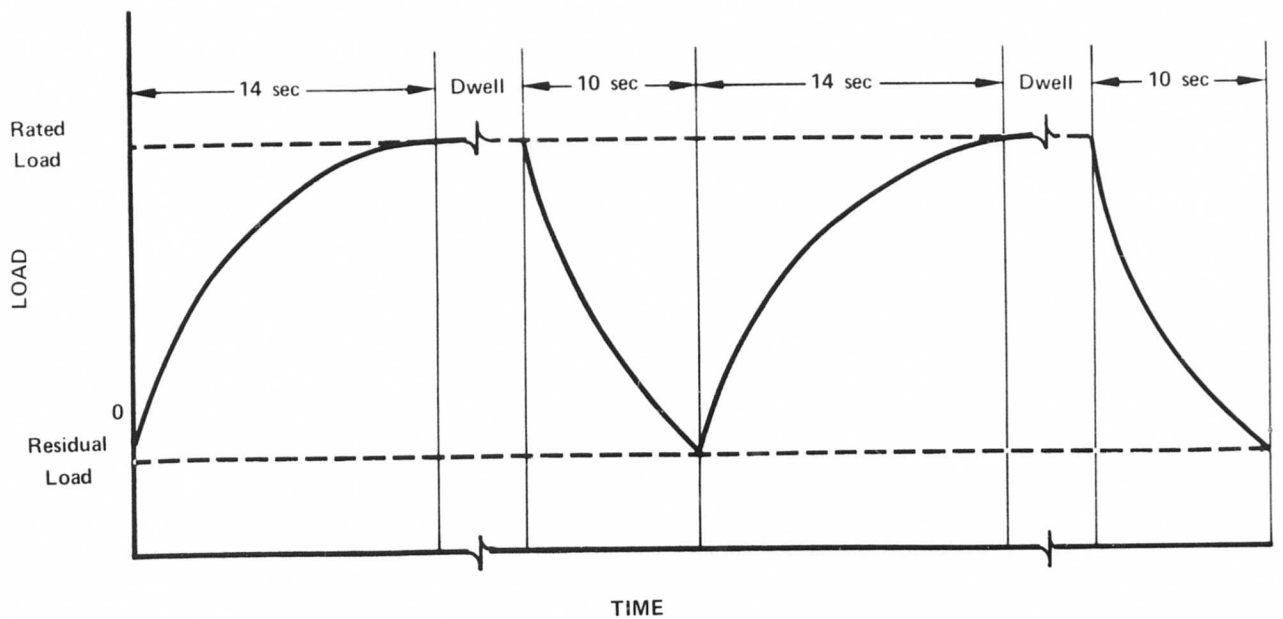

Specimen	Dwell Time
215	0
216	1 min
217	0
218	3 min
219	0

Figure 96. Typical Biaxial Specimen Load Cycle.

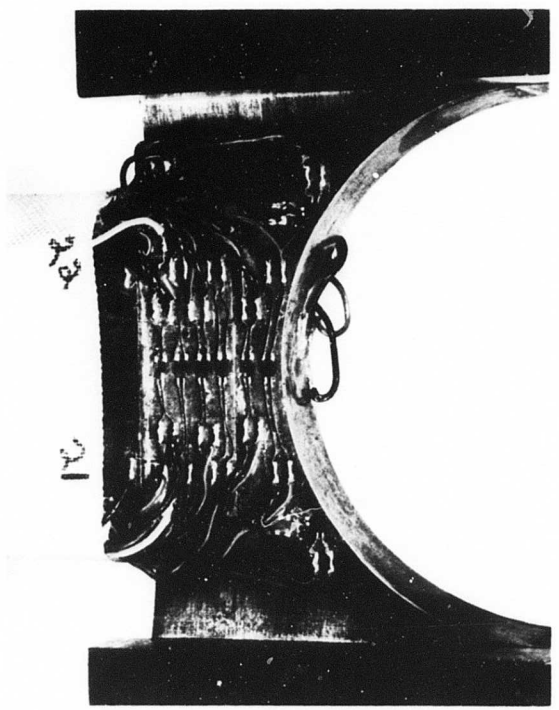

Figure 97. Biaxial Specimen Strain Gages.

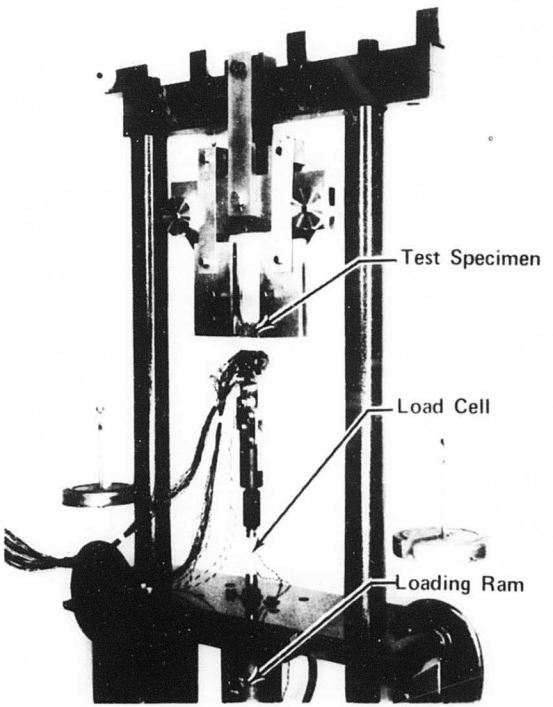

Figure 98. Strain Gage Test Setup.

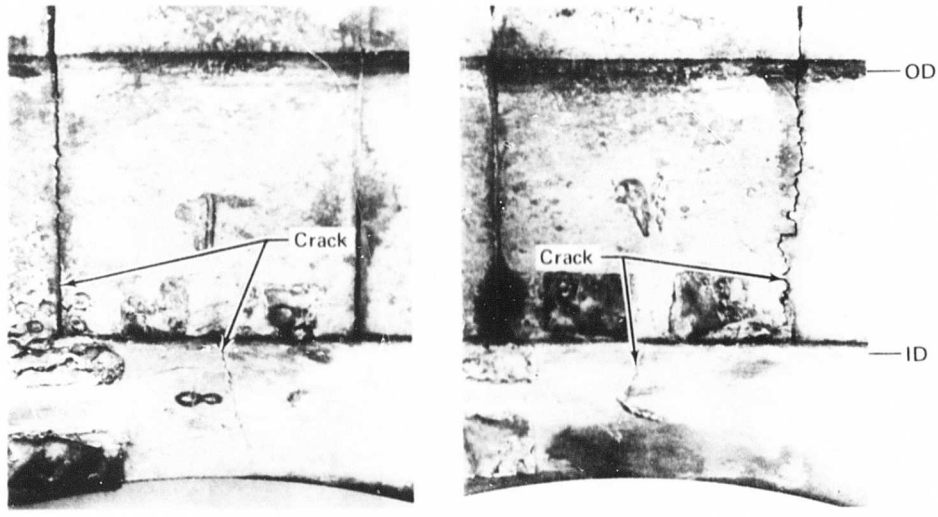

Figure 99. Cracking of Specimen (SN 215) After 4700 Cycles.

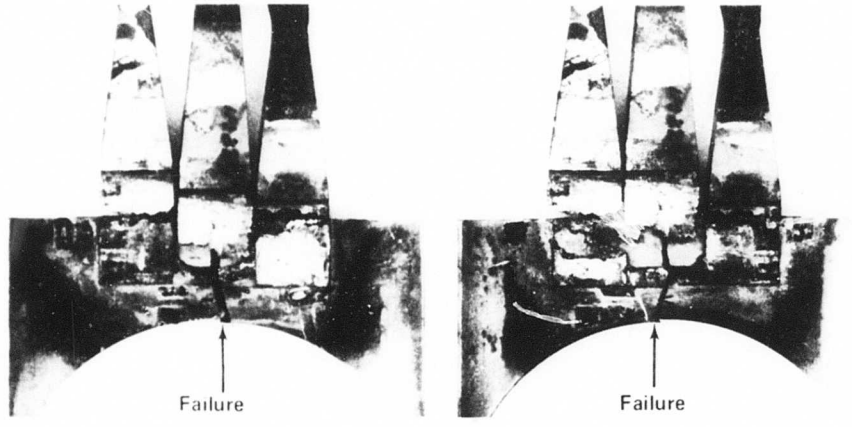

Figure 100. Failure of Specimen (SN 215) After 4754 Cycles.

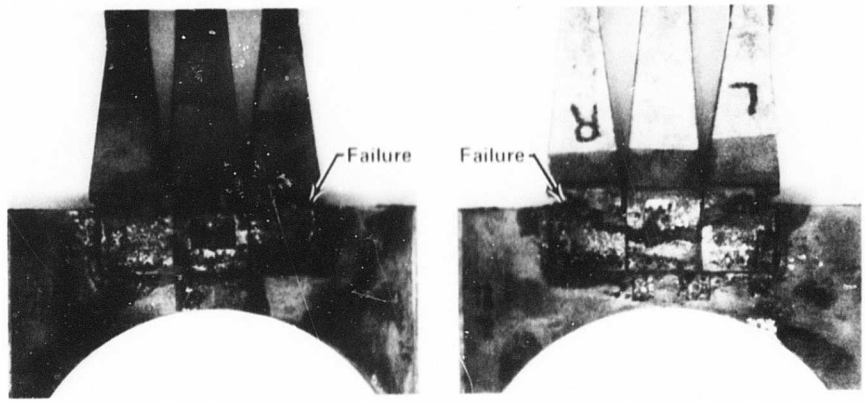

Figure 101. Failure of Specimen (SN 218) After 2605 Cycles.

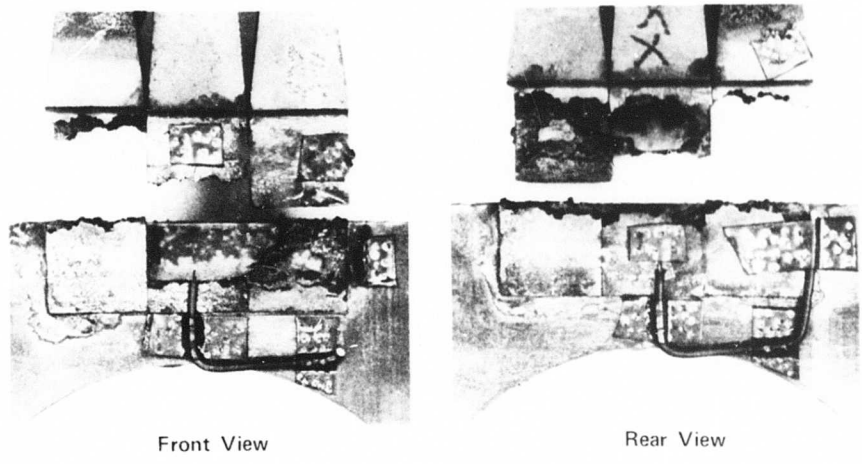

Figure 102. Failure of Specimen (SN 216) After 30 Cycles.

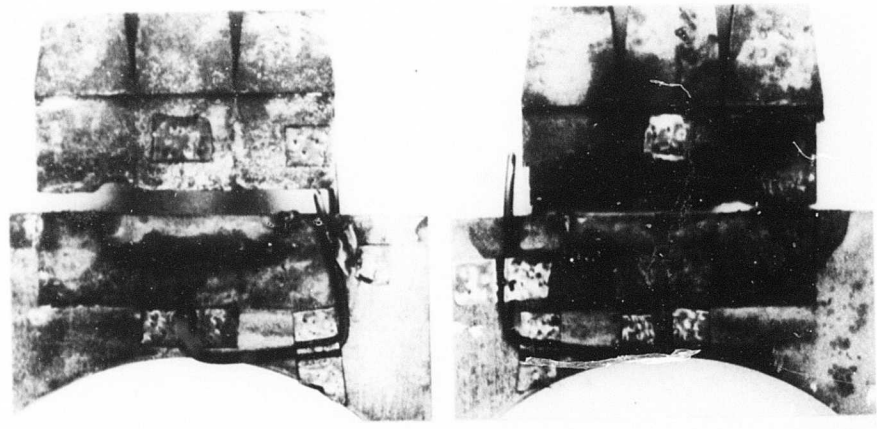

Figure 103. Failure of Specimen (SN 219) Upon Initial Loading.

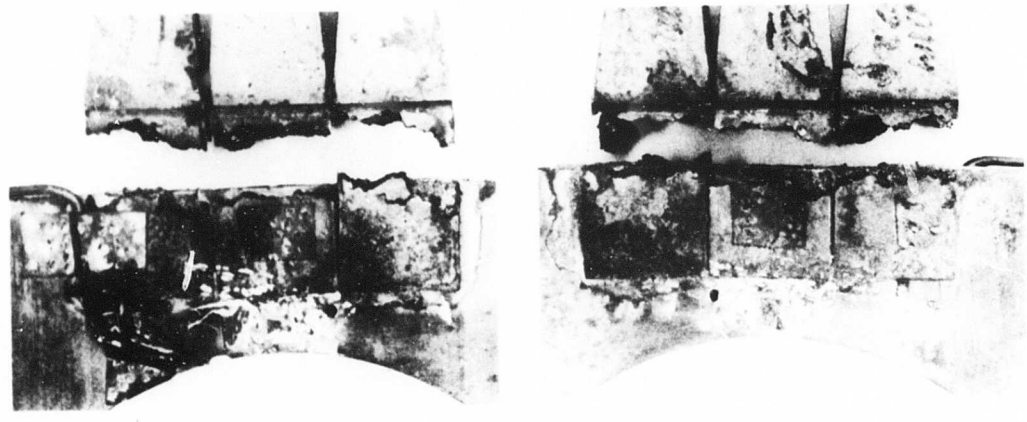

Figure 104. Failure of Specimen (SN 217) After 319 Cycles.

Figure 105. Photomicrograph of Braze Joint (Specimen SN 218).

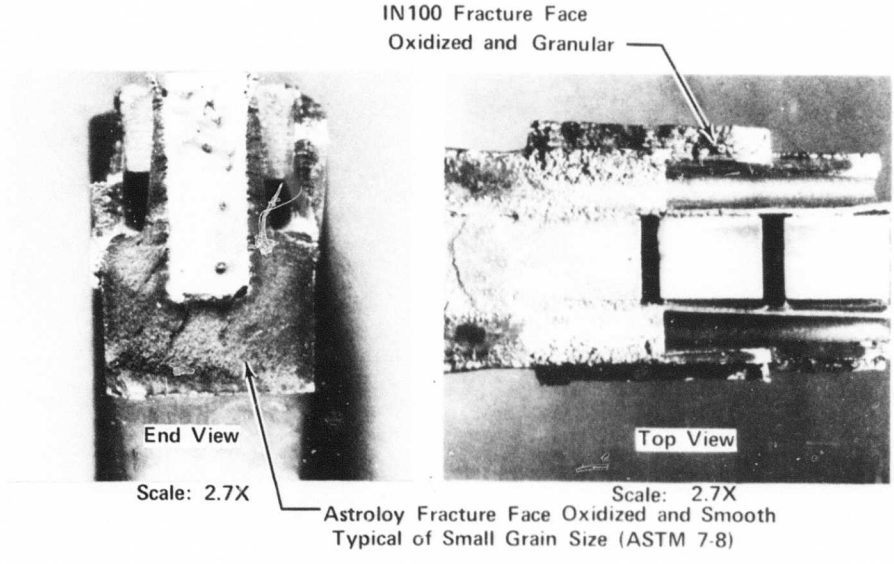

Figure 106. Test Specimen (SN 215) Fracture Faces.

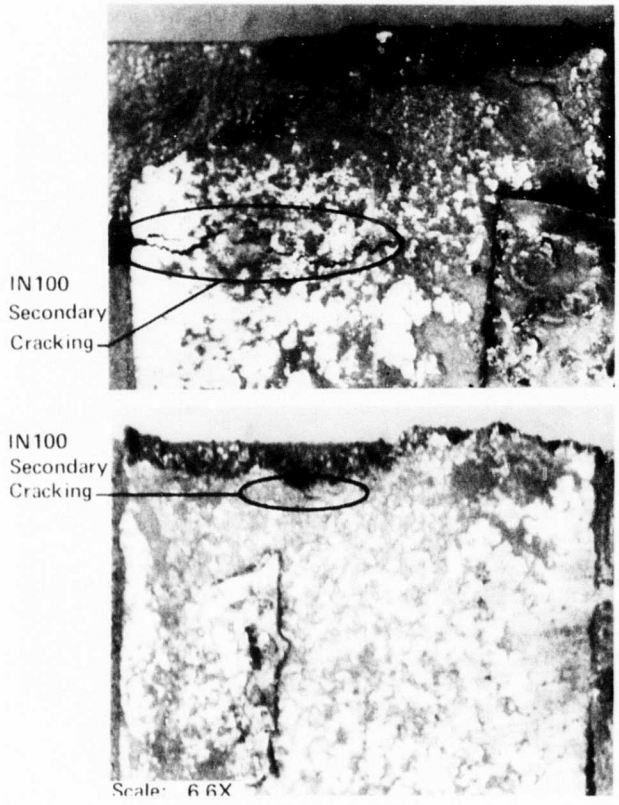

Figure 107. Stress Rupture Failure of Specimen (SN 218).

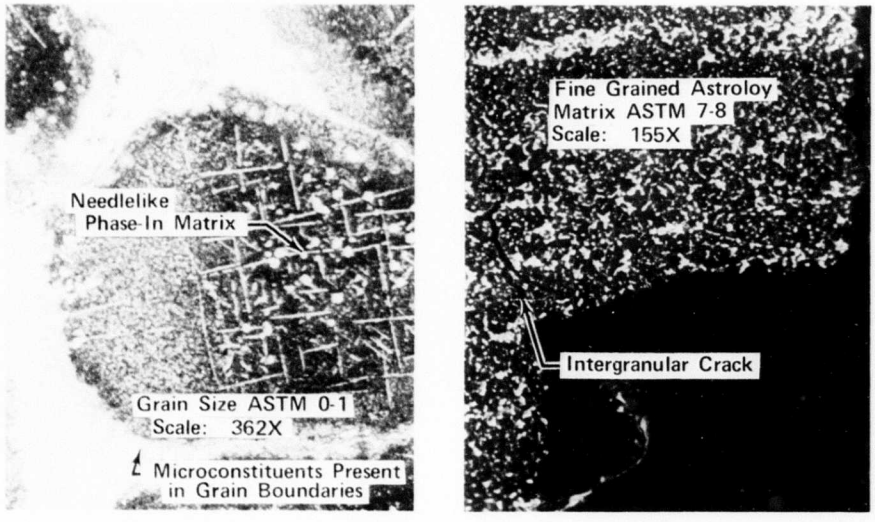

Figure 108. Alteration of Astroloy Microstructure.

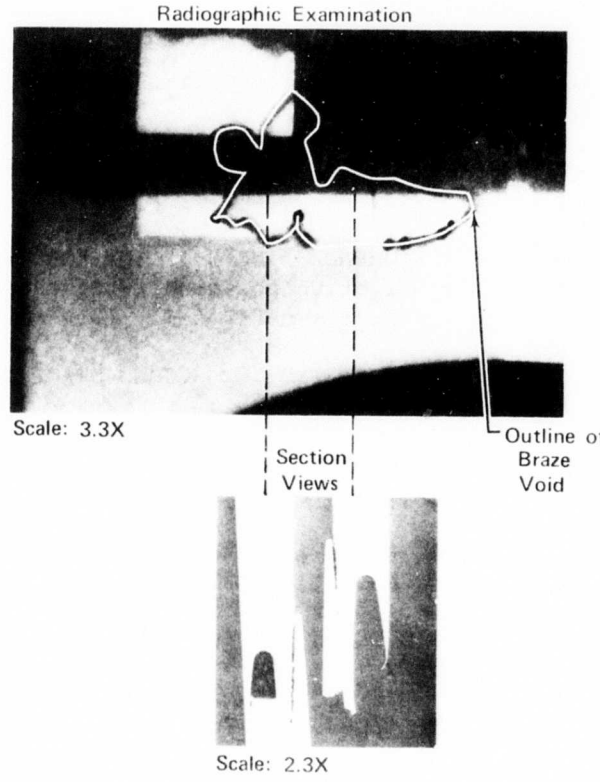

Figure 109. Test Specimen (SN 216) Braze Void.

9.0 SELECTED BIBLIOGRAPHY

1. ALLISON T63 AND AUBISQUE, Flight International, Vol 81, February 15, 1962, pp. 251 and 252.

2. Bowden, A. T., and W. Hryniszak, THE DEVELOPMENT OF SMALL GAS TURBINES OF LOW WEIGHT AND HIGH PART LOAD EFFICIENCY, International Developments in Heat Transfer ASME, 1963, pp. 190-199.

3. Boyle, J. H., PRODUCTION OF INTEGRALLY-CAST AIRFOIL COMPONENTS FOR SMALL GAS-TURBINE ENGINES, ASME, 62-GTP-5.

4. Chapman, W. I., CHRYSLER'S GAS TURBINE CAR: POWERPLANT DESIGN CHARACTERISTICS, SAE Preprint, January 13-17, 1964, p. 23.

5. Conrad, J. D., and N. Mochel, OPERATING EXPERIENCE WITH HIGH TEMPERATURE STEAM TURBINE ROTORS AND DESIGN IMPROVEMENTS IN ROTOR BLADE FASTENING, ASME Trans 80, August 1958, pp. 1210-24.

6. HIGH TEMPERATURE TURBINE COMPONENT DEVELOPMENT FOR USAAML SMALL GAS TURBINE PROGRAM, Curtis-Wright Corporation, Wright Aeronautical Division, Monthly Technical Report Numbers 4-13, 1964-65.

7. Defries, R. S., CAST-WELDED BOEING 502 SECOND STAGE TURBINE, Allegheny Ludlum Steel Corporation, March 1956.

8. Dollin, F., SOME DESIGN PROBLEMS ARISING IN THE DEVELOPMENT OF VERY LARGE HIGH SPEED TURBINES, Proc of IME, Vol 177, No. 9, 1963.

9. Eliseev, V. A., and A. A. Krinskii, IMPROVING GAS TURBINE RELIABILITY, Vestnik Mashinostroeniya, No. 7, July 1966.

10. Fessler, H., CENTRIFUGAL STRESSES IN TURBO-ALTERNATOR ROTORS, Proc of IME, Vol 173, No. 29, 1959.

11. 1964 GAS TURBINE SPECIFICATIONS, Gas Turbine, Vol 5, No. 1, January-February 1964.

12. Glukharev, E. G., THE FLEXIBILITY AND SHAPE OF THE FIR-TREE ROOT TEETH IN TURBINE BLADES, Energomashinostroene', No. 11, 1960 (Russian).

13. Haigh, R. A., and M. L. Murdoch, ANALYSIS OF CENTRIFUGAL STRESSES IN TURBINE WHEELS, Journal of Mechanical Eng Science, Vol 5, No. 1, March 1963, pp. 66-74.

14. Heywood, R. B., TENSILE FILLET STRESSES IN LOADED PROJECTIONS, Proc I. Mech E, Vol 159, 1968.

15. Hill, H. C., PROGRESS OF GAS TURBINE TRUCK TESTS, SAE Transactions, Vol 6, No. 3, July 1952.

16. Holms, A. G., and A. J. Repko, CORRELATION OF FIR-TREE-TYPE TURBINE BLADE FASTENING STRENGTH WITH MECHANICAL PROPERTIES OF MATERIALS, ASME Transactions, August 1957.

17. Hoppe, C. H., Jr., DESIGN STUDY FOR THE MECHANICAL ATTACHMENT OF BRITTLE MATERIAL BLADES TO GAS TURBINE ROTORS, J. C. Carter Company, April 1954.

18. Hoyle, R. D., TRANSIENT TEMPERATURE STRESSES IN AXIALLY SYMMETRICAL SYSTEMS WITH SPECIAL APPLICATION TO SOLID ROTOR OF STEAM TURBINE, Proc IME, V. 169, N. 31, 1955, pp. 553-62.

19. Johnson, Robert A., CENTRIFUGAL STRESSES IN ROTORS OF ARBITRARY CROSS-SECTION, AD 475 365L, 1965, p. 44.

20. Karen, H. P., and G. E. Trevaskis, DEVELOPING NEW MANUFACTURING METHODS TO REDUCE COSTS IN SMALL GAS TURBINES, SAE, January 1967.

21. Karp, P. I., C. H. Sayre, and R. L. Probst, INVESTIGATION OF THE FABRICATION OF STRUT SUPPORTED STAINLESS STEEL TURBINE BLADES BY SINTERED LOOSE SPHERICAL POWDER TECHNIQUES, Federal-Mogul-Bower Bearings, Inc, February 1956.

22. Kucera, J., O. Kerkovsky, and V. Nezval, METHOD OF MANUFACTURING THERMAL TURBINE ROTORS, USAF Foreign Technology Division, AD 476 118, December 1965.

23. Leikin, A. S., DISTRIBUTION OF BENDING FORCES IN TURBINE BLADE ROOTS, Russian Engineering Journal, No. 1, 1964.

24. Leikin, A. S., INCREASING THE STRENGTH OF FIR-TREE JOINTS IN TURBINE BLADES, Russian Engineering Journal, No. 3, 1964.

25. Leikin, A. S., ON THE GENERAL NONUNIFORMITY OF STRESS DISTRIBUTION IN TURBINE BLADE JOINTS DUE TO THE INFLUENCE OF THE BLADE SHAPE, AN SSR Mech and Mechanical Engr, 1960 (Russian).

26. Leist, K., and H. Ostenrath, TORQUE VARIATION OF SMALL TWO-SHAFT GAS TURBINES, U. S. Army Foreign Science and Technology Center, AD 478150, December 1965.

27. Lynn, E. K., EXPERIMENTAL STRESS ANALYSIS IN DESIGN OF LIQUID HYDROGEN PUMP ROTOR, Experimental Mech, 2, 12, December 1962, pp. 19A-23A.

28. Macke, Harry J., STRESS ANALYSIS OF FIR-TREE DOVETAIL FASTENING FOR TURBINE BUCKETS, Doctoral Thesis Submitted to the Faculty of Arts and Sciences of Harvard University, May 1951.

29. Meyer, A. J., Jr., Kaufman, Albert, and W. C. Caywood, INVESTIGATION OF MECHANICAL FASTENINGS FOR SOLID TURBINE BLADES FROM DUCTILE MATERIALS, NACA, August 1954.

30. Mustafin, C. G., CALCULATING THE CLEARANCES IN THE FIR-TREE JOINTS OF MOVING TURBINE BLADES, Russian Engineering Journal, No. 7, 1962, pp. 8-12.

31. Mustafin, C. G., TOOTH FLEXIBILITY AND CLEARANCE IN TURBINE FIR-TREE ROOT JOINTS, Russian Engineering Journal, Vol XLVI, No. 2.

32. Newton, R. E., A PHOTOELASTIC STUDY OF STRESSES IN ROTATING DISCS, Journal of Applied Mech, Vol 7, No. 2, June 1940.

33. Nickols, L. W., COMPARATOR FOR TURBINE BLADE ROOTS, Engineering, Vol 179, No. 4660, May 20, 1955.

34. Pattee, H. E., and R. M. Evans, BRAZING FOR HIGH TEMPERATURE SERVICE, DMIC Report 149, February 21, 1961.

35. PHOTOELASTIC INVESTIGATION OF TRANSIENT STRESSES AROUND BLADE ROOTS OF TURBINE DISKS, Tecnica Italiana, Vol 31, November 1966, pp. 607-615.

36. Piwonka, T. S., BI-METAL CASTING, TRW Metals Division, October 8, 1968.

37. Ryan, J. J., and J. T. Rettaliata, PHOTOELASTIC ANALYSIS OF STRESSES IN A STEAM TURBINE BLADE ROOT, ASME Transactions, August 1940.

38. Seleznev, K. P., GAS TURBINE ROTOR TEMPERATURE FIELD WITH COOLING AIR BLOWN THROUGH SLOTS IN ROOT ATTACHMENTS, AD 627113, December 21, 1965.

39. SINGLE ROTOR ENGINE-FEASIBILITY FINAL REPORT, Curtiss-Wright Corporation, WAD, AD 642257, July 23, 1966, p. 33.

40. Sobolev, S. P., TAIL JOINING OF WORKING TURBOMACHINE BLADE, Foreign Technology Division, Wright-Patterson AFB, August 1967.

41. Sokolov, B. P., CONDITIONS AFFECTING THE ROOT JOINTS OF GAS TURBINE MOVING BLADES, Izvestiya AN USSR OTN, No. 5, 1958 (Russian).

42. Sorenson, Gordon, DON'T OVERLOOK LOW-FREQUENCY STRESSES IN DESIGNING SMALL GAS TURBINES, SAE Journal, June 1957.

43. Sorenson, Gordon, EXPERIMENTAL STRESS ANALYSIS IN SMALL TURBINES, SAE Annual Meeting, Detroit, Preprint 33, January 14-18, 1957, p. 19.

44. SOUND REVEALS STRESS PATTERNS, Iron Age, Vol 191, No. 5, January 31, 1963, pp. 58-59.

45. Spinks, L. J., THE AUSTIN TURBINE MOTORCAR ENGINE, The Oil Engine and Gas Turbine, Vol 24, No. 282, February 1957.

46. Spinks, L. J., THE SECOND RUSTON GAS TURBINE, The Oil Engine and Gas Turbine, Vol 25, No. 289, September 1957.

47. SUPERALLOY CASTINGS ARE MEETING SMALL TURBINE BLADE LIFE NEEDS, SAE Journal, Vol 76, No. 6, June 1968.

48. Thurgood, D. A., CENTRIFUGAL STRESSES IN SINGLE WHEEL AND HUB, Engineering, Vol 212, No. 5522, November 24, 1961, pp. 869-70.

49. Turunen, W. A., and J. S. Collman, THE GENERAL MOTORS RESEARCH GT-309 GAS TURBINE ENGINE, SAE Preprint R430, October 1965, p. 65.

50. Wahl, A. M., EFFECTS OF THE TRANSIENT PERIOD IN EVALUATING ROTATING DISK TESTS UNDER CREEP CONDITIONS, ASME, Journal of Basic Engineering, March 1963.

51. Warnock, R. E., R. W. Martini, and J. H. Boyle, APPLICATION OF HIGH TEMPERATURE MATERIALS FOR INTEGRALLY CAST TURBINE COMPONENTS, SAE 650706, October 18-21, 1965.

52. Weaving, J. H., SMALL GAS TURBINE, Inst Mechanical Engrs Proceedings, Automobile Division, 1961-62.

53. Weidhuner, D. D., MILITARY POTENTIAL OF THE SMALL GAS TURBINE, ASME 66-GT-91.

54. West, J. and P. Ryan, BLADE ROOT FOR SPLIT DISC EXPERIMENTAL MULTI-STAGE AIR TURBINE, Engineer, Vol 220, December 31, 1965.

55. Wilkinson, Paul H., BABY TURBOJETS, Aviation Age, Vol 16, No. 3, September 1951, pp. 30-31.

APPENDIX I

BLADE/DISK ATTACHMENT LITERATURE SURVEY

The literature on blade/disk attachment methods was reviewed to provide background for the preliminary selection of attachment designs for this program. This survey included experience within United Aircraft Corporation, available domestic and foreign literature, patent search, and a manufacturing vendor survey. Particular emphasis was directed toward procuring information applicable to the small, high-temperature turbines defined for U. S. Army Contract DAAJ02-68-C-0071.

Studies of small, high temperature gas turbine engines indicate that rotor speeds are limited by blade/disk attachment stress. Therefore, to increase substantially the performance of small gas turbine engines, attachment methods must be improved significantly. To obtain further insight into this problem, a survey of all available literature concerned with root attachments was conducted. The reports received were screened for techniques that would be applicable to this program. Literature sources employed in this survey were previously presented in Table II.

The following paragraphs summarize the information obtained in this survey.

1. Fir-Tree Attachment

Most existing gas turbine engines use some form of fir-tree root design to attach the turbine blades to the disk rim. However, the shape, size, and number of teeth of the various joint designs vary greatly, indicating wide differences of opinion on the best fir-tree tooth design for a given application.

Meyer, Kaufman, and Caywood[29] made a preliminary investigation of mechanical attachments made from ductile materials. In their study of the four more important basic configurations (shown in Figure 110), the authors found that the fir-tree design was far superior to any other root design tested; the fir-tree had the highest percentage of area available to support tensile loads without a loss in shear area because of its multitooth construction. Typical percentages of available tensile and shear area for each configuration are presented in Figure 110, along with the method of calculation. Because the fir-tree root design was found to be the strongest attachment scheme for ductile materials, the authors conducted an extensive investigation of the variations in the fir-tree configuration. In an effort to establish design criteria, the analysis included three specific fir-tree root designs: one with six pairs of small teeth, one with six pairs of large teeth, and one with only three pairs of large teeth. These three designs are illustrated in Figure 111. The

authors concluded from their tests that the strengths of these three fir-tree root joints depended only on the total tensile and shear area available to support the centrifugal and gas bending loads and that strength was not directly affected by the number or size of the teeth providing these areas. As strength is not sacrificed, use of a root joint with the fewest number of large teeth is desirable to reduce the manufacturing costs associated with machining fir-tree teeth to close tolerances. However, a compromise in fillet radius (see Figure 112) is necessary to maintain a strong joint because increased fillet radii tend to decrease the available areas supporting the shear load.

The effect of fillet radius size on the strength of fir-tree joints was studied by Homs and Repko[16] by running elevated-temperature, time-dependent spin tests on turbine rotors. The authors correlated the results of the spin tests with the mechanical properties of materials derived from laboratory stress rupture tests. They concluded that the smooth bar stress rupture test was inadequate as a measure of material strength for fir-tree root joints and indicated that the notched bar strength was a suitable measure of fir-tree strength when the notch radius was representative of the fillet radius of the joint.

Recent analytical studies have indicated that, to achieve maximum strength from a fir-tree joint, it is necessary to consider the distribution of forces within the joint. Leikin[24] discovered that local stress concentrations in the spaces between the joint teeth could be reduced by increasing the fillet radii and providing inclined working surfaces on the teeth. In addition, to reduce the general nonuniformity of stress distribution in the root joints resulting from airfoil camber, Leikin indicates that the airfoil should be situated as far as possible from the first section of the joint as illustrated by the distance "d" in Figure 112. This allows the load to become more uniform before being transmitted to the teeth because the teeth are further from the plane of load application. Leikin indicates that another method of increasing stress uniformity is to rotate the joint relative to the airfoil so that the chord of the airfoil at the root section is parallel to the longitudinal plane of symmetry of the joint. This condition will exist if $\gamma = 0$ deg in Figure 112 and has the effect of redistributing the mass of the airfoil more evenly over the root joint. For the same purpose, it is also advantageous to make the centers of gravity of the airfoil and root joint coincide. The first teeth of a fir-tree joint usually support a higher load than the remaining teeth in the joint. The first teeth run at higher temperatures, and the greater thermal expansion in this area tends to unload the remaining fir-tree teeth. In an earlier investigation by Leikin[23], this effect was found to exist. A reduction in load on the first teeth was accomplished by increasing the tooth clearance in this area; however, this more uniform load distribution increased the bending moment on the disk rim. It was also learned that as the ratio of the radial depth of the joint to the mean thickness of the blade root in the circumferential direction decreases, the loads supported by the teeth and the bending moments along the blade root are distributed more uniformly. This again had the effect

of slightly raising the relative value of the bending moment on the disk rim. The additional bending moment may be offset by a material selection that increases the ratio of the modulus of elasticity of the blade root material to that of the disk material. This augments the relative flexibility of the teeth on the disk, resulting in a reduction of the bending moment on the disk rim; it also provides for a more even distribution of both the loads sustained by the teeth and the bending moment along the blade root. Leikin also discovered in this study that an increase in the wedge angle of the blade root from 30 to 50 deg tends to equalize the distribution of the applied load on the teeth. However, this amplified the nonuniformity of the bending moment distribution along the blade root and disk rim.

Mustafin[30] reports that one method of attaining a reasonably equal load distribution among all the joint teeth is to adjust the clearances between the disk and the blade root teeth. This is done in such a manner that they diminish from a maximum clearance for the pair of teeth which is subject to the maximum load to zero clearance for the pair which is subject to the lightest load. Therefore, to obtain an equal load throughout all the teeth, it is necessary that during assembly (when the joint is not subject to load), only the pair of teeth situated in the section subject to the smallest load should be in contact.

In another investigation, Mustafin[31] indicates that several theoretical approaches to the design of turbine fir-tree joints include a flexural analysis based on the assumption that the root teeth are cantilevered, of variable section, and rigidly joined to the root of the blade. Such an analysis ignores the effects of the flexibility of the joint teeth, which can increase the radial displacement of the root by a factor of 2.2 - 2.5. As a result of additional experimental investigation, Mustafin reports that the blade root thickness has no effect upon tooth deflection, which is completely elastic until the mean shear stress in the section immediately under the load reaches approximately 60% of the material yield stress.

Fir-tree root joint failures in operating gas turbines are frequently the result of high cycle fatigue. It is of extreme importance therefore to consider design measures for increasing the strength of such joints under vibratory loading. These measures consist essentially of: (1) reducing the maximum local stresses in the spaces between the teeth, (2) improving the distribution of the steady stresses and reaction forces, and (3) reducing the level of vibratory stresses in the joint. Meyer, Kaufman, and Caywood[29] learned that large teeth and large fillets have high cycle fatigue advantages. The large fillets reduce the stress concentrations in the spaces between the teeth, decreasing steady-state stress levels and permitting higher vibratory stress levels. Also, the large teeth do not require the strict machining tolerances necessary for uniform load distribution on small teeth. This results in a loose joint providing increased capability for vibration damping.

Leikin[24] reports that since the first teeth of fir-tree root joints are subjected to high steady and vibratory loads, it is necessary to reduce the steady load applied to the first teeth so that the peak stress (steady plus vibratory) does not exceed the material limits. Leikin suggests two basic methods for attaining this condition. The first is to choose the blade and disk materials so that the coefficient of thermal expansion of the disk is greater than that of the blade root. Assuming that all teeth on the blade root are in uniform contact with the teeth on the disk during assembly, this ensures that the distance between the first and last tooth (see Figure 113) on the disk will be greater than the distance between corresponding teeth on the blade root at operating temperature. This has the effect of providing a clearance between all the teeth of the joint except the teeth subjected to the smallest load (those nearest the center of the disk). The maximum clearance is between the first teeth, thus relieving the steady load on the first teeth. The other method is to make the pitch of the teeth on the disk greater than that of the teeth on the blade root. This has the same effect of providing the most clearance between the first teeth and reducing the load on the first teeth. For extreme operating conditions, both methods could be applied simultaneously. Leikin indicates in the same report that the damping of vibrations in a fir-tree joint is substantially increased by a reduction in the steady tensile load on the first teeth of the joint and redistributing this load proportionately among the remaining teeth. By proper adjustment of the load, it is possible to approximately double the work done by damping, and the amplitude of the vibratory load may be reduced by 20%. In short blades, where the ratio of the airfoil span height to the chord of the airfoil at the root section does not exceed 2.7, the general damping capacity of the blade may be more than trebled, reducing the level of vibratory load by approximately 35%.

In a study performed by Eliseev and Krinskii[9], fatigue failures occurring at the first recess in the fir-tree joint were eliminated by: (1) reducing the stress concentration at the first recess by increasing the fillet radius (shown in Figure 112) and consequently increasing the moment of inertia of the section, (2) extending the root in the axial direction to further increase the moment of inertia, and (3) modifying the blade locking inserts so as to bear upon the blade roots rather than on the disk in order to damp out blade oscillations.

2. Dovetail Attachment

This type attachment, shown in Figure 114, is a relatively simple mechanical attachment that can be easily fabricated, incorporates large radii, and involves no pins or auxiliary attachments other than a locking device to retain the blade in the disk. Dovetail attachments have been primarily used in compressor applications where joint efficiency is not a critical problem. The stress concentration factor (the ratio of the true maximum stress to the nominal stress calculated by ordinary formulas of mechanics) is low for dovetail attachments; however, the limited amount of shear area available to support the blade results in a relatively inefficient joint.

Hoppe[17] reported that the dovetail root design is especially suited for brittle materials because of its low stress concentration factor and the large radii that can be achieved. Hoppe developed a modification to the dovetail design which was found to increase the strength of the joint by 28%. The modification entailed rotating the blade root about the centroidal axis of the airfoil and providing flat loading surfaces to support the applied load. Hoppe indicated that the optimum amount of root rotation depended on the camber of the airfoil. As shown in Figure 114, the rotated root design aligns the airfoil over the longitudinal centerline of the dovetail. Hoppe states that the selection of flat loading surfaces is based on consideration of the method of fabrication of the root. The bearing stress on the surfaces is a function of the total area in contact and also depends upon the absence of local imperfections which cause stress concentrations. The former may be calculated, but the latter is determined primarily by the accuracy with which the loading surfaces are fabricated. In production, the blade root contour would probably be machined by grinding, and the corresponding disk slot would be broached. Hoppe indicates that the accuracy of each of these fabricating techniques should be better for flat surfaces rather than curved. It is Hoppe's opinion therefore that the incorporation of flat loading surfaces in conjunction with rotating the root should achieve maximum strength from the dovetail design. It is apparent that maximum joint strength will be attained when the area of the attachment is proportioned so that the blade root and the disk rim are of equal strength. The optimum ratio of the blade root area to the disk rim area varies with operating temperature, time-to-failure, and material selection.

3. Integrally Cast Attachment

One-piece rotors (integral blades and disk) offer cost advantages and positive cooling air sealing if other design requirements can be achieved. Boyle[3] found that this approach permitted dramatic cost savings over conventional designs with individual blades and a separate disk because it eliminated costly grinding and broaching operations on the blade roots and disk slots. In spite of the cost advantages, most turbine wheels for small engines are still being made with individual blades. One reason is that while the cast high-temperature alloys provide excellent properties for the blades, these same alloys are less than ideal as disk materials because of reduced ductility at disk operating temperatures. This is a difficult problem, since the trend in turbine blade materials is toward refractory alloys with inherently poor ductility. In addition, the intricate cooling passages required for some advanced, high-temperature service airfoils present a difficult coring problem in integral castings. Another objection to the one-piece construction is that casting damage or casting defects can result in loss of a sizeable investment through rejection of the complete rotor assembly. Karen and Trevaskis[20] indicated that reevaluation of allowable casting imperfections must be studied by the engine manufacturer to offset this risk.

One solution to obtaining optimized blade and disk materials in integral assemblies is to make the turbine wheel by a bimetal casting process. Bimetal casting as reported by Piwonka[36] is the casting of a metal directly to a part already in a solid state to produce an integral product. The second metal may be identical or dissimilar to the first, and the bonds may be of two types: mechanical or metallurgical. A mechanical bond is a mere anchoring of the two members by a wedging effect or the like. A metallurgical bond is a fusion bond, where the second melted casting has been joined to the first, forming a completely solidified zone. A combination of these two bonds may also be obtained, which permits an attachment design combining an integral joint with mechanical features (such as a fir-tree).

4. Welded Attachment

This attachment method was found by Curtiss-Wright[6] to incorporate weight savings and potential production oriented features. Other advantages are high joint efficiency, no leakage of cooling air, and separate blade and disk manufacture. One major disadvantage of this attachment design has been the inability of achieving good weld joints and developing a positive, nondestructive method of inspecting the welds. Problems of this nature were encountered by Curtiss-Wright. A split-disk approach could also be used with welded designs. Welding two disk halves together would eliminate the use of bolts and thus reduce the large cross-sectional disk area required to maintain acceptable stress levels around the bolt holes. However, the solid welded attachment does not have the damping characteristics of the mechanical attachment designs and must withstand higher vibratory stresses. In addition, a high conductivity heat path exists as a result of the solid joint and requires additional attention to disk cooling. Karen and Travaskis[20] studied a composite turbine rotor composed of a separate outer ring containing turbine blades which was welded to a center disk. Karen and Travaskis found three advantages to this design: (1) the use of a lower cost material in the disk, (2) less metal in each pour resulting in lower casting costs, and (3) elimination of loss in structural integrity due to porosity in the disk.

5. Split-Disk Attachment

This design was studied in order to develop turbine rotor hardware capable of individual blade replacement, ease of providing cooling air to each blade, and efficient cooling air sealing. Curtiss-Wright's[6] layout studies indicate that a hollow front disk half and a solid rear disk half with a circumferential fir-tree attachment potentially provided the desired features. Preliminary thermal analyses indicated excellent temperature, stress, and deformation compatibility between each disk half. However, subsequent stress analyses indicated that separating moments on the disk halves were being generated by centrifugal force. The modification required to eliminate these separating moments moved the hub sections of the disk halves apart axially, more nearly radially under the fir-tree portions of the disks. The adverse effect of this modification was to

lower the critical speed of the system into the operating range of the engine. This necessitated an additional redesign of the support system to allow the first critical speed to occur below the normal operating range and the second critical speed above the operating range. This attachment design, which attained the desirable feature of interchangeability of rotor blades, had the attendant disadvantages of high weight and close tolerance requirements of the fir-tree joint to assure proper tooth loading. The main difficulty associated with this scheme was the design of the disk halves to maintain thermal and mechanical strain compatibility.

West and Ryan[54] studied the use of a tapered root tank in conjunction with the split disk attachment design. They discovered that the bending moment on the disk sides due to the centrifugal load is proportional to the axial distance from the point of application of load to the disk element being studied. This distance is shown as the "effective arm" in Figure 115. This effective arm was reduced to a minimum in the authors' design through the use of a tapered root tang. West and Ryan also found that the use of L-section rings in conjunction with the split-disk design transformed the bending loads in the disk halves into compressive loads and allowed the root to support a higher load than a conventional configuration.

6. Pinned Attachment

Pin type attachments are attractive because they are easy to fabricate, permit individual blade replacement, and are relatively economical. Pinned attachments have much lower rim loading efficiency than fir-tree designs, however, since only a small percentage of the disk rim circumference can be loaded. Pinned attachments will be discussed in the following three design categories: (1) pins-in-sectional shear, (2) pins-in-compression, and (3) pins-in-longitudinal shear. Schematics of these basic designs are shown in Figure 116.

a. Pins-in-Sectional Shear

Investigation of this design by Hoppe[17] disclosed that the major problem is to provide sufficient shear area in the pins. To use this type attachment, the pin area must be kept reasonably small. Round pins are desirable to permit fabrication of the pin retaining holes in the wheel rim by drilling and reaming rather than by broaching. However, round pins of sufficient shear area reduce the blade base neck width and thus raise the stress level above a practical value. A lower stress level can be obtained by using noncircular pins.

Spinks[45] reported that a pinned blade attachment was used in the Austin turbine motorcar engine. The root of each blade was in the form of a tang that was drilled in the axial direction to take the pin. The tang fitted into a circumferential groove machined in the rim of the disk. The pins were a push fit and entered from the forward side of the disk. Blade replacement could be accomplished without damaging the blades or

disk by removing the pins. With all the blades fully assembled, a slight circumferential slippage was permitted in an attempt to provide a measure of vibration damping.

b. Pins-in-Compression

Hoppe[17] reports that this type attachment allows the blade base and the rotor segment to interlock with each other such that the pin size does not limit the blade neck width. Because the pin is in compression it can be made of relatively soft material and does not require an additional ductile material insert to distribute the bearing loads. Using small round pins, which do not limit the tensile area of the attachment, the maximum allowable load is considerably reduced; however, noncircular pins permit higher loading. This is caused by the additional shear area afforded by the noncircular pins.

c. Pins-in-Longitudinal Shear

Round pin type attachments are attractive because they are easy to fabricate and assemble in mass production, and because the attaching pins may be made of a ductile material to distribute the bearing loads evenly across the lands of the blade base. However, in conditions where the attachment is highly stressed, a high strength pin material must be selected to withstand large shear loads and will require ductile inserts for load distribution. Hoppe[17] concluded that the basic weakness of this type of attachment was that insufficient space existed to provide adequate blade and disk lugs as well as satisfactory attaching pins. Increasing the attachment space by utilizing less than the optimum number of blades per disk reduces the structural limitations of the attachment; however, associated with this compromise is a reduction in turbine aerodynamic performance.

7. Brazed Attachment

The brazed attachment offers a compromise between the mechanical and integral attachment designs. Its major advantages are: (1) positive sealing of blade cooling air, and (2) separate blade and disk manufacture. However, a major disadvantage of this scheme is inadequate joint inspection techniques. The possibility of insufficient braze coverage requires that some form of dependable nondestructive inspection technique be developed. Also, this type attachment does not have the inherent damping characteristics of the mechanical attachments because the blades are rigidly attached to the disk. In addition, a highly conductive heat path exists between the blade and the disk due to the solid construction of the joint. This results in higher transient and steady-state temperatures in the attachment and may create low cycle fatigue problems if the blade and disk materials are extremely dissimilar. Much of the difficulty associated with high temperature brazing is related to the characteristics of the base metals. The very elements that impart strength, oxidation resistance, and corrosion resistance to these metals at elevated temperatures are the elements that often impair the brazing properties of the filler metals.

Pattee and Evans[34] report that brazing alloys are selected on the basis of their wetting properties, their resistance to oxidation and corrosion, and their compatibility with the base metals. The difficulty incurred in brazing high strength alloys for use in gas turbines is that braze alloys usually contain small percentages of aluminum and/or titanium. These elements have a strong affinity for oxygen and form refractory oxides which reduce strength and are very difficult to remove. Other major problems are: (1) embrittlement of the base metal, and (2) severe reduction in the tensile strength and stress-rupture life of the base metal, consequently requiring additional heat treatment of the joint.

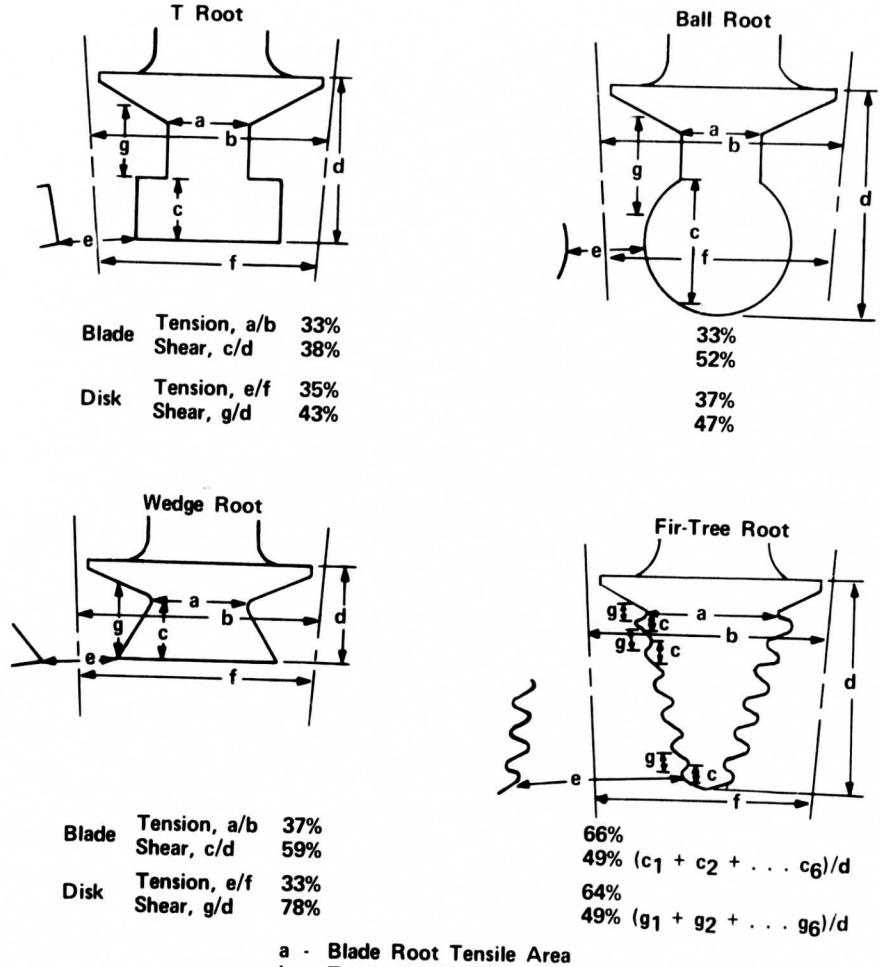

Figure 110. Basic Root Attachment Configurations.

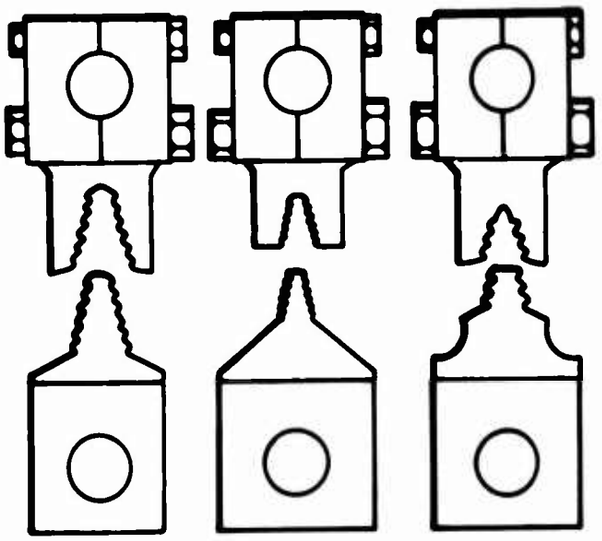

Figure 111. Fir-Tree Test Specimens.

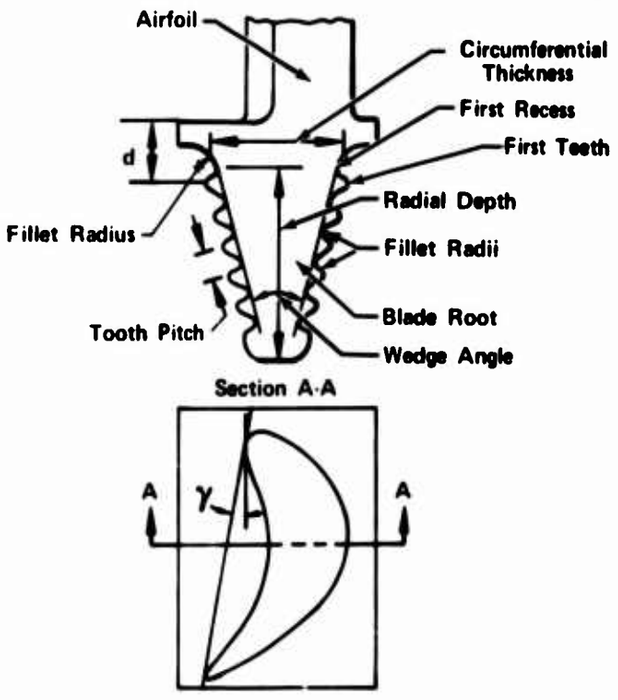

Figure 112. Fir-Tree Nomenclature.

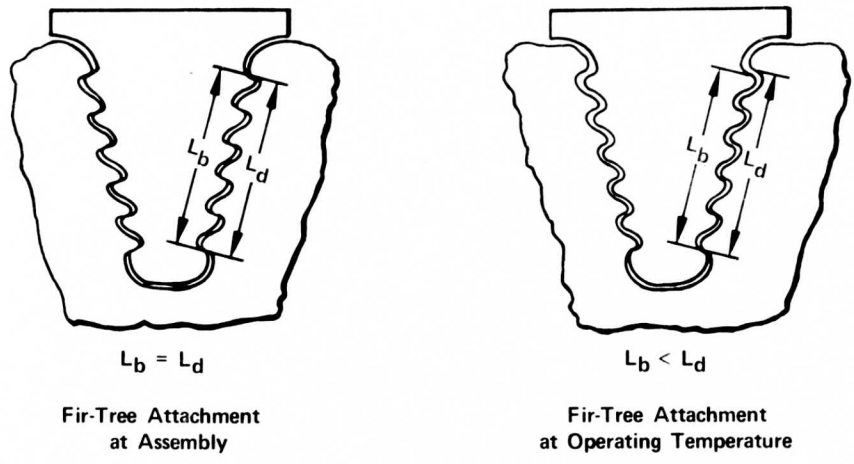

Figure 113. Fir-Tree Root Attachment.

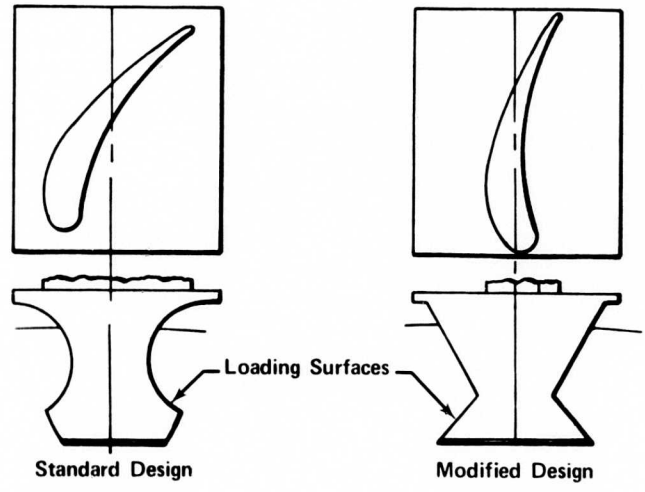

Figure 114. Dovetail Attachment.

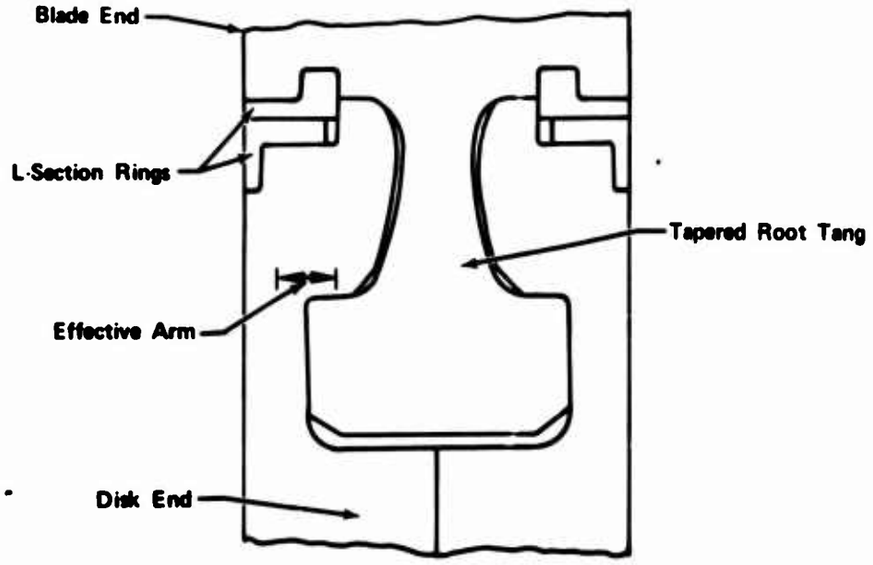

Figure 115. Split-Disk Tapered Root Tang Attachment.

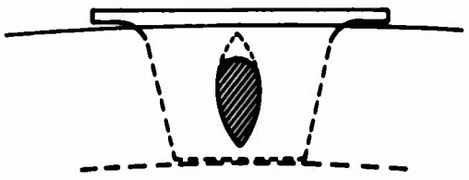

a. Pin-in-Sectional Shear

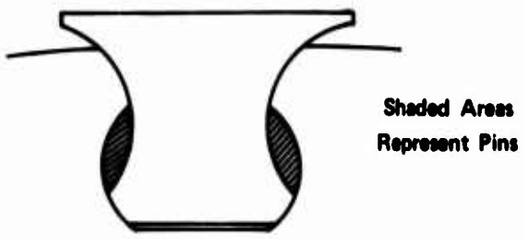

b. Pin-in-Compression

c. Pin-in-Longitudinal Shear

Figure 116. Pinned Attachment.

APPENDIX II
BIMETAL CASTING

An evaluation of this new fabrication technique was undertaken with the knowledge that it could not be incorporated into this program as a blade/disk attachment design because the time required to obtain fundamental strength data was not compatible with the program schedule. However, due to the potential advantages of this concept in the field of small turbine development, preliminary joint strength data for the bicasting process was obtained under a separately funded program.

Simple pull specimens as shown in Figure 117 were fabricated: seven butt joints to evaluate tensile strength, and seven tang joints to evaluate shear strength.

The specimens were cast of PWA 658 (IN 100) using a two-pour technique. Following the initial pour, a mold was formed that held the first part and contained gating near the mating surface so that the second pour metal flowed past the mating surface, promoting surface melting and oxide removal at the junction.

A joint line could not be detected by either visual or radiographic examination, and a complete metallurgical bond appeared to exist in all specimens (see Figure 118). The radiographic inspection of the eight specimens in the section poured last indicated severe shrinkage* at a location away from the joint. It was the opinion of the casting vendor that the shrinkage could be eliminated by optimizing the mold temperature and the cooling rate.

The butt-joint specimens were machined into typical tensile and creep rupture specimens having cylindrical gage sections and threaded shanks. The tang joint specimens were machined with a flat gage section to test the combined tensile and shear strength.

Tensile and creep rupture tests were conducted on the equipment discussed in Section 5.1. Tensile tests were conducted at room temperature with a cross-head speed of 0.05 in./min; creep rupture tests were conducted at 1400°F. Test data are presented in Table XXV. The eight specimens with severe casting shrinkage failed in the shrinkage region and did not develop the IN 100 specification strength. All specimens that failed within the bicast joint met the material strength specifications for IN 100. No distinguishing strength characteristics were noted between the butt or tang type joints since the bond appeared to have parent material strength.

These initial results indicate that the bicast fabrication technique is a potentially feasible method of blade/disk attachment that should be considered for further development.

*Shrinkage refers to the metallurgical contraction during solidification that results in large quantities of microscopic voids that adversely affect material strength.

TABLE XXV. BICAST SPECIMEN TEST DATA

Material: PWA 658

A. Creep Rupture @ 1400°F

Specification No.	Joint Type	Stress (ksi)	Life (hr)	Elongation (%)	Satisfied Material Specifications
1	Tang	85.0	3.1	-	No*
2	Tang	85.0	0.1	-	No*
3	Butt	85.0	12.0	1.2	No*
4	Butt	70.0	18.5	0.7	No*
5	Butt	85.0	29.3	2.1	Yes
6	Butt	70.0	500.**	-	Yes
7	Tang	85.0	231.0	7.8	Yes
8	Tang	85.0	80.7	5.4	Yes
9	Tang	85.0	10.7	3.4	No*
10	Tang	85.0	94.5	6.1	Yes
11	Tang	85.0	210.2	8.9	Yes

B. Tensile

Specification No.	Joint Type	Test Temperature (°F)	Ultimate (ksi)	Yield (ksi)	Elongation (%)	Satisfied Material Specifications
1	Tang	1400	104.9	-	2.0	No*
2	Butt	1400	89.8	-	-	No*
3	Butt	1400	121.0	112.3	4.0	Yes*
4	Butt	70	115.8	102.2	10.0	Yes*
5	Butt	70	112.8	106.8	5.0	No*
6	Tang	1400	141.5	103.8	7.0	Yes
7	Tang	1400	123.5	95.0	4.0	Yes

TABLE XXV - Continued

C. PWA 658 Specifications

1. Creep Rupture @ 1400°F

Stress (ksi)	Life (hr)	Elongation (%)
70.0	300.0	1.5
85.0	23.0	1.5

2. Tensile

Temperature (°F)	Ultimate (ksi)	Yield (ksi)	Elongation (%)
70.0	115.0	95.0	5.0
1400.0	112.0	94.0	2.0

*Failure occurred outside test zone within area of high shrinkage.

**Discontinued test

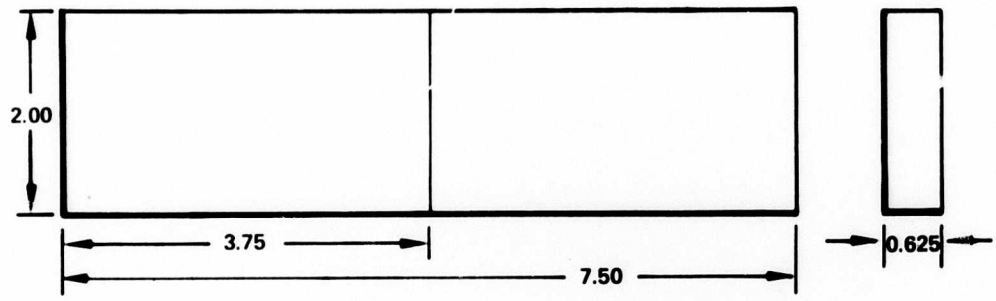

a. Butt Joint

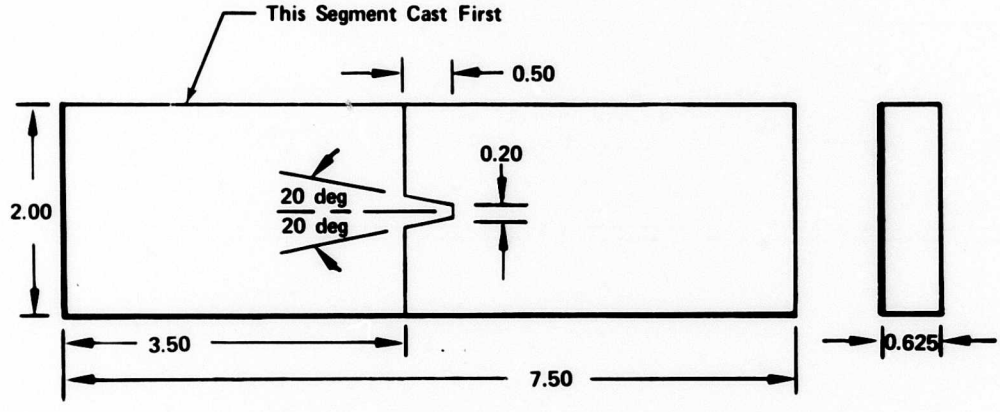

b. Tang Joint

Figure 117. Bicast Test Specimens.

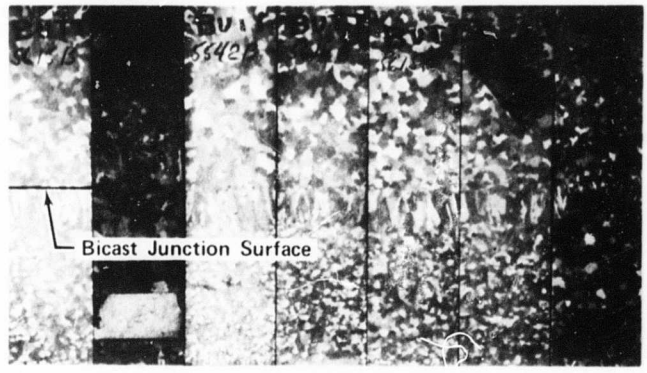

Bicast Test Bars (Butt Joint)

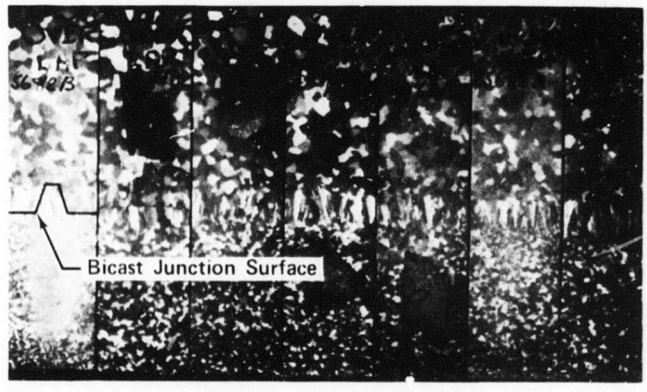

Bicast Test Bars (Tang Joint)

Scale: 0.25X

Figure 118. Bicast Bars.

UNCLASSIFIED

Security Classification

DOCUMENT CONTROL DATA - R & D

(Security classification of title, body of abstract and indexing annotation must be entered when the overall report is classified)

1. ORIGINATING ACTIVITY (Corporate author)

Pratt & Whitney Aircraft
Division of United Aircraft Corporation
Florida Research and Development Center
Box 2691, West Palm Beach, Florida 33402

2a. REPORT SECURITY CLASSIFICATION

Unclassified

2b. GROUP

3. REPORT TITLE

Turbine Blade/Disk Fabrication Investigation

4. DESCRIPTIVE NOTES (Type of report and inclusive dates)

Final Report

5. AUTHOR(S) (First name, middle initial, last name)

Kelch, George W.
Nelson, Richard W.

6. REPORT DATE	7a. TOTAL NO. OF PAGES	7b. NO. OF REFS
September 1970	175	55

8a. CONTRACT OR GRANT NO.	9a. ORIGINATOR'S REPORT NUMBER(S)
DAAJ02-68-C-0071	USAAVLABS Technical Report 70-53
b. PROJECT NO. Task 1G162203D14413	
c.	9b. OTHER REPORT NO(S) (Any other numbers that may be assigned this report)
d.	PWA FR-3827

10. DISTRIBUTION STATEMENT

This document is subject to special export controls, and each transmittal to foreign governments or foreign nationals may be made only with prior approval of US Army Aviation Materiel Laboratories, Fort Eustis, Virginia 23604.

11. SUPPLEMENTARY NOTES	12. SPONSORING MILITARY ACTIVITY
	U. S. Army Aviation Materiel Laboratories Fort Eustis, Virginia

13. ABSTRACT

This report describes an investigation of blade/disk attachment methods for small gas turbine engines. The investigation included analytical and experimental evaluations of selected attachment methods potentially suitable for a 2-lb/sec axial flow turbine with 2500°F turbine inlet temperature.

A literature survey of attachments for small axial flow turbines yielded six candidate methods for further analytical study. The three most promising approaches were evaluated experimentally to determine the superior attachment technique. This attachment scheme was optimized by additional uniaxial experimental testing and final proof-testing by subjecting biaxial specimens to cyclic loads at the attachment design temperature.

DD FORM 1 NOV 1473 REPLACES DD FORM 1473, 1 JAN 64, WHICH IS OBSOLETE FOR ARMY USE.

UNCLASSIFIED

Security Classification

KEY WORDS	LINK A		LINK B		LINK C	
	ROLE	WT	ROLE	WT	ROLE	WT
Turbine Blade/Disk Attachment						
Fir-Tree						
Brazing						
Electron-Beam Welding						
Bicast						